Null steering based beamforming techniques

Leng, Shuang

2011

Leng, S. (2011). Null steering based beamforming techniques. Doctoral thesis, Nanyang Technological University, Singapore.

https://hdl.handle.net/10356/46288

https://doi.org/10.32657/10356/46288

NULL STEERING BASED BEAMFORMING TECHNIQUES

LENG SHUANG

School of Electrical & Electronic Engineering

A thesis submitted to the Nanyang Technological University
in partial fulfillment of the requirement for the degree of
Doctor of Philosophy

2011

Statement of Originality

I hereby certify that the work embodied in this thesis is the result of original research and has not been submitted for a higher degree to any other University or Institution.

....

Date **LENG SHUANG**

Acknowledgments

I would like to express my heartfelt gratitude and appreciation to my advisor, Prof. Ser Wee. He had been very involved, providing advice, suggestions and encouragement throughout the project. Without his guidance and support, this thesis would not have been possible.

I would also like to thank all the colleagues in Center for Signal Processing, for their kind support and help in the past four years.

I would like to dedicate this thesis to my wonderful parents. There is no doubt in my mind that without their continued support and counsel I could not have completed this process.

Finally, I wish to acknowledge the love, encouragement and support of my wife, Lin Qing.

Contents

Abstract

Null steering techniques have been used extensively for interference suppression purposes in communications where the desired signal is weak compared with the interfering signals. In null steering algorithms, the weights of an antenna array are selected such that the directional pattern has nulls in particular directions. In this manner, undesirable interference, jamming signals, or noise can be reduced or completely eliminated. One of the pioneering null steering algorithms is Davies method [11]. Using Davies method, the null positions can be tracked one after another without affecting other null positions. Because of its ability to steer independent nulls, the Davies method has been attracting considerable interest for use in adaptive array processing. The Davies method has been further developed in [12], where a fast null steering algorithm was presented. Using this algorithm, the complex zeros of the array are adjusted individually in a cyclical manner to track individual interferences. The research work in this thesis focus on several novel developments based on the Davies method and the null steering algorithm in [12].

Since look direction constraint is not used in the Davies method as well as the null steering algorithm in [12], they are of great advantage in scenarios where the desired signal is weak compared with the interferences. However, in

the environment where the desired signal is stronger or not significantly weaker than the interferences, a deep null will be placed in the direction of interest resulting in desired signal loss. In this thesis, we first study and propose an adaptive beamformer derived from a constrained null steering design. With the new method, the null positions can be selectively tracked so that the interference signals can be rejected while the desired signal is picked up by the array. The main advantages of the new null steering beamformer are the simplicity, faster convergence rate and lower complexity.

The need for a broad null often arises when the direction of arrival (DOA) of the unwanted interference may vary slightly with time or the actual angle may dithering, and where a comparatively sharp null would require continuous steering for obtaining a reasonable value for the signal-to-interference ratio (SIR). In this thesis, we present an implementation of adaptive null steering beamformer for flexible broad null control, based on constrained recursive updating of array response zeros and spatial finite impulse response (FIR) filters. The design allows the beamformer to form broad nulls and control their widths readily. The new method is of great advantage for sensor array in which the number of array elements is very large compared with the number of interferences the array is designed to suppress. The new beamformer is useful and effective in the environment where both stationary and moving interference signals exist since it can steer both sharp and controlled broad nulls in the appropriate directions.

The basic structure of null steering algorithm in [12] assumes an all-zero model. In this thesis, we develop a new fast infinite impulse response (IIR) array processing based null steering system to investigate the design and performance if the null steering structure is extended to take the form of a pole-zero model.

Specifically, in the new design, the entire adaptive array is implemented by using two IIR arrays and the complex zeros of the array system will be repetitively updated one by one in a cyclical manner through a sequence of adjustment cycles. The proposed design is very effective and useful in the sense that without applying any additional constraint it will result in a nearly flat gain in the antenna pattern, except zero gains at the null directions.

The problem of determining DOA of multiple narrowband plane waves using sensor arrays has received significant attention in the array signal processing literature. In this thesis, we improve the null steering algorithm in [12] with least-square based preprocessing and show that both the least-square based null steering structure and the IIR array processing based null steering structure can be used to estimate the DOA. Moreover, computer simulations show that the new DOA estimation methods are robust to the sensor gain and phase perturbations.

List of Abbreviations and Symbols

Abbreviations

ASV	array steering vector
CMT	covariance matrix taper
DOA	direction of arrival
DOF	degree of freedom
DSFT	discrete-space Fourier transformer
DTFT	discrete-time Fourier transformer
ESPRIT	Estimation of Signal Parameters via Rotational Invariance Techniques
EVD	eigenvalue decomposition
FIR	finite impulse response
IDSFT	inverse discrete-space Fourier transformer
IDTFT	inverse discrete-time Fourier transformer
IIR	infinite impulse response
LCMV	linearly constrained minimum variance
LMS	least mean square

MSC	multiple sidelobe canceller
MSE	mean-square error
MUSIC	MUltiple SIgnal Classification
MVDR	minimum variance distortionless response
NLMS	normalized least mean square
NMSE	normalized mean-square error
NSASC	null steering algorithm with single constraint
NSAMC	null steering algorithm with multiple constraints
QR-RLS	QR decomposition-based recursive least squares
RLS	recursive least squares
SIR	signal-to-interference ratio
SINR	signal-to-interference-plus-noise ratio
SMI	sample matrix inversion
SNR	signal-to-noise ratio
SVD	singular value decomposition
UCA	uniform circular array
ULA	uniform linear array

Symbols

a	scalar
$\mathbf{a}$	vector
$\mathbf{A}$	matrix
$(\cdot)^*$	complex conjugate of a vector or matrix
$(\cdot)^H$	complex conjugate transpose of a vector or matrix
$(\cdot)^T$	transpose of a vector or matrix
$\|\cdot\|_2$	Euclidean norm
$E\{\cdot\}$	expectation operator
A_m	amplitude of narrowband signal
d	inter-element distance of uniform linear array
K	number of snapshots
M	number of signals
N	number of sensors in the array
$\mathbf{I}$	identity matrix
$\mathbf{R}$	covariance matrix
$\hat{\mathbf{R}}$	the sample average covariance matrix
$\mathbf{R}_s$	covariance matrix of impinging sources
$\mathbf{R}_{\mathrm{n}}$	covariance matrix of noise
$\hat{\mathbf{R}}_{CMT}$	covariance matrix for CMT based MVDR beamformer
σ_m^2	the signal power of the mth source
σ_{n}^2	the noise power
ω_0	operating frequency of narrowband signal
$s(t)$	array incident signal
$i(t)$	array incident interference

$\mathbf{v}(\omega_0, \theta, \phi)$	array steering vector
$\mathrm{n}(t)$	noise component
$\mathbf{n}(t)$	array received noise vector
p	output power of array processor
$\hat{p}$	optimal output power of array processor
t	time index
θ_m	incident azimuth angle of the mth source
ϕ_m	incident elevation angle of the mth source
α_m	phase shift of the signal
ϕ_n	nth phase setting for Davies beamformer
τ_m	time delay of arrival
μ	feedback factor
$D(z)$	directional pattern of array processor
b_n	zero of directional pattern
ρ	desired misadjustment
$\mathbf{w}$	array weight vector
$\hat{\mathbf{w}}$	estimated optimal array weight vector
$x_n(t)$	array received signal at the nth sensor
$\mathbf{x}(t)$	array received signal snapshot
$y(t)$	array output signal
$\vec{\mathbf{u}}_m$	unit vector in the incident direction of the mth source
$\mathbf{u}_n$	the nth eigenvector
λ_n	the nth eigenvalue
λ	wavelength
$\vec{\mathbf{r}}_n$	position vector of nth sensor
v	propagation speed of signal

Σ	the eigenvalue matrix
$\mathbf{U}$	the eigenvector matrix
$\mathbf{U}_{\mathrm{n}}$	basis of noise subspace
$\mathbf{U}_s$	basis of signal subspace
$\mathbf{T}_{CMT}$	taper for CMT based beamformer

List of Figures

List of Tables

Chapter 1

Introduction

1.1 Background and Motivation

Array signal processing has been studied for some decades as an attractive method for signal detection and estimation in harsh environments. An array of sensors can be applied to achieve spatial filtering which weakens the interference power (null steering) and enhances the signal strength (beamforming). It has found many applications in radar, radio astronomy, sonar, wireless communication, seismology, speech acquisition, medical diagnosis and treatment [1, 2, 3], etc.

Null steering techniques have been used extensively for interference suppression purposes in communications where the desired signal is weak compared with the interfering signals. Suppose a receiver wants to receive signals from any directions without knowing where they are coming from and in the presence of interferences. In this scenario, we do not know the direction of interest and it is better not to have a particular beam pointing to a specific direction but

to have equal gain in all directions except in direction of interferences. This is easily achievable by null steering algorithms where the weights of an antenna array are selected such that the radiation pattern has nulls in particular directions. In this manner, undesirable interference, jamming signals, or noise can be reduced or completely eliminated.

The major advantages of null steering algorithms are simplicity and fast convergence rate. One of the pioneering null steering algorithms is Davies method [11]. Using Davies method, the null positions can be tracked one after another without affecting other null positions. Because of its ability to steer independent nulls, the Davies method has been attracting considerable interest for use in adaptive array processing. The Davies method has been further developed in [12], where a fast null steering algorithm was proposed. Using this algorithm, the complex zeros of the array are adjusted individually in a cyclical manner to track individual interferences. Since only one zero is adjusted at any instance, the complexity required to implement the algorithm is low and the convergence behaviour is significantly faster.

When the direction of interest is known, beamforming techniques can be utilized to form a particular beam pointing to that direction. A beamformer is a processor used in conjunction with an array of sensors to provide a versatile form of spatial filtering. The sensor array collects spatial samples of propagating wave fields, which are processed by the beamformer. The objective is to not only concentrate the array to signals coming from the direction of interest, but also to reduce interference and noise for better signal-to-interference-plus-noise ratio (SINR).

Beamformers are classified as either data independent or statistically opti-

mum, depending on how the weights are chosen. The weights in a data independent beamformer do not depend on the array data and are chosen to present a specified response for all signal/interference scenarios. The weights in a statistically optimum beamformer are chosen based on the statistics of the array data to optimize the array response. The typical statistically optimum beamformer are the linearly constrained minimum variance (LCMV) beamformers [4, 5, 6, 7, 8].

The statistics of the array data are usually unknown and may change over time so adaptive algorithms are typically used to determine the weights. The adaptive algorithm is designed so the beamformer response converges to a statistically optimum solution. The constrained least mean square (LMS) algorithm is a popular weight adaptation algorithm. The primary virtue of the LMS algorithm is its simplicity. However, its convergence characteristics depend on the external noise environment and may be unacceptably slow in the situation where strong interferences exist.

One alternative to LMS is the exponentially weighted recursive least square (RLS) algorithm. The convergence of RLS weight adaptation algorithm is often faster than that obtained using the LMS algorithm. Recently, QR-RLS based beamformers [9, 10] have been proposed. The potential advantages of QR-RLS based method include numerical stability and pipelined structure in implementation. However, one drawback for RLS weight adaptation algorithm is its high computational complexity.

To improve the speed of the LMS algorithm without sacrificing too much of its implementation simplicity, the null steering algorithms for beamforming applications need to be investigated. Constrained null steering algorithms [14, 53]

were presented to ensure that the look direction response remains unchanged when a particular null is being updated. However, in these algorithms, the look direction constraint must be satisfied in each null update process. Therefore, more research works still need to be carried out on how null steering algorithm can be used for the scenario where the direction of signal of interest is known. In this thesis, we study and propose an adaptive beamformer derived from a constrained null steering design. The designed beamformer has faster convergence rate and lower computational complexity.

In recent years, there has been a considerable interest in obtaining broad null sectors in linear arrays. The need for a broad null often arises when the direction of arrival (DOA) of the unwanted interference may vary slightly with time or the actual angle may be dithering, and where a comparatively sharp null would require continuous steering for obtaining a reasonable value for the signal-to-interference ratio (SIR).

Recently, several authors exploited the idea of artificial broadening of the beampattern nulls in unknown interfering directions. One common approach is the covariance matrix taper (CMT) based minimum variance distortionless response (MVDR) beamformer [15, 16, 17, 18]. It is a filterbank method that the optimum weights are chosen to minimize the output power of moving interference signals and, at the same time, to maintain a distortionless response towards the desired signal. This effectively places deep broad nulls canceling interference from sources in directions other than the one of interest. The implementation of CMT based MVDR beamformer suffers from being computationally cumbersome, especially for large arrays [19]. This is due to the requirement to evaluate a vector-matrix product containing the inverse of large dimensional data co-

variance matrix. Numerous adaptive algorithms can be used to solve CMT based MVDR beamforming problem. Some of the more widely used methods are sample matrix inversion (SMI) [42], LMS [31], normalized LMS (NLMS) and QR-RLS [10]. However, the major disadvantage of LMS and NLMS is that their convergence behavior is very slow in severe jamming situation. The drawback of SMI and QR-RLS is their high computational cost.

Quite a few papers have proposed to synthesize the antenna array pattern with prescribed broad nulls by minimizing the mean-square error (MSE) between the desired and the generated beam patterns [20, 21, 22]. Sidelobe constraints in the interference direction are added to the least-squares criterion in order to form a broad null. Main difficulties in implementing the constrained optimization algorithm include: 1) The explicit function of the desired pattern is hard to obtain; 2) The integration of the squared-error function may not be easy to calculate; 3) The computation load increases as a matrix inversion with large size is required.

The similarity between uniform linear array (ULA) beamformer and temporal finite impulse response (FIR) filter makes filter design methods applicable for beampattern synthesis. As depicted in [23, 24], the impulse response of an FIR filter is directly employed as the array coefficients. However, the designed beamformers are data independent. Moreover, additional undesirable broad nulls will be generated due to the symmetrical shapes in the beampatterns.

In this thesis, the beamformer derived from a constrained null steering design is further developed for the scenario when interferences are moving. Hence, broader null can be generated using the same structure.

The basic null steering structure discussed in [12] assumes an all-zero model

and it will be useful to investigate the design and performance if it is extended to take the form of a pole-zero model. Hence, in this thesis, we present an infinite impulse response (IIR) array processing based null steering algorithm.

DOA estimation is a basic and important technique in array signal processing. Many high-resolution direction-finding approaches have been presented to solve the problem in the recent years. Those approaches were based on the techniques such as maximum-likelihood [25] and MUSIC [26]; One typical DOA estimator based on maximum-likelihood method is MVDR estimator [27], which finds the maximum-likelihood estimate of the power arriving from a point source in certain direction assuming all other sources as interferences. However, the computational burden associated with those approaches is quite high and makes them difficult for high-speed applications. Compared to MUSIC method, ESPRIT [28] method does not need to search for spectral peak, so it has advantage of less calculation, higher precision and suitable for real time application. However, the ESPRIT method is a one dimensional method, thus in the case of low signal-to-noise ratio (SNR) the estimation error can be high. Therefore, we study and investigate null steering algorithms for DOA estimation application. It will be shown in this thesis that the same null steering structure can also be used to estimate the DOA.

1.2 Objectives

The objective of this thesis is to study the null steering algorithms, develop beamforming algorithms based on that structure for some communications scenarios, and compare them with the existing beamforming approach.

1.3 Major Contributions of Thesis

The main contributions of this thesis are the followings:

1. An adaptive beamformer derived from a constrained null steering design is proposed. The main advantage of the new beamformer is its simplicity and lower complexity. The analyses and investigations on the convergence behavior, rules for sidelobe direction selection, ratio parameter and the effect of number of elements are also provided.

2. An online implementation of an adaptive null steering beamformer for flexible broad null control, based on constrained recursive updating of array response zeros and spatial FIR filters, is presented. The design allows the beamformer to form broad nulls and control their widths readily.

3. A new fast null steering system employing IIR array preprocessing is presented and analyzed. The new algorithm is of considerable interest in communications where the desired signal is weak compared with the interfering signals or where the desired signal can be easily separated out. The proposed method is very effective and useful in the sense that without applying any additional constraint it will result in a nearly flat gain in the antenna pattern, except zero gains at the null directions.

4. The applications of null steering algorithms on DOA estimation are presented and discussed in details. With null steering algorithm, the complex zeros of the array directional pattern are repetitively updated one at a time. Then, a relationship between the updated zeros and the DOA angles is established so that the angles can be quickly estimated. In ad-

dition, the performance of the proposed approach with sensor gain and phase perturbations is also discussed.

1.4 Organization of Thesis

The remainder of this thesis is organized as follows. Chapter 2 provides the background materials of adaptive null steering and beamforming techniques. The basic principle and structure of adaptive beamformer are explained. The definition of the signal and noise model and formulations of the array processors are presented. The array geometry and the well studied LCMV beamformer are discussed. The conventional CMT based robust beamformer is also presented.

In Chapter 3, we present an adaptive beamformer derived from a constrained null steering design. The analyses and investigations on the convergence behavior, rules for sidelobe direction selection, ratio parameter and the effect of number of elements are also provided.

An online implementation of adaptive null steering beamformer for flexible broad null control is proposed in Chapter 4. The proposed implementation has relatively simple design and the ability to control each individual broad null readily.

In Chapter 5, a new fast null steering system which takes the form of a pole-zero model will be presented and analyzed. The entire array system is implemented by using two IIR arrays.

In Chapter 6, we study and investigate the application of null steering technique in DOA estimation. The new method establishes a relationship between the updated zeros and the DOA angles so that the angles can be quickly es-

timated. The robustness of the new algorithm to the sensor gain and phase perturbations is also investigated using analysis and computer simulations.

Finally, Chapter 7 provides some concluding remarks and future work for possible extensions.

Chapter 2

An Overview of Spatio-Temporal Array Processing: Models and Structures

2.1 Introduction

In this chapter, the framework for the design of adaptive beamformer will be presented. The chapter begins with an introduction to the basic principle and concepts in array processing. This is followed by the mathematical notations, signal and noise models that are relevant to the major part of this thesis. An overview of array beamformers is also given. Uniform linear array (ULA), which is frequently used in the subsequent chapters for simulations and performance evaluations, is also discussed in this chapter. The basic structure of the minimum variance beamformer is reviewed and briefly discussed.

2.2 Principle of Adaptive Beamformer

An adaptive array is a system consisting of an array of sensor elements and a real-time adaptive signal receiver-processor that automatically adjusts the array beampattern by weighting the input of the individual elements. These weights can be chosen based on various algorithms [7, 29, 30, 31]. The received signals are obtained by means of an array of sensors located at different points in space in the field of interest. The aim of array processing is to extract useful characteristics of the received signal field (e.g., its signature, direction, speech of propagation). The collected signals at sensors are combined cleverly so as to enhance the signal-to-noise ratio (SNR) of target signal, to characterize the signal wave field, and to track the signal sources as they move in space.

With distributed sensors, the array processing exploits not only the temporal information, but also the spatial information of signals. The temporal-spatial processing greatly extends the capability in information extraction. This technique has received great interest in past decades. In this thesis, we focus on the array processor in beamforming applications for signal detection and enhancement.

The interest in using adaptive beamforming began in 1950s to solve the new problems in satellite communications. In [32], the theoretical basis for the operation of adaptive beamformer was given. The multiple sidelobe canceller (MSC) proposed by Appelbaum [29] consists of a main antenna with high gain and one or more auxiliary antenna elements. With properly chosen auxiliary antenna weights, it is then possible for the auxiliary channels to cancel the main channel interference component. The overall system then has a response of zero in the direction of interference sources. Widrow et al. [30] proposed the use of

a reference signal and the array weights could be chosen to minimize the mean square error between the adaptive array output and this reference signal. The weights can also be chosen to directly maximize the signal-to-interference-plus-noise ratio (SINR) [7]. Frost [31] has suggested a least mean square (LMS) based linearly constrained minimum variance (LCMV) beamforming algorithm, where the desired signal is preserved while minimizing contributions to the output due to interfering signals and noise arriving from directions other than the direction of interest.

Most of the pioneering works on adaptive arrays focus on antenna array for communication and radar applications. Another important application of adaptive array is the acoustic application, e.g. sonar, which works with low frequency signals. Although the signals as well as systems are different in those applications, the adaptive array techniques developed in communication and radar can be used in sonar too. The differences are rather in technologies than in principles. For specific applications, there are special problems of adaptive array. Nevertheless they have similar principle.

An important concept in adaptive array is the classification of the array depending on the frequency operating bandwidth. According to such classification, adaptive arrays may be of narrowband or broadband type. A bandwidth exceeding 15% deviation from the centre frequency is usually accepted as a broadband criterion. Although in principle no distinctions exist between the two situations, in practice, the technical means used to implement the array weights are different. In this thesis, we focus on the array processor in narrowband applications. Unless it is specially mentioned, the array processing refers to narrowband beamforming in this thesis.

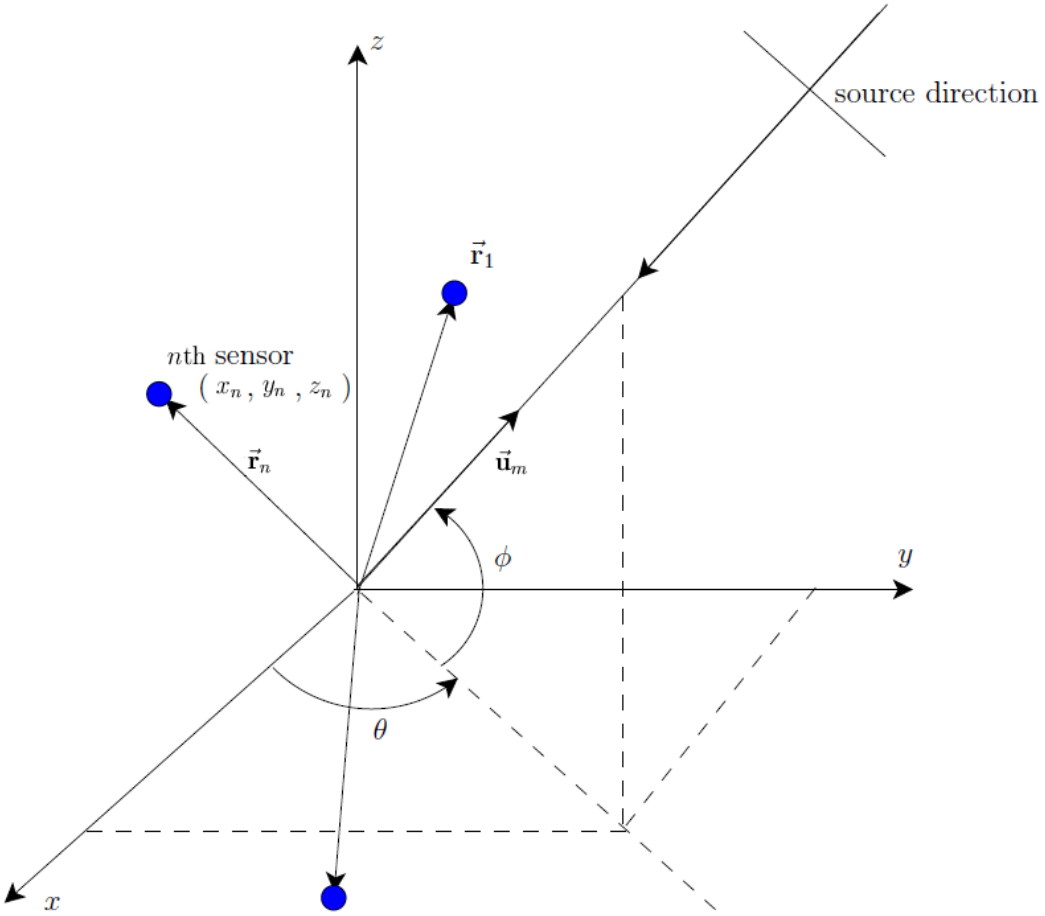

Figure 2.1: Array with arbitrary geometry

2.3 Signal Representation in Array Processing

In most of the array processing examples, it is assumed that each signal consists of a point source which is located at a far distance away from the array, i.e., the array is located in the far field of the point sources. Thus each directional signal impinging on the array is considered as a plane wave. This is the typical scenario of conventional array processing.

2.3.1 The Signal Representation of Beamformer

As the array system shown in Fig. 2.1, it is assumed that the signal environment consists of M plane waves, each arriving at the array from a distinct direction, and that all the plane waves are narrowband, with the same frequency ω_0. The noiseless signal produced at the nth sensor of the array due to the mth plane wave can be expressed as follows:

$$s(n, m, t) = A_m e^{j(\omega_0(t-\tau_{nm})+\alpha_m)} \tag{2.1}$$

where t is the time, A_m is the amplitude of the signal produced, α_m is the phase displacement, τ_{nm} is the time delay at the nth sensor.

The expression for τ_{nm} is given by

$$\tau_{nm} = \frac{\vec{\mathbf{u}}_m \cdot \vec{\mathbf{r}}_n}{v} \tag{2.2}$$

where $\cdot$ denotes the dot product, $\vec{\mathbf{u}}_m$ is the unit vector in the incident direction (θ_m, ϕ_m) of the mth source, $\vec{\mathbf{r}}_n$ is the position vector of the nth sensor, and v is the speed of the propagating wave. The vectors $\vec{\mathbf{u}}_m$ and $\vec{\mathbf{r}}_n$ can be expressed as

$$\vec{\mathbf{u}}_m = \begin{bmatrix} \cos\phi_m \cos\theta_m \\ \cos\phi_m \sin\theta_m \\ \sin\phi_m \end{bmatrix} \tag{2.3}$$

and

$$\vec{\mathbf{r}}_n = \begin{bmatrix} x_n \\ y_n \\ z_n \end{bmatrix} \tag{2.4}$$

respectively.

Substituting (2.3) and (2.4) into (2.2), τ_{nm} can be expressed as

$$\tau_{nm} = \frac{1}{v}[(x_n \cos\theta_m + y_n \sin\theta_m)\cos\phi_m + z_n \sin\phi_m] \tag{2.5}$$

The coordinate of each array element, $\vec{\mathbf{r}}_n$, is assigned by taking the centre of gravity of the array as the origin, such that

$$\sum_{n=0}^{N} \vec{\mathbf{r}}_n = 0 \tag{2.6}$$

The selection of the centre of gravity of the array as the coordinate origin will ensure that the array is equipped with the rotational invariance property [33]. This property is important as one would expect the array to have the same characteristic irrespective of whether the source is rotated in θ and/or ϕ or the array rigidly rotated by the corresponding $-\theta$ and/or $-\phi$ with a fixed source.

The sensor received signal in (2.1) can be represented by its complex amplitude, $s(n, m)$, defined by

$$\begin{aligned} s(n,m) &= A_m e^{-j(\omega_0 \tau_{nm} + \alpha_m)} \\ &= (A_m e^{j\alpha_m}) e^{-j\omega_0 \tau_{nm}} \\ &\triangleq a_m e^{-j\omega_0 \tau_{nm}} \end{aligned} \tag{2.7}$$

The signal in (2.7) describes the noiseless signal output at the nth sensor. In practice, the array received signal also contains noise. In many array processing examples, the noise is assumed to be a white, ergodic random process.

The output from each element in the array is customarily filtered to the same narrowband frequency occupied by the actual received signal.

The observed signal at the nth sensor, $x_n(t)$ can be expressed as the sum of the noiseless signals produced by all the plane waves and the white noise as follows:

$$x_n(t) = \sum_{m=1}^{M} a_m e^{-j\omega_0 \tau_{nm}} + \mathrm{n}_n(t) \tag{2.8}$$

where $\mathrm{n}_n(t)$ is the complex random noise. Let $\mathbf{x}(t)$ be the vector of the observed signals derived at the output of the sensor elements, i.e.

$$\mathbf{x}(t) = [x_1(t) \quad x_2(t) \quad \cdots \quad x_N(t)]^T \tag{2.9}$$

where the superscript T denotes vector transpose.

Substitute (2.8) into (2.9), it follows that

$$\mathbf{x}(t) = \sum_{m=1}^{M} a_m \mathbf{v}_m(\omega_0, \theta_m, \phi_m) + \mathbf{n}(t) \tag{2.10}$$

where $\mathbf{v}_m(\omega_0, \theta_m, \phi_m)$ is the array steering vector (ASV) of the mth source given by

$$\mathbf{v}_m(\omega_0, \theta_m, \phi_m) = \begin{bmatrix} e^{-j\omega_0 \tau_{m1}} \\ e^{-j\omega_0 \tau_{m2}} \\ \vdots \\ e^{-j\omega_0 \tau_{mN}} \end{bmatrix} \tag{2.11}$$

and $\mathbf{n}(t)$ is the received noise vector given by

$$\mathbf{n}(t) = [\mathrm{n}_1(t) \quad \mathrm{n}_2(t) \quad \cdots \quad \mathrm{n}_N(t)]^T \tag{2.12}$$

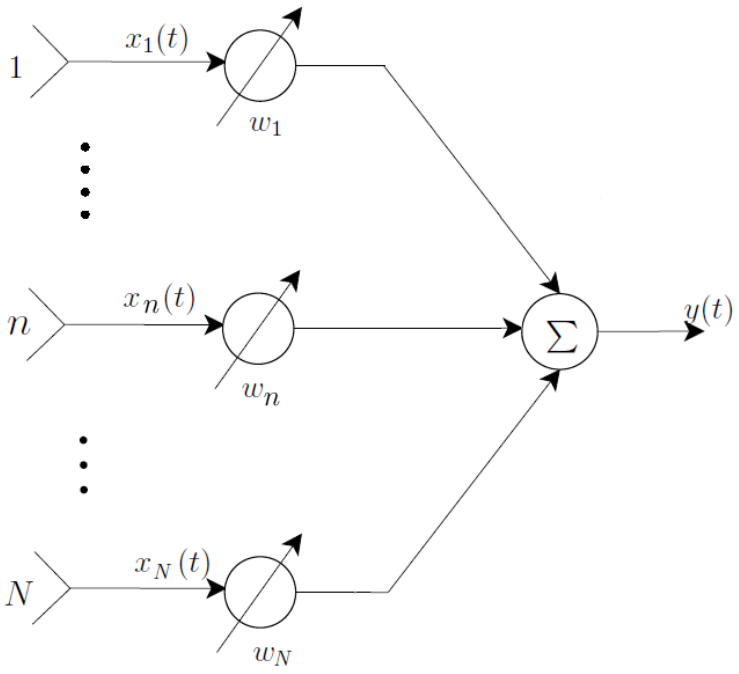

Figure 2.2: Narrwoband beamformer with N sensors

The structure of a narrowband beamformer comprising of N sensors is shown in Fig. 2.2. The sensor-collected signals, $x_n(t)$, $n = 1, \ldots, N$, are weighted by w_n, $n = 1, \ldots, N$ and summed up to form the output signal $y(t)$

$$y(t) = \sum_{n=1}^{N} w_n^* x_n(t) = \mathbf{w}^H \mathbf{x}(t) \tag{2.13}$$

where $\mathbf{w}$ denotes the complex weight vector and $(\cdot)^H$ denotes the Hermitian transpose.

$$\mathbf{w} = [w_1 \quad \cdots \quad w_n \quad \cdots \quad w_N]^T \tag{2.14}$$

For the sources that can be modeled by stationary stochastic process, the mean output power from the array system is given by

$$p(\mathbf{w}) = E\{|y(t)|^2\} = \mathbf{w}^H \mathbf{R} \mathbf{w} \tag{2.15}$$

where $E\{\cdot\}$ denotes the expectation operator, and $\mathbf{R}$ is the $N \times N$ dimensional array covariance matrix defined by

$$\mathbf{R} = E\{\mathbf{x}(t)\mathbf{x}^H(t)\} \tag{2.16}$$

2.3.2 The Covariance Matrix of Beamformer

The covariance matrix $\mathbf{R}$ in (2.16) is the statistical second-order property of the impinging signals. In real applications, $\mathbf{R}$ is estimated using the received array snapshots. The estimated array covariance matrix, $\hat{\mathbf{R}}$, is given by

$$\hat{\mathbf{R}} = \frac{1}{K}\sum_{k=1}^{K}\mathbf{x}(k)\mathbf{x}^H(k) \tag{2.17}$$

where K is the number of snapshots, and $\mathbf{x}(k)$ is a column vector consisting of the kth sampled data of all the N sensors. When K approaches infinity, the estimated $\hat{\mathbf{R}}$ asymptotically approaches the true one, assuming that the sensor signals are ergodic.

When all the impinging sources and the noise are mutually uncorrelated or noncoherent, the array correlation matrix $\mathbf{R}$ is a non-negative matrix, and is given by

$$\begin{aligned}\mathbf{R} &= \sum_{m=1}^{M}\sigma_m^2\mathbf{v}(\omega_0,\theta_m,\phi_m)\mathbf{v}^H(\omega_0,\theta_m,\phi_m) + \mathbf{R}_{\mathrm{n}} \\ &\triangleq \mathbf{R}_s + \mathbf{R}_{\mathrm{n}}\end{aligned} \tag{2.18}$$

where σ_m^2 is the power of the mth source,

$$\sigma_m^2 = E\{|a_m|^2\} \tag{2.19}$$

and $\mathbf{R}_{\mathrm{n}}$ is the covariance matrix of the background white noise, $\mathbf{R}_s$ is the covariance matrix of the impinging directional sources. When the noise is white,

$$\mathbf{R}_{\mathrm{n}} = \sigma_{\mathrm{n}}^2 \mathbf{I} \tag{2.20}$$

where σ_{n}^2 is the power of noise and the matrix $\mathbf{I}$ is an identity matrix.

The eigen-decomposition (EVD) of the covariance matrix plays an important role in array processing algorithms and thus its structure will be explored further. It can be decomposed and expressed in the following form:

$$\begin{aligned} \mathbf{R} &= \mathbf{U}\Sigma\mathbf{U}^H \\ &= \sum_{n=1}^{N} \lambda_n \mathbf{u}_n \mathbf{u}_n^H \end{aligned} \tag{2.21}$$

where $\Sigma = diag(\lambda_1, \lambda_2, \cdots, \lambda_N), \lambda_1 \geq \lambda_2 \geq \cdots \geq \lambda_N$ is the eigenvalue matrix and $\mathbf{U} = [\mathbf{u}_1\ \mathbf{u}_2\ \cdots\ \mathbf{u}_N]$ is the corresponding eigenvector matrix, such that

$$\mathbf{R}\mathbf{u}_n = \lambda_n \mathbf{u}_n, \quad n = 1, \cdots, N \tag{2.22}$$

An important property of the EVD of the matrix $\mathbf{R}$ is that, the eigenvalues λ_i of $\mathbf{R}$ is

$$\lambda_n = \begin{cases} \gamma_n + \sigma_{\mathrm{n}}^2, & 1 \leq n \leq M \\ \sigma_{\mathrm{n}}^2, & M+1 \leq n \leq N \end{cases} \tag{2.23}$$

where γ_n is the nth eigenvalue of the matrix $\mathbf{R}_s$.

Splitting the eigenvector matrix into

$$\mathbf{U} = [\mathbf{U}_s \ \mathbf{U}_{\mathrm{n}}] \tag{2.24}$$

where

$$\begin{aligned} \mathbf{U}_s &= [\mathbf{u}_1 \ \mathbf{u}_2 \ \cdots \ \mathbf{u}_M], \\ \mathbf{U}_{\mathrm{n}} &= [\mathbf{u}_{M+1} \ \cdots \ \mathbf{u}_N] \end{aligned} \tag{2.25}$$

Then, the matrix $\mathbf{U}_s$ is the eigen-basis of the so-called signal subspace, and the matrix $\mathbf{U}_{\mathrm{n}}$ is the eigen-basis of the noise subspace. The ASV of each signal is a linear combination of the column vectors of $\mathbf{U}_s$, i.e.,

$$\mathbf{v}(\omega_0, \theta_m, \phi_m) \in span(\mathbf{U}_s) \tag{2.26}$$

2.4 Array Geometry - Uniform Linear Array

The inter-element time delay in (2.2) is defined for an arbitrary array system. In practice, the geometry of the array system is well defined and hence the inter-element time delay can be expressed in a simplified form. One commonly used array geometry, namely uniform linear array (ULA) is examined in this section. In this thesis, we focus on the beamforming techniques using ULA system.

In many applications, such as sonar, radar and seismology, it is necessary to use antenna arrays with a very directive characteristic to meet the demand of long distance communication. The ULA is very simple in design and is found to be suitable for these applications as it has very high directivity.

A ULA consists of a number of sensor elements, which are equally spaced in a straight line. For an N-element ULA, with all the elements placed along the

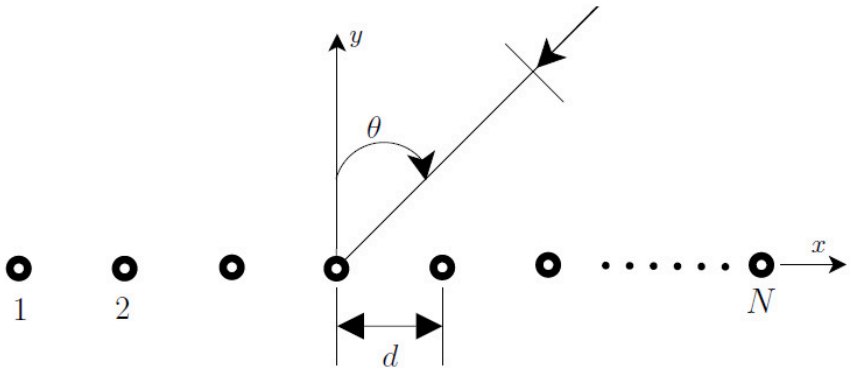

Figure 2.3: Uniform linear array with N sensors

x-axis as shown in Fig. 2.3, the inter-element time delay at the nth element can be derived from (2.2) by setting $y_n = z_n = 0$ and $\phi_n = 0°$, i.e.,

$$\tau_n = \frac{x_n sin\theta}{v} \tag{2.27}$$

where θ is the incident angle of the directional source measured from the y-axis (broadside), and x_n is the x-coordinate of the nth element.

Taking the centre of the array as the reference, it follows that

$$\tau_n = \left[(n-1) - \frac{N-1}{2}\right] \frac{d \sin\theta}{v} \tag{2.28}$$

where d is the inter-element spacing.

2.5 Linearly Constrained Minimum Variance Array Beamformer

Most of the well studied array beamformers are LCMV beamformers. The optimal weight vector of the LCMV beamformer is obtained by minimizing the

output variance subject to a set of linear constraints. In this section, we briefly introduce the typical narrowband beamformer used in array processing.

The structure of a narrowband beamformer comprising of N sensors is shown in Fig. 2.2. The adaptive beamformer adjusts its weight vector $\mathbf{w}$ automatically according to specific criterion without the requirement on the information of the stochastic property of the signals. A famous representative of the LCMV beamformer, the Capon beamformer [34], is designed to minimize its mean output power subject to a unity gain constraint in the look direction as an indirect way of rejecting noise and interferences incident on the array. The optimal weight vector $\hat{\mathbf{w}}$ is the solution of the following constrained optimization problem

$$\begin{cases} \min\limits_{\mathbf{w}} & \mathbf{w}^H\mathbf{R}\mathbf{w} \\ s.t. & \mathbf{v}^H(\theta_0)\mathbf{w} = 1 \end{cases} \tag{2.29}$$

where $\mathbf{v}^H(\theta_0)$ is the nominal ASV corresponding to the assumed target direction θ_0. Using the Lagrange multipliers methodology [35], the optimal weight vector $\hat{\mathbf{w}}$ is given as [5]

$$\hat{\mathbf{w}} = \frac{\mathbf{R}^{-1}\mathbf{v}(\theta_0)}{\mathbf{v}^H(\theta_0)\mathbf{R}^{-1}\mathbf{v}(\theta_0)} \tag{2.30}$$

The optimal output power of the array beamformer, i.e., the power of the target signal, is

$$\hat{p} = \frac{1}{\mathbf{v}^H(\theta_0)\mathbf{R}^{-1}\mathbf{v}(\theta_0)} \tag{2.31}$$

2.6 Summary

In this chapter, the basic concepts of the array processing were discussed. The signal models used in array processing for narrowband array applications were

presented. The basic structures of the array beamformers were also discussed. A brief introduction to the widely used ULA was given. The LCMV beamformer was also summarized.

Chapter 3

Adaptive Beamformer Derived from A Constrained Null Steering Design

3.1 Introduction

As discussed in Chapter 2, a beamformer forms a beam to a desired direction and the purpose is to enhance the signal-to-noise ratio (SNR) in that direction. The principle of conventional linearly constrained minimum variance (LCMV) beamformer is briefly introduced in Chapter 2. The computational load of LCMV beamformer can be high and the adaptive or tracking speed can be slow for time-varying environments.

The conventional null steering algorithms [11, 12] are of great advantage in scenarios where the desired signal is weak compared with the interference signals, so that undesirable interferences, or jamming signals can be reduced

and the desired signal will not be in a null. The advantages of null steering algorithms are simplicity and faster convergence rate. Therefore, to improve the speed of the conventional adaptive beamforming algorithm, the null steering algorithms for beamforming applications need to be investigated. A constrained null steering algorithm [14] was presented to ensure that the look direction response remain unchanged when a particular null is being updated. However, in this algorithm, the look direction constraint must be satisfied in each null update process. Hence, more research works still need to be carried out on how null steering algorithm can be used for the scenario where not only the interferences need to be suppressed but also the desired signal needs to be preserved.

In this chapter, the null steering algorithms with single and multiple constraints (NSASC, NSAMC) are proposed. Using these methods, the zeros can be selectively tracked so that the interferences can be rejected while the desired signal is concentrated on by the array. The main advantage of NSASC/NSAMC is its simplicity. When compared with conventional least mean square (LMS) based LCMV beamforming algorithm, NSASC and NSAMC converge in a faster manner. Compared with QR-recursive least square (QR-RLS) based minimum variance distortionless response (MVDR) beamformer, NSASC and NSAMC have lower complexity. Furthermore, due to their cascade configurations, signal self-nulling problem for conventional beamformer can be resolved.

Detailed analysis and investigation of the convergence behavior, rules for sidelobe direction selection, ratio parameter and the effect of number of elements for NSASC/NSAMC are also provided in this chapter. Note that throughout this chapter, the direction of desired signal is assumed to be roughly known.

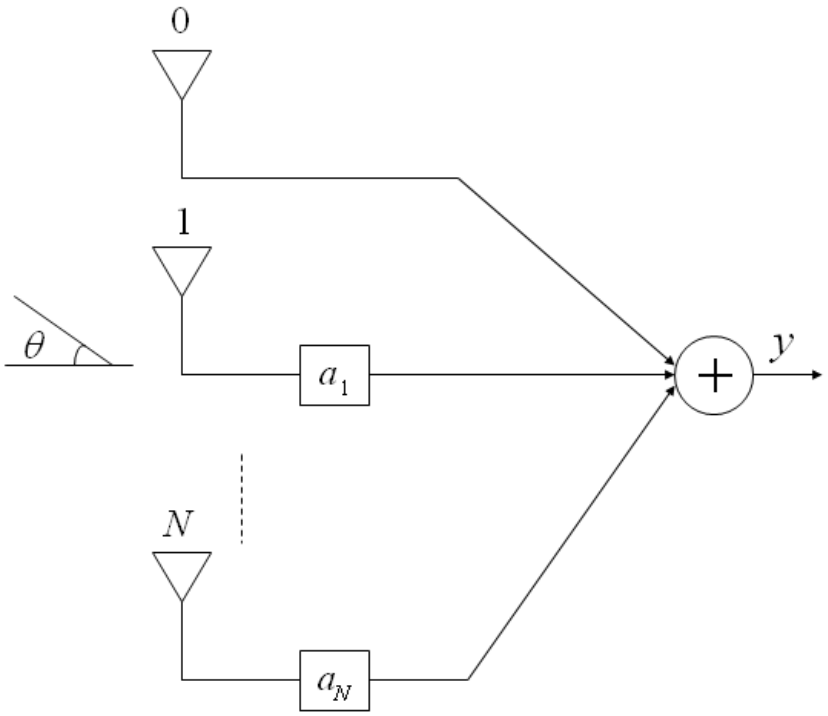

Figure 3.1: The power inversion array

The remainder of this chapter is organized as follows. The power inversion array is discussed in Section 3.2. Section 3.3 briefly summarizes the Davies null steering algorithm [11] and the fast null steering method presented in [12]. The proposed NSASC and NSAMC are presented in Sections 3.4 and 3.5. Section 3.6 provides the average convergence behavior analysis. The simulation results are given in Section 3.7. Finally, Section 3.8 gives the summary.

3.2 Power Inversion Array

Fig. 3.1 shows the structure of linear uniformly spaced narrowband power inversion array with $N + 1$ elements. The directional pattern of the array is given by

$$D(z) = 1 + a_1 z^{-1} + a_2 z^{-2} + a_3 z^{-3} + \ldots + a_N z^{-N} \tag{3.1}$$

where

$$z = e^{j2\pi d \sin\theta/\lambda} \tag{3.2}$$

λ is the wavelength. Such a polynomial may be represented as the product of N factors giving the N zeros of the directional pattern.

$$D(z) = (1 - b_1 z^{-1})(1 - b_2 z^{-1}) \ldots (1 - b_N z^{-1}) \tag{3.3}$$

where b_n is the nth complex zero of the directional pattern. By choosing

$$b_n = e^{j\phi_n} \tag{3.4}$$

the array will have N perfect nulls at directions satisfying

$$\phi_n = \frac{2\pi d \sin\theta_n}{\lambda} \tag{3.5}$$

Since an array with $N+1$ elements only has N independent response zeros, without loss of generality, the noise environment will be assumed to consist of N independent interferences with powers $p_1, \ldots, p_N$ at directions $\theta_1, \ldots, \theta_N$, respectively, measured from the normal of the array as indicated in Fig. 3.1. In addition, each array element will also be assumed to generate independent receiver noise of power p_0. From (3.1)-(3.4), the output power from the array is

$$E[|y|^2] = \sum_{i=1}^{N} p_i \left[\prod_{n=1}^{N} |e^{j\gamma_i} - e^{j\phi_n}|^2 \right] + p_0 \left[1 + \sum_{n=1}^{N} |a_n|^2 \right] \tag{3.6}$$

where

$$\gamma_i = \frac{2\pi d \sin\theta_i}{\lambda} \tag{3.7}$$

When all the interferences have powers much greater than receiver noise, the second term in (3.6) due to receiver noise will be small compared with the first term due to the interferences, unless the nulls controlled by $\phi_1, \ldots, \phi_N$ correspond to the interferences' directions as given by $\gamma_1, \ldots, \gamma_N$. Thus, when the processing employed by the array is adjusted to minimize the output power, each of the strong interferences will eventually be tracked by at least one of the nulls. However, when the background noise level is close to the interference level, the second term in (3.6) will be comparable to the first term and the tracking errors of the interferences will become large.

3.3 Conventional Null Steering Algorithms

Null steering algorithms are used to cancel a plane wave arriving from a certain direction and thus produces a null in the response pattern in the direction of arrival (DOA) of the plane wave [36].

3.3.1 Davies Null Steering Algorithm

As discussed in Chapter1, the major disadvantage of LMS algorithm is that its convergence characteristics depend on the external noise environment and may be unacceptably slow in situations where strong interferences exist. To improve the speed of the LMS algorithm without sacrificing too much of its implementation simplicity, the Davies method [11] can be employed as the underlying array processing structure. By using Davies method, the null positions can be tracked one after another without affecting other null positions.

Fig. 3.2 shows the structure of the narrowband Davies method for a linear

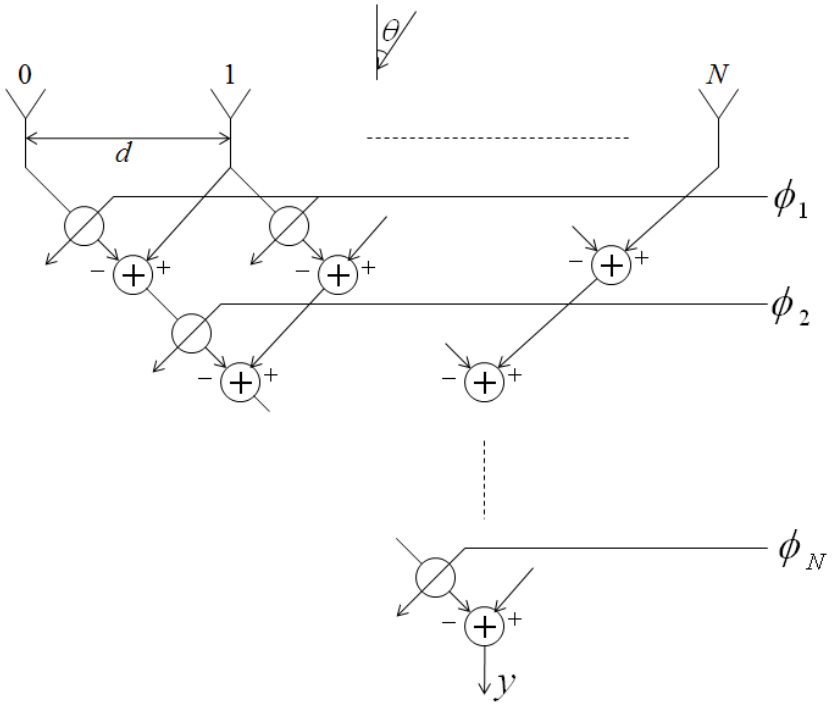

Figure 3.2: The Davies null steering algorithm [11]

array with $N+1$ elements. It consists of N sets of phase shifters and summers and has a directional pattern given by

$$D(z) = \prod_{n=1}^{N} (z - e^{j\phi_n}) \tag{3.8}$$

where ϕ_n is the nth phase setting. From (3.2) and (3.8),the nth null in the directional pattern is at a direction given by

$$\sin\theta = \phi_n \lambda / 2\pi d \tag{3.9}$$

Thus, each of the N phase shifter settings steers an independent null of the array. Since nulls can be independently steered, and the number of variables needed to be controlled is small, an adaptive array based on this method can be envisioned to have a better performance in tracking interferences than the

conventional system based on power inversion array. Therefore, we use the basic structure of Davies null steering algorithm as the basis in this thesis.

3.3.2 Fast Null Steering Algorithm

The fast null steering algorithm [12] for narrowband arrays is briefly summarized in this section. Using this algorithm, which was developed based on the theory of Davies null steering method, the complex zeros of the array are repetitively updated and thus the nulls are placed in the directions of interference signals.

The directional pattern of power inversion array is given as (3.3). Now suppose zero b_1 is to be updated to track the strongest interference signal. From (3.3), the directional pattern of the array is given by:

$$D(z) = (1 - b_1 z^{-1})\hat{D}(z) \tag{3.10}$$

where

$$\begin{aligned} \hat{D}(z) &= (1 - b_2 z^{-1})(1 - b_3 z^{-1}) \dots (1 - b_N z^{-1}) \\ &= 1 + c_1 z^{-1} + c_2 z^{-2} + \dots + c_{N-1} z^{-(N-1)} \end{aligned} \tag{3.11}$$

can be seen as the directional pattern of an N-element array with the coefficients $1, c_1, c_2, \dots, c_{N-1}$.

From (3.10) and (3.11), $D(\theta)$ can be expressed as

$$D(z) = \hat{D}(z) - b_1 \hat{\hat{D}}(z) \tag{3.12}$$

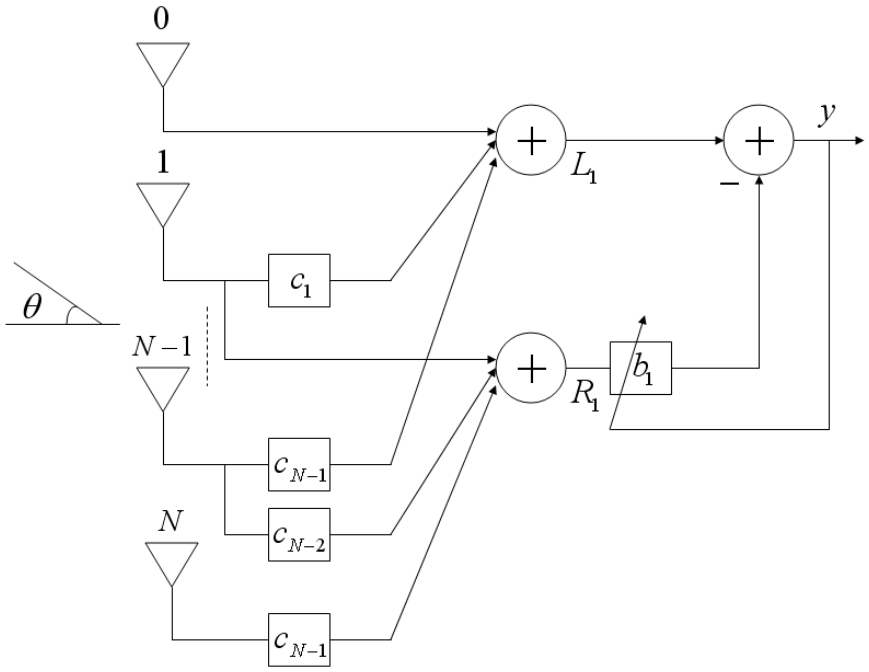

Figure 3.3: Array structure for updating b_1

where

$$\hat{\hat{D}}(z) = z^{-1} + c_1 z^{-2} + \ldots + c_{N-1} z^{-N} \tag{3.13}$$

Therefore, the processing of (3.12) can be implemented by using the structure in Fig. 3.3.

The output of the array is given by

$$y = L_1 - b_1 R_1 \tag{3.14}$$

Using the theory of power inversion array, the zero b_1 can be tracked by minimizing the array output power.

From (3.14), the output power is given by

$$E[|y|^2] = E[|L_1|^2] - E[L_1 R_1^*] b_1^* - E[L_1^* R_1] b_1 + E[|R_1|^2] b_1 b_1^* \tag{3.15}$$

By carrying out differentiation with respect to b_1^*

$$\frac{\partial E[|y|^2]}{\partial b_1^*} = E[|R_1|^2]b_1 - E[L_1 R_1^*] \tag{3.16}$$

From (3.16), the average output power will be minimized if b_1 is given by its optimal value

$$b_{1opt} = \frac{E[L_1 R_1^*]}{E[|R_1|^2]} \tag{3.17}$$

Thus, the zero b_1 is eventually updated and a null is placed in the direction of the strongest interference signal. Now suppose zero b_2 is to be updated in the next cycle to track the second strongest interference signal. The same updating procedure described above for b_1 can be applied to the adjustment of b_2, except that the coefficients in Fig. 3.3 need to be changed accordingly. The update of the second zero will not affect other null positions, which is the key feature of Davies algorithm. The zeros can also be iteratively updated using LMS algorithm with the arrival of each new data sample.

$$b_1 \rightarrow b_1 + \mu_1 y R_1^* \tag{3.18}$$

Note here that the update in (3.18) is run for sufficient number of iteration for b_1 to be converged before attending to b_2. μ_1 is the feedback factor and its significance will be discussed later.

The fast null steering algorithm can therefore be summarized by the flow chart in Fig. 3.4. As can be seen, the complex zeros of the array system are adjusted individually in a cyclic manner to suppress the interferences. One simple stopping criterion for the zero tracking process can be the array output power,

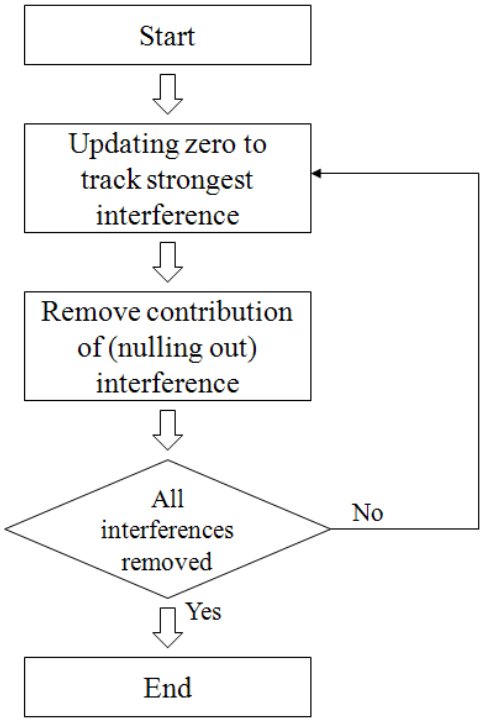

Figure 3.4: Flow chart of fast null steering algorithm

since the information on whether untracked signals exist in the environment can be obtained by measuring the array output power as each zero is being updated.

3.4 Proposed Null Steering Algorithm With Single Constraint

The look direction constraint is not used in the algorithm above. Therefore, this algorithm is of great advantage in communication scenario where a radio wants to receive signals from any directions without knowing where they are coming from and in the presence of interferences. In this scenario, the direction of interest is not known and it is better not to have a particular beam pointing to a specific direction but to have equal gain in all directions except in direction of

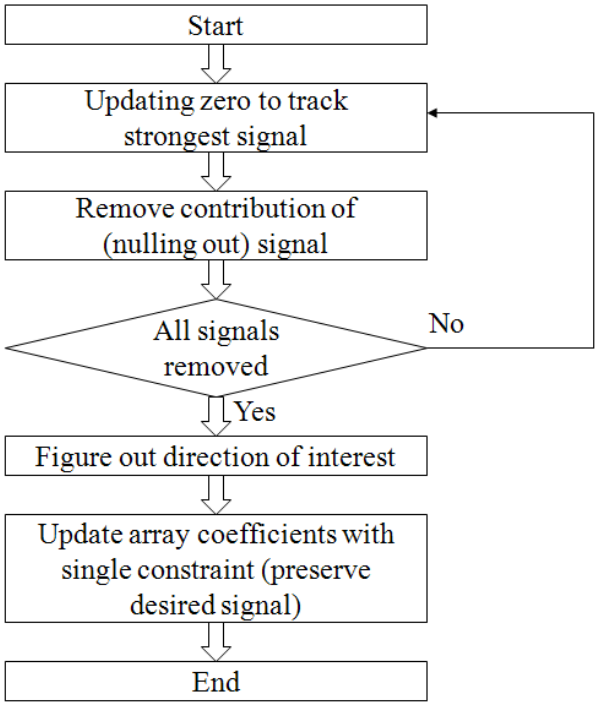

Figure 3.5: Flow chart of NSASC

interferences. The null steering algorithm is also suitable for the scenarios where the desired signal is weak compared with the interference signals. However, in the environment where the desired signal is stronger or not significantly weaker than the interference sources, one zero corresponding to the desired signal will be updated. A null will, therefore, be placed in the direction of interest by the array.

The null steering algorithm with a single constraint (NSASC) is proposed in this section. With NSASC, the desired signal will preserve while the nulls in the direction of interference signals will remain. The main advantage of this algorithm is its simplicity.

The NSASC is described by the flow chart in Fig. 3.5.

Fig. 3.6 shows the block diagram of NSASC. The array structure in Block

I is same as that presented in last section. The purpose of Block I is to track the desired signal as well as the interference sources in the environment after collecting enough number of data samples. The number of training samples is chosen such that the zero being updated will close to its optimal value as discussed in [12]. Since it is assumed that the direction of desired signal is roughly known, we can easily figure out the zero closest to direction which corresponds to the signal of interest. The accuracy of the assumed known DOA of the desired signal will depend on how well NSASC can handle nearby interference. Consider the scenario where the desired signal is impinging on the array from the DOA centered at θ_s and the DOA of the nearest interference that NSASC can handle is $\theta_i = \theta_s \pm \Delta\theta$, then the assumed DOA θ of the desired signal will be in the range of $\theta \in [\theta_s - \Delta\theta, \theta_s + \Delta\theta]$.

With the information of zeros obtained from Block I, the array coefficients in Block II can be adjusted to suppress the interference signals while maintain a fixed gain in the look direction.

To illustrate how the coefficients in Block II can be easily adjusted and without any loss of generality, assume that there exist one desired signal and two interferences in the environment, and a 4-element array is used.

From (3.3), the directional pattern of the system in Block I is

$$D_I(z) = (1 - b_s z^{-1})(1 - b_1 z^{-1})(1 - b_2 z^{-1}) \tag{3.19}$$

where b_s, b_1, b_2 correspond to the zeros for the desired signal, interference 1 and interference 2, respectively.

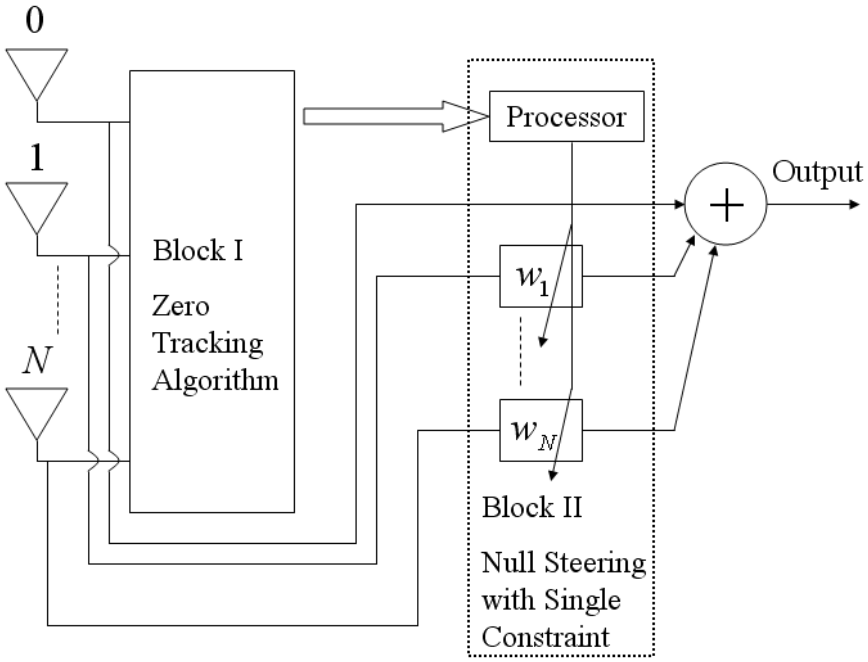

Figure 3.6: Block diagram of null steering algorithm with single constraint

Let the directional pattern of Block II be

$$\begin{aligned} D_{II}(z) &= (1-\gamma z^{-1})(1-b_1 z^{-1})(1-b_2 z^{-1}) \\ &= \mathbf{w}^T \mathbf{z} \end{aligned} \tag{3.20}$$

where

$$\mathbf{w} = \begin{bmatrix} 1 \\ w_1 \\ w_2 \\ w_3 \end{bmatrix} = \begin{bmatrix} 1 \\ -(\gamma + b_1 + b_2) \\ \gamma b_1 + \gamma b_2 + b_1 b_2 \\ -\gamma b_1 b_2 \end{bmatrix} \tag{3.21}$$

is the array coefficients to be adjusted and

$$\mathbf{z} = [1 \quad z^{-1} \quad z^{-2} \quad z^{-3}]^T. \tag{3.22}$$

Note that in (3.20), a new unknown parameter γ is introduced and to be

calculated based on the look direction constraint. The zeros b_1 and b_2 remain in the directional pattern so that the two interference signals can be suppressed.

In order to recover the desired signal with no amplitude and phase distortion, a unity gain in the look direction is defined, that is

$$\mathbf{w}^H \mathbf{v}(\theta_s) = 1 \tag{3.23}$$

where $\mathbf{v}(\theta_s)$ is the array steering vector (ASV) in the direction of desired signal. For uniform linear array (ULA), the ASV takes the form

$$\mathbf{v}(\theta_s) = [1 \quad exp(-j2\pi u_s) \quad exp(-j2\pi 2u_s) \quad exp(-j2\pi 3u_s)]^T \tag{3.24}$$

where

$$u_s = \frac{d \sin \theta_s}{\lambda} \tag{3.25}$$

From (3.21), (3.23) and (3.24), the value of parameter γ can be easily obtained, since γ is the only unknown. With γ and from (3.21), the array coefficients in Block II can be adjusted. Thus, we obtain the directional pattern with two nulls in the direction of interferences and a unity gain in the direction of interest.

The computational complexity in terms of multiplications is calculated and compared to the complexity of the LMS based LCMV method and adaptive QR-RLS method. Table 3.1 shows the comparison of computational complexity for different methods using N elements and K data samples.

It is evident that NSASC becomes convenient in terms of computational complexity with respect to the QR-RLS scheme. NSASC and LMS based LCMV

Table 3.1: Comparison of computational complexity for LCMV, QR-RLS and NSASC

Method	Number of real multiplications
LMS based LCMV	$2KN + 2K$
QR-RLS	$10KN + 30KN^2$ [41]
NSASC	$2KN + 3K + 6N - 8$

method have almost equal computational complexity.

3.5 Proposed Null Steering Algorithm With Multiple Constraints

The algorithm in the previous section is designed for use as a fast constrained null steering algorithm to preserve the desired signal. The null steering algorithm with multiple constraints (NSAMC) is proposed in this section. In this algorithm, by incorporating more constraints, the same basic structure can also function like a beamformer, where the output SINR of the mainbeam is enhanced with a decreased sidelobe level.

The flow chart of NSAMC is shown in Fig. 3.7. The idea of NSAMC is to relax the unity gain constraint in the look direction. Consider the 4-element array discussed above and the same directional pattern as in (3.20) is defined for the array in Block II. Now instead of single constraint in the look direction, we impose multiple constraints which consist of:

- A flexible gain α in the look direction, that is

$$\mathbf{w}^H \mathbf{v}(\theta_s) = \alpha \tag{3.26}$$

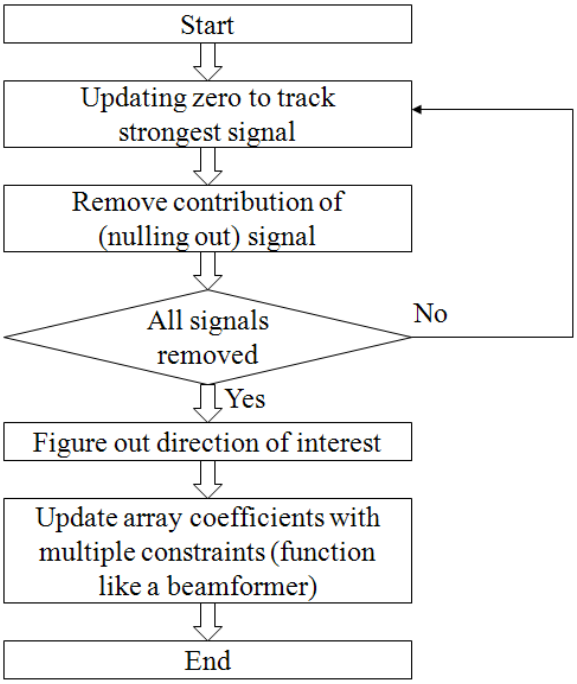

Figure 3.7: Flow chart of NSAMC

- A flexible gain β in a sidelobe direction θ_n, that is

$$\mathbf{w}^H \mathbf{v}(\theta_n) = \beta \tag{3.27}$$

- A predefined ratio between α and β,

$$\frac{\alpha}{\beta} = \kappa \tag{3.28}$$

The reason why we set the three constraints is to lower the sidelobe level and improve the mainlobe to sidelobe ratio. Note that in (3.28), κ is defined as the ratio between the look direction gain and a chosen sidelobe direction gain. The larger the ratio, the lower the array response in the chosen sidelobe direction, and greater noise suppression can be achieved in this direction θ_n.

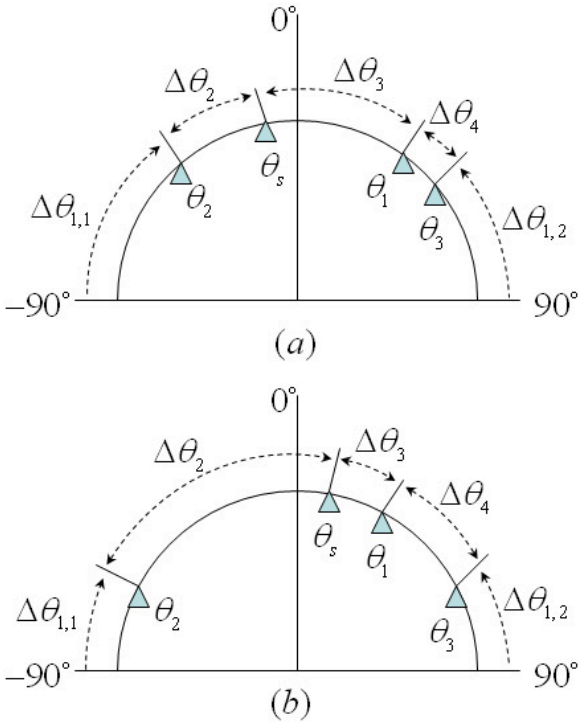

Figure 3.8: Rules for sidelobe direction selection

The rules to pick the sidelobe direction θ_n in (3.27) can be summarized as follows:

Step 1: For an environment where there exist one desired signal and M interference sources, $M+1$ spatial regions can be formed. As shown in Fig. 3.8(a) and (b), where one desired signal and three interferences are coming from the directions $\theta_s, \theta_1, \theta_2$ and θ_3, respectively, we can form four spatial regions $\Delta\theta_m,\ m = 1, \ldots, 4$. Note here that the spatial region $\Delta\theta_1$ consists of two sub-spatial regions $\Delta\theta_{1.1}$ and $\Delta\theta_{1.2}$.

Step 2: The spatial regions are prioritized by the descending order of absolute value of angle difference. In Fig. 3.8(a), we have $|\Delta\theta_1| = (|\Delta\theta_{1.1}| + |\Delta\theta_{1.2}|) > |\Delta\theta_3| > |\Delta\theta_2| > |\Delta\theta_4|$. Therefore, the spatial region $\Delta\theta_1$ has the highest priority and $\Delta\theta_4$ has the lowest priority.

Step 3: The middle point of sidelobe directions in the spatial region with highest priority is selected as θ_n in (3.27). This is due to the fact that the array response over this range of directions before constraints are imposed is usually higher, and therefore the overall sidelobe level can be reduced as much as possible after applying NSAMC. For Fig. 3.8(a), we have

$$\theta_n = \theta_3 + \frac{|\Delta\theta_1|}{2} \tag{3.29}$$

Similarly for Fig. 3.8(b), where spatial region $\Delta\theta_2$ has the highest priority, we have

$$\theta_n = \theta_2 + \frac{|\Delta\theta_2|}{2} \tag{3.30}$$

To illustrate how NSAMC works, we continue the assumption made in last section that there exist one desired signal and two interferences in the environment.

From (3.21), (3.24), (3.26), (3.27) and (3.28), we have the following equation

$$\begin{bmatrix} 1 & w_1 & w_2 & w_3 \end{bmatrix} \begin{bmatrix} 1 & 1 \\ exp(-j2\pi u_s) & exp(-j2\pi u_n) \\ exp(-j2\pi 2u_s) & exp(-j2\pi 2u_n) \\ exp(-j2\pi 3u_s) & exp(-j2\pi 3u_n) \end{bmatrix} = \alpha \begin{bmatrix} 1 \\ \\ \frac{1}{\kappa} \end{bmatrix}^T \tag{3.31}$$

Since the array coefficients w_N is a function of unknown parameter γ, equation (3.31) can be easily solved for the values of γ and α.

Note that in this case, the gain α obtained in the look direction may be a complex number, resulting in amplitude and phase distortion of the desired signal. Thus, the structure for NSAMC is shown in Fig. 3.9, where Block III is

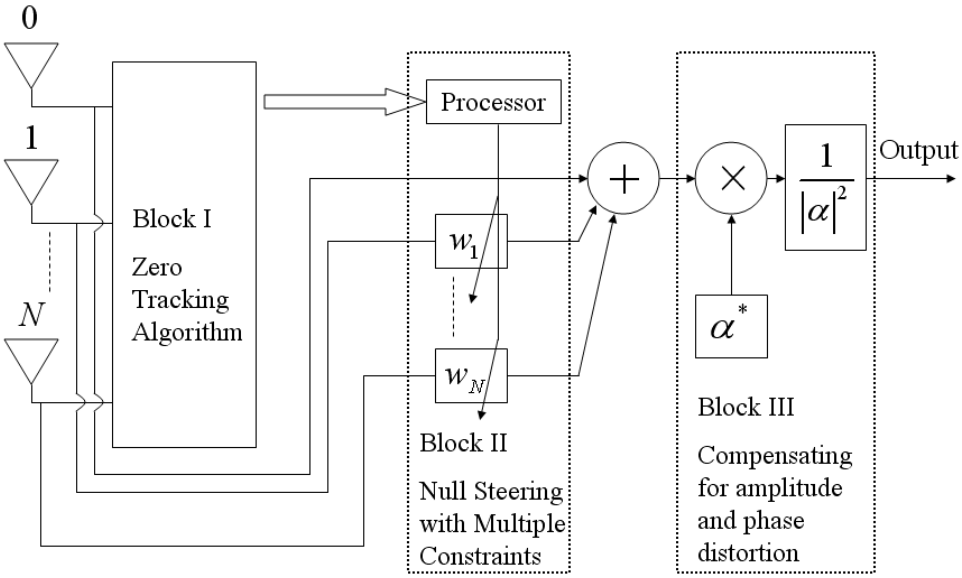

Figure 3.9: Block diagram of null steering algorithm with multiple constraints

to compensate for the desired signal distortion.

For the algorithm here using N elements and K data samples, we have the following:

- Number of real multiplications:$2KN + 3K + 10N - 12$

Although adding more constraints, the complexity only increases by a small amount compared with NSASC and is still lower than that of QR-RLS based method.

A summary of the algorithms in Sections 3.4 & 3.5 is given in Table 3.2.

3.6 Average Convergence Behaviour

The convergence behaviour of NSASC and NSAMC in the two sections above are totally controlled by Block I, since the processings in other blocks are not

Table 3.2: Summary of the algorithms

NSASC in section 3.4	NSAMC in section 3.5
Track desired signal and interferences using method in [12] to get corresponding zeros in (3.19)	
• Calculate parameter γ using equations (3.21) (3.23) and (3.24)	• Choose sidelobe direction in (3.27)
• Adjust array coefficients using equation (3.21)	• Define ratio in (3.28)
	• Calculate parameters γ, α and β using equations (3.28) and (3.31)
	• Adjust array coefficients using equation (3.21)
	• Form Block III in Fig. 3.9 for compensation of signal distortion

involved in the update process. The average convergence behaviour of the zero being updated in the current adjustment cycle can be obtained by taking ensemble average of (3.18), giving

$$E[b_1] \rightarrow E[b_1] + \mu_1 E[yR_1^*]. \tag{3.32}$$

Using (3.14) and (3.17) then yields

$$E[\Delta b_1] \rightarrow \{1 - \mu_1 E[|R_1|^2]\} E[\Delta b_1] \tag{3.33}$$

where

$$\Delta b_1 = b_1 - b_{1opt} \tag{3.34}$$

is the difference between b_1 and its optimal value.

From (3.33), after K iterations, the value of $E[\Delta b_1]$ at the end of the current adjustment cycle $E[\Delta b_{1end}]$ is related to that at the beginning of the cycle $E[\Delta b_{1int}]$ by

$$E[\Delta b_{1end}] = \{1 - \mu_1 E[|R_1|^2]\}^K E[\Delta b_{1int}]. \tag{3.35}$$

Clearly, if the feedback factor μ_1 is such that

$$|1 - \mu_1 E[|R_1|^2]| < 1, \tag{3.36}$$

$E[b_1]$ will converge towards its optimal value. The magnitude of $1 - \mu_1 E[|R_1|^2]$ is dependent on the value of μ_1, which is, in turn, constrained by the tolerable amount of additional output noise generated by the jittering of b_1. The additional output noise resulting from this phenomenon is often measured in terms of the misadjustment of the algorithm. For the LMS algorithm (3.18), the misadjustment can be shown to be given roughly by [29]

$$\rho_1 = \frac{1}{2}\mu_1 E[|R_1|^2] \tag{3.37}$$

Using (3.37), (3.35) becomes

$$E[\Delta b_{1end}] = \{1 - 2\rho_1\}^K E[\Delta b_{1int}] \tag{3.38}$$

Therefore, given the desired misadjustment ρ_1 for b_1, $E[b_1]$ will converge towards its optimal value with a time constant of

$$\tau_1 \approx \frac{1}{2\rho_1} \tag{3.39}$$

From (3.39), the time constant for the convergence of $E[b_1]$ depends only on the ρ_1, the misadjustment desired. Clearly, for all the complex zeros to have the same convergence time constant, the misadjustments contributed by them must also be roughly equal. Thus, given the total misadjustment tolerable ρ_T, the misadjustment due to the adjustment of each complex zero is

$$\rho_1 = \frac{\rho_T}{N} \tag{3.40}$$

so that (3.39) becomes

$$\tau_1 \approx \frac{N}{2\rho_T} \tag{3.41}$$

From (3.37), the feedback factor μ_1 is related to $E[|R_1|^2]$, where the array has no prior knowledge and therefore has to be estimated and updated continuously. For this purpose, the recursive equation

$$\frac{1}{\mu_1} \rightarrow \left(1 - \frac{2\rho_T}{N}\right)\frac{1}{\mu_1} + |R_1|^2 \tag{3.42}$$

can be used to update μ_1 every data sample so that the convergence time constant for $1/\mu_1$ is also roughly the same as that for $E[b_1]$.

Therefore, the convergence behaviour of NSASC and NSAMC depends only on the misadjustment and is significantly faster. For the LMS based LCMV beamforming technique, the time constant associated with the mth interference source is given by [31]

$$\tau_m \approx \frac{1}{4\mu\sigma_m}; \quad m = 0, 1, \ldots, M-1 \tag{3.43}$$

where σ_m is the eigenvalue of array input covariance matrix $\mathbf{R}$ corresponding to the mth interference source. From (3.43), we can see that the convergence behavior of LMS based LCMV beamformer is dependent on the external noise environment. The output power due to each individual interference converges with different time constants, and it is the large differences in convergence time constants that leads to the slow overall convergence behaviour in the situation where strong interferences exist. It has also been shown in [3] that the convergence rate of LMS based LCMV beamformer is governed by the eigenvalue spread of covariance matrix $\mathbf{R}$. For large eigenvalue spread, convergence can be very slow.

3.7 Simulation Results

Some simulation results will now be presented to verify the above theoretical results. The simulated array is assumed to be a 4-element linear array with interelement spacing of $\lambda/2$.

The simulated environment consists of a desired signal of power 20 dB arriving from $-30°$, and two independent interference signals of power 40 dB and 40 dB, assumed to be located at 24° and 27° to the array normal. Finally, independent white Gaussian noise of power 0 dB is added to each sensor element to account for the presence of ambient isotropic noise and other broadband sources of noise. Note here that the same simulation parameters as that in reference [12] are used here. For some communication scenarios, e.g. Wi-Fi communication,

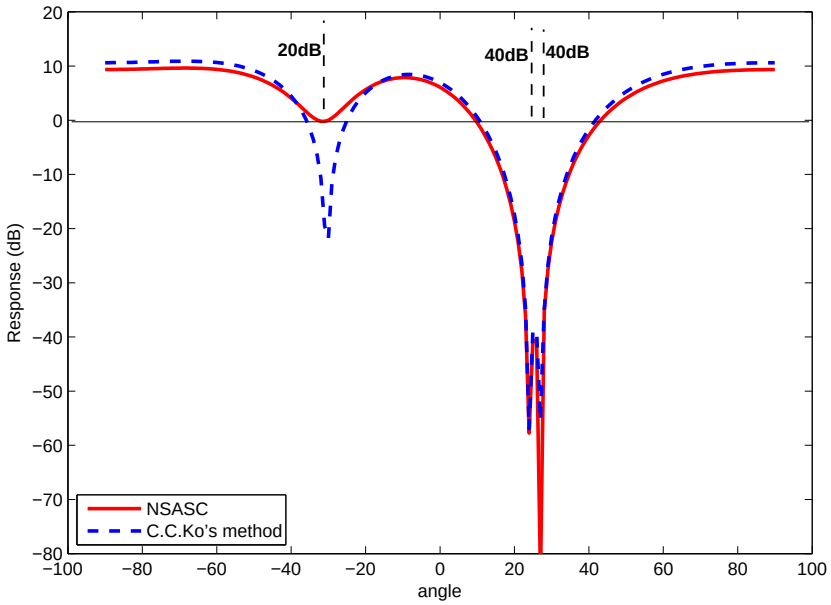

Figure 3.10: Directional patterns for C.C.Ko's method [12] and NSASC

20 dB SNR is considered to be low signal (i.e. large noise).

Fig. 3.10 shows the directional patterns for C.C. Ko's method [12] and NSASC. As seen in the figure, by using C.C. Ko's method, a deep null is placed at $-30°$, i.e. in the direction of desired signal, and two deep nulls are placed in the directions of interference signals. Thus, this array system will reject all data signals, including the desired signal and the interferences. Our objective is to get rid of the null in the direction of interest and impose a unity gain to it.

By using NSASC, the two deep nulls steered in the directions of interference signals remain unchanged. A unity gain in the look direction is achieved so that the desired signal will preserve.

Note that with the three zeros obtained in Block I and using NSASC, the parameter γ in (3.20) can be easily calculated. This γ does not relate to the zeros of the directional pattern of the array in Block II, since we use the degree

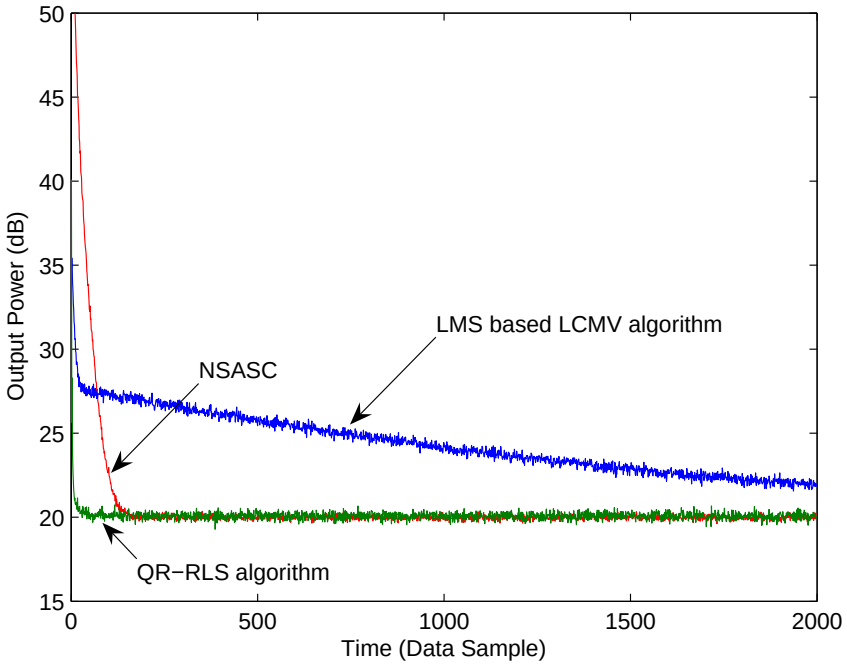

Figure 3.11: Stochastic output power convergence behaviors of LCMV, QR-RLS and NSASC

of freedom (DOF) to impose a gain in the look direction.

Fig. 3.11 compares the average output power convergence curves of using LCMV, QR-RLS and NSASC, averaged over 500 runs. The desired misadjustment for all algorithms is 5%. Since the processing in Block II in NSASC does not need to be involved in the update process, the convergence behavior of the whole system will be totally controlled by Block I. As can be seen, NSASC converges in a faster manner compared with LMS based LCMV beamformer. The QR-RLS algorithm [10] and NSASC have similar convergence behavior. The square root of the normalized mean-square error (NMSE) as a function of the number of data samples is plotted in Fig. 3.12. One can also observe from the figure that NSASC has better convergence behaviour compared with LMS based LCMV method.

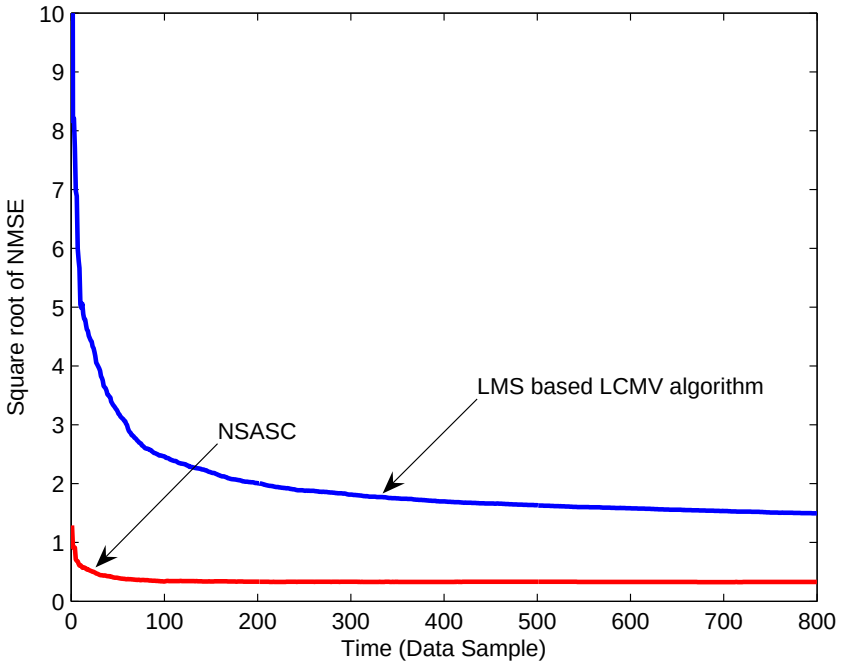

Figure 3.12: Square root of the NMSE as a function of length of data samples using LCMV and NSASC

Now some simulation results for the NSAMC will be presented. Consider the same simulated array and environment discussed above, by applying the rules in Section 5, the gain β in (3.27) can be imposed to the sidelobe direction of $-88.5°$. The ratio in (3.28) is set to be 20. Fig. 3.13 shows the directional patterns for LMS based LCMV beamformer [31], QR-RLS MVDR beamformer [10] and NSAMC. One observes from the figure that the peak sidelobe level (PSL) obtained by using LCMV and QR-RLS MVDR method is -10 dB. While NSAMC allows the achievement of a lower PSL which is around -18 dB. We also note that the null depths for NSAMC reach deeper levels, resulting in better performance in terms of interferences rejection capabilities.

Now we look at another environment where two interferences of power 70 dB and 55 dB are located at $40°$ and $-30°$ to the array normal and the desired

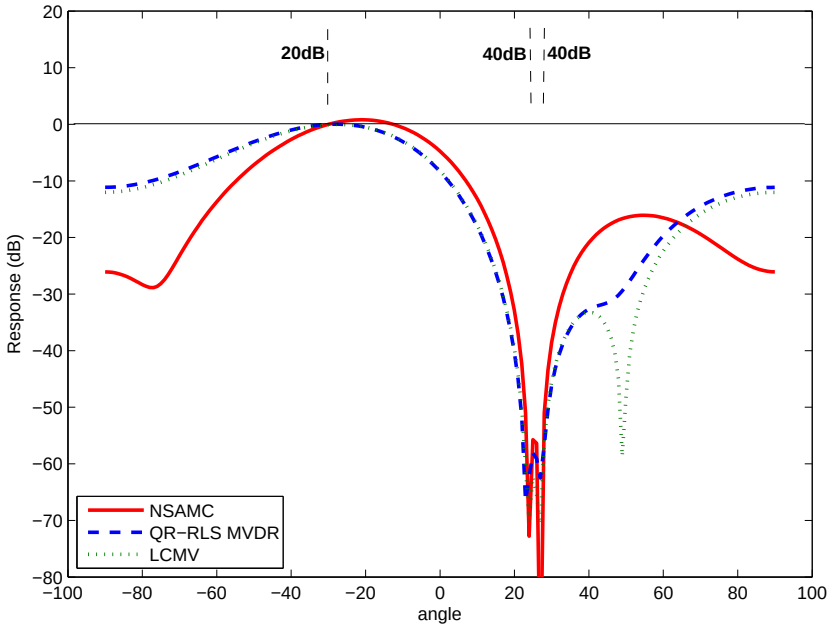

Figure 3.13: Directional patterns for LCMV, QR-RLS MVDR and NSAMC, θ_n chosen to be $-88.5°$

signal of power 40 dB arrives from the broadside direction. By applying the rules in section 4.4, the gain β in (3.27) can be imposed to the sidelobe direction of $-85°$. The gain ratio in (3.28) is 20. Fig. 3.14 shows the directional patterns for LCMV, QR-RLS MVDR and NSAMC. As shown in the figure, overall lower sidelobe level can be achieved by using NSAMC.

As another example, the simulated array is assumed to be a 5-element linear array. Three 40 dB interferences are located at $-80°$, $60°$ and $70°$, respectively, and the desired signal of power 20 dB is coming from $5°$. By applying the rules for sidelobe direction selection stated in section 4.4, four spatial regions can be formed and the gain β in (3.27) is imposed to $-37.5°$. The gain ratio in (3.28) is set to be 60. The directional patterns for LCMV, QR-RLS MVDR and NSAMC are shown in Fig. 3.15. For this simulated example, the spatial region between

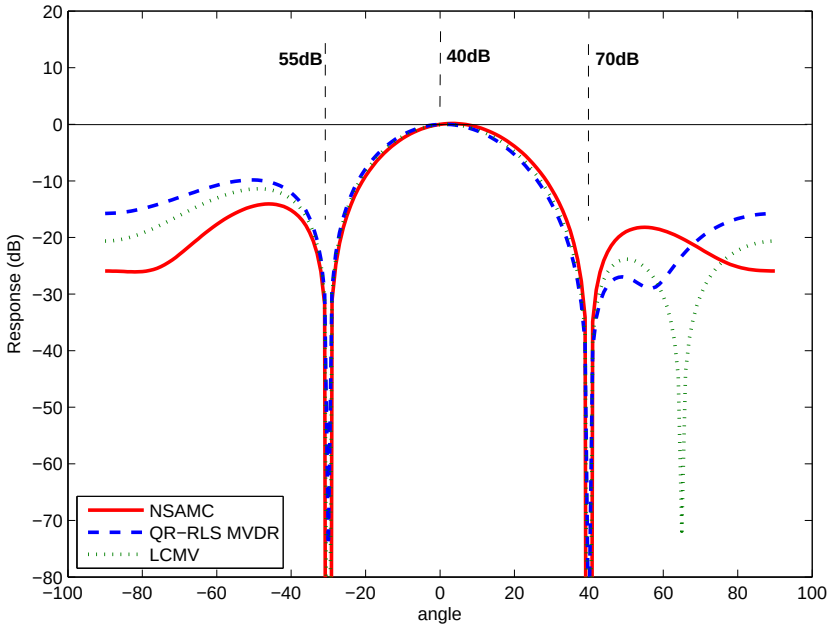

Figure 3.14: Directional patterns for LCMV, QR-RLS MVDR and NSAMC in another scenario, θ_n chosen to be $-85°$

60° and 70° has the lowest priority. The dash line in Fig. 3.16 shows the array response when θ_n in (3.27) is chosen to be 65°. One can observe that, in this case, the overall sidelobe level cannot be reduced. This is due to the fact that the array response over the spatial region between 60° and 70° is low before imposing constraints, as shown by the dot line in Fig. 3.16. Therefore, we are unable to lower the overall sidelobe level while applying NSAMC if θ_n is chosen from the range of directions in this spatial region with lowest priority.

Now the significance of the choice of ratio in (3.28) will be shown here by simulation. This predefined ratio between the look direction gain and a chosen sidelobe direction gain also affects the array output SNR. For the same environment of Fig. 3.14, the directional patterns for NSAMC with gain ratios 20, 200 and 10000 are shown in Fig. 3.17. As can be seen, the array response in the

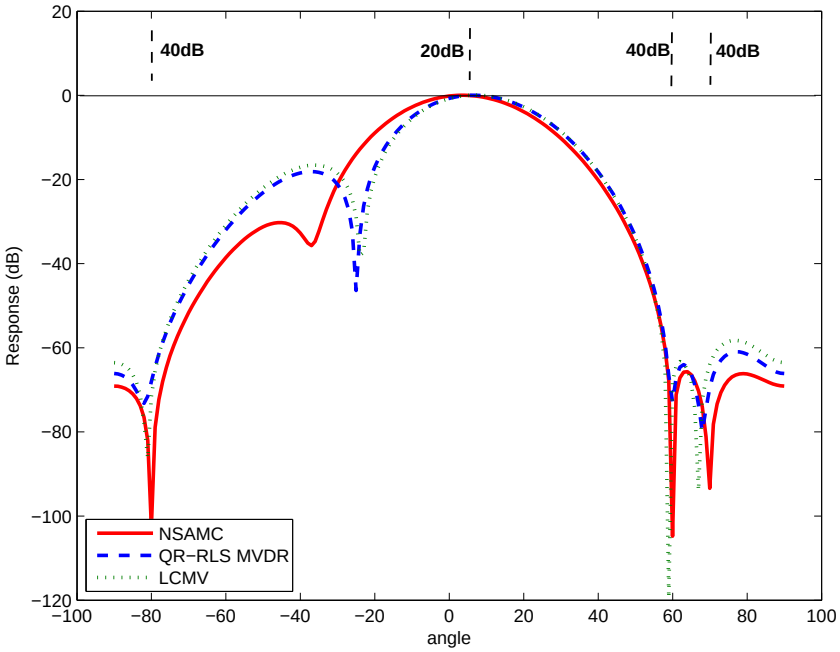

Figure 3.15: Directional patterns for LCMV, QR-RLS MVDR and NSAMC in another scenario, θ_n chosen to be $-37.5°$

direction of $-85°$ becomes lower with increasing gain ratio. Therefore, the noise level at the array output can be reduced when bigger gain ratio is employed. It can also be seen from the figure that we obtain a deep null in the direction of $-85°$ by using a very big gain ratio and therefore significant noise reduction can be achieved around the chosen sidelobe direction of $-85°$.

Fig. 3.18 shows the directional patterns for a 4, 5, and 6-element array when NSAMC is employed in the environment of Fig. 3.14. Note that as the number of elements increases and the array has more unused DOFs, additional nulls start to be formed in the sidelobes as a result of reducing the amount of receiver noise at the array output. These nulls are not directed at any physical interferences. With the misadjustment due to each zero being the same, these noninterference nulls will have a higher jitter when compared with those track-

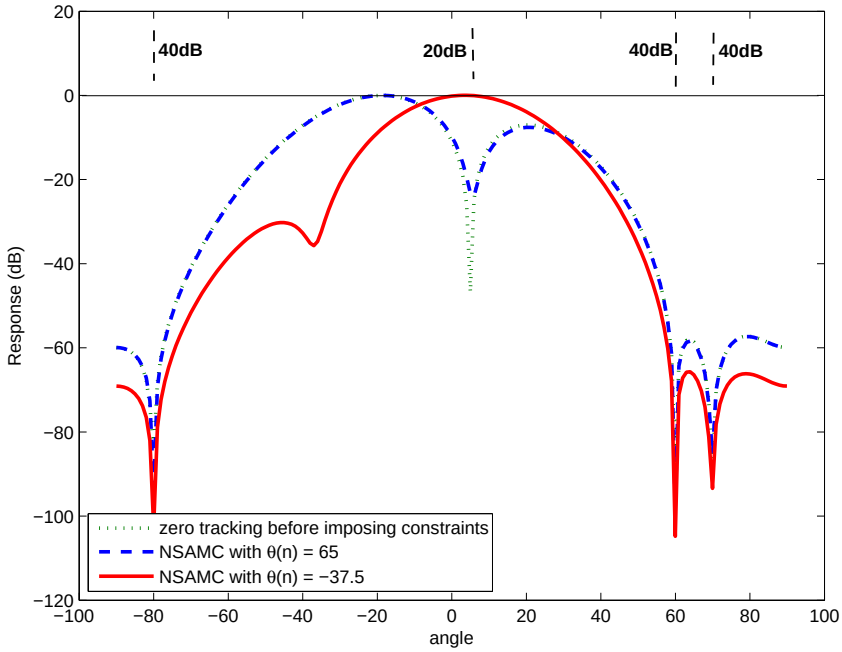

Figure 3.16: Directional patterns for NSAMC with different θ_n

ing actual interferences. However, in the array of interest where the principal objective is to receive a look direction signal while minimizing interferences from other directions, the possibly large variations of the noninterference nulls in the sidelobes are not really a matter of concern, particularly as the array response in the look direction is being constrained to be unity. Nevertheless, apart from reducing the overall misadjustment level, one approach to decrease the jittering of noninterference nulls and perhaps also increase the speed of the algorithm is to identify the zeros which are not tracking physical interferences by measuring the array output power as each zero is being updated. Those zeros deemed to be not tracking physical interferences can then be adjusted based on the other interference tracking zeros or, alternatively, not updated at all.

We look at the case when a 5-element linear array is employed in Fig. 3.18.

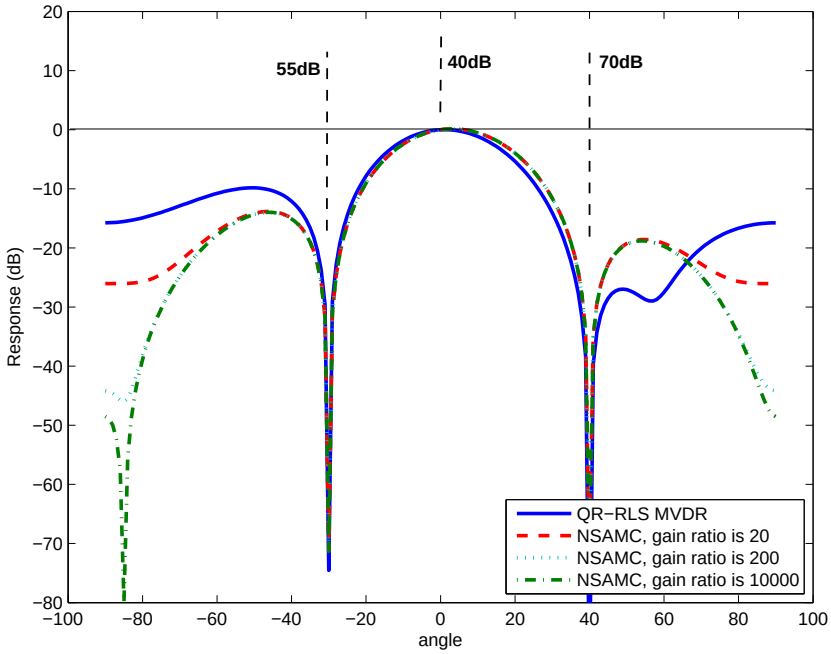

Figure 3.17: Directional pattern for NSAMC with different gain ratios

The initial nulls of the array are chosen so that the first and last elements have unity equivalent weights and all the other elements have zero equivalent weights [12]. Table 3.3 summarizes the null steering status at each stage. Note here that the updated null directions have been rounded to integers. The array has 4 DOFs in its pattern and places maximum of 4 perfect nulls in certain directions. The first zero being updated will converge towards its optimal value at the end of the first adjustment cycle and a null is placed in the direction of strongest interference signal. The output power after first null steering is 75 dB, which can be an indication that some other signals exist in the environment. Therefore, we continue updating the next zero and the null directions after second null steering are also shown in Table 3.3. As can be seen, a null towards the second strongest interference signal is formed. We now proceed to the next update cycle since the output power after second null steering is still high. The

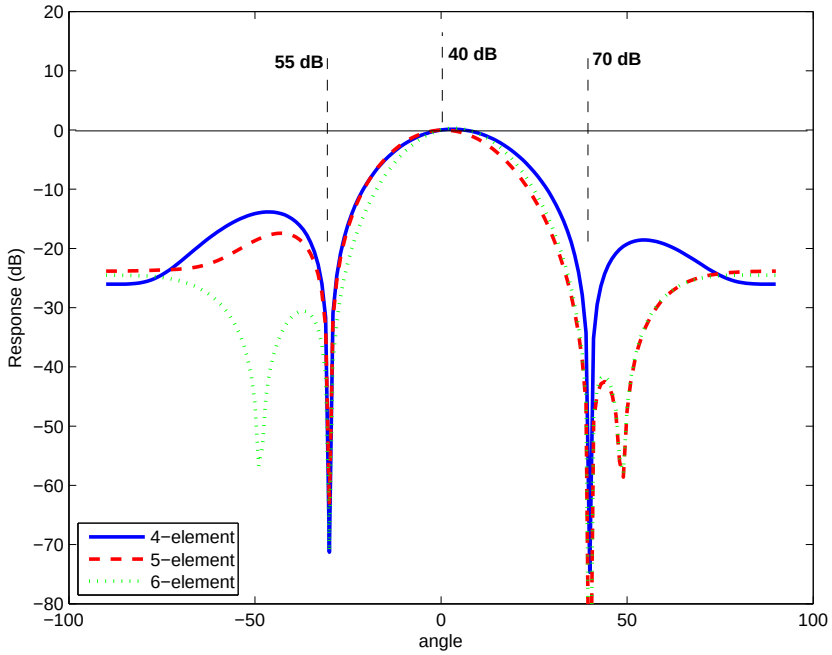

Figure 3.18: Directional patterns for a 4-, 5-, and 6-element array using NSAMC in the environment of Fig. 3.14

update process will end after the third null steering since the output power now is very low. Therefore, we have updated three nulls out of the four to track the signals existing in the environment. The zero corresponding to the null direction of 49° does not need to be updated.

Now consider the same scenario as Fig. 3.14 with steering vector assumed to be located at 0°. The desired signal is coming from 1°, hence resulting in a steering vector error problem. Fig. 3.19 shows the directional patterns for LCMV beamformer and NSAMC under this steering vector error scenario. Since the LCMV beamformer tries to minimize the total output power while maintain a fixed gain in the look direction, it will produce a null in the actual desired signal direction. This phenomenon is often referred to as signal self-nulling. For NSAMC, the desired signal direction will be first obtained in Block I. Therefore,

Table 3.3: Summary of the null steering status

Actual desired signal and interference directions (degree)	0 40 -30
Power of desired signal and interferences (dB)	40 70 55
Initial null directions	-49 -14 14 49
Null directions after first null steering	-49 -14 40 49
Output power after first null steering	75
Null directions after second null steering	-30 -14 40 49
Output power after second null steering	35
Null directions after third null steering	-30 0 40 49
Output power after third null steering	-5

the system can still steer to the actual data signal direction.

3.8 Summary

The null steering algorithms with single and multiple constraints (NSASC, NSAMC) were proposed. Using the new method, the null steering structure can function like a beamformer. When compared with conventional LMS based LCMV beamforming algorithm, NSASC and NSAMC converge in a faster manner; and compared with QR-RLS based MVDR beamformer, NSASC and NSAMC have lower complexity. Furthermore, due to their cascade configurations, signal self-nulling problem for conventional beamformer can be resolved.

The proposed algorithm works well in the environment where stationary

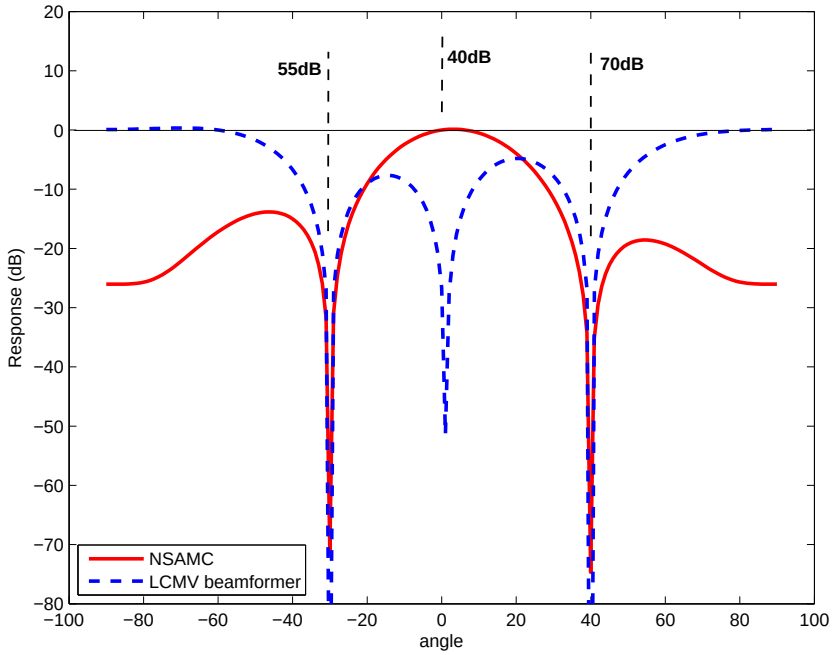

Figure 3.19: Directional patterns for LCMV and NSAMC under steering vector error scenario

interference sources exist. It enhances the output SINR by placing sharp nulls in the direction of interferences. The algorithms can be further developed for another scenario when interferences are moving. The research work on how broader null can be generated using the same structure will discussed in the next chapter.

The basic null steering structure assumes an all-zero model and it will be useful to investigate the design and performance if it is extended to take the form of a pole-zero model. That will be discussed in Chapter 5.

In addition, the same null steering structure can also be used to estimate the DOA and it will be discussed in Chapter 6.

Chapter 4

Adaptive Null Steering Beamformer Implementation For Flexible Broad Null Control

4.1 Introduction

As discussed in Chapter 2, the beamforming systems have found applications in radar, sonar and communication systems for minimizing degradation in signal-to-noise ratio (SNR) performance owing to unwanted interference. It is achieved by means of arranging for a null in the antenna's pattern response to coincide with the direction of interference and at the same time forming a beam toward the desired signal.

In recent years, there has been a considerable interest in obtaining broad null sectors in linear array. The need for a broad null often arises when the direction of arrival (DOA) of the unwanted interference may vary slightly with time or

the actual angle may dithering, and where a comparatively sharp null would require continuous steering for obtaining a reasonable value for the signal-to-interference ratio (SIR).

Recently, several authors exploited the idea of artificial broadening of the beampattern nulls in unknown interfering directions. One common approach is the covariance matrix taper (CMT) based minimum variance distortionless response (MVDR) beamformer [15, 16, 17, 18]. It is a filterbank method that the optimum weights are chosen to minimize the output power of moving interference signals and, at the same time, to maintain a distortionless response toward the desired signal. This effectively places deep broad nulls canceling interference from sources in directions other than the one of interest. The implementation of CMT based MVDR beamformer suffers from being computationally cumbersome, especially for large arrays. This is due to the requirement to evaluate a vector-matrix product containing the inverse of large dimensional data covariance matrix. Numerous adaptive algorithms can be used to solve CMT based MVDR beamforming problem. Some of the more widely used methods are sample matrix inversion (SMI) [42], least mean square (LMS) [31], normalized LMS (NLMS) and QR-recursive least square (QR-RLS) [10]. However, the major disadvantage of LMS and NLMS is that their convergence behavior is dependent on the external noise environment and can be very slow in severe jamming situation. The drawback of SMI and QR-RLS is their high computational cost.

Quite a few papers have proposed to synthesize the antenna array pattern with prescribed broad nulls by minimizing the mean-square error (MSE) between the desired and the generated beam patterns [20, 21, 22]. Sidelobe constraints in the interference direction are added to the least-squares criterion in

order to form a broad null. Main difficulties in implementing the constrained optimization algorithm include: 1) The explicit function of the desired pattern is hard to obtain; 2) the integration of the squared-error function may not be easy to calculate; 3) the computation load increases as a matrix inversion with large size is required.

In Chapter 3, we presented the null steering algorithm with multiple constraints for beamforming application. The proposed algorithm works well in the environment where stationary interfering sources exist. It enhances the output signal-to-interference plus noise ratio (SINR) by placing sharp nulls in the direction of interferences and forming a beam in the direction of interest. In this chapter, the algorithm will be further developed for the scenario when interferences are moving.

Our contribution in this chapter is twofold. (i) The LMS and QR-RLS implementations of CMT based MVDR beamformer are developed. The potential drawbacks of the implementations are discussed. (ii) An implementation of adaptive null steering beamformer for flexible broad null control is presented. Using the proposed design, the series of null steering beamformers are first implemented by decomposing the original array into several subarrays. A spatial finite impulse response (FIR) filter is used in the design to suppress any moving interference. Since an all-zero model is assumed and the concept of subarrays is used, the new method is of great advantage for sensor array in which the number of array elements is very large compared with the number of interferences the array is designed to suppress. The new beamformer is useful and effective in environments where both stationary and moving interference signals exist, since it can steer both sharp and controlled broad nulls in the appropriate di-

rections. When compared with LMS CMT based broad null synthesis method, the proposed beamformer has a faster convergence rate; and compared with the QR-RLS CMT based broad null synthesis method, the proposed method has a lower complexity.

The remainder of this chapter is organized as follows. The next section introduces the array signal model used in this chapter. Section 4.3 briefly summarizes the CMT based robust beamformer. The LMS and QR-RLS implementations of CMT beamformer are also developed. The proposed beamformer implementation for flexible broad null control is presented in Section 4.4. The simulation results are given in Section 4.5. Finally, Section 4.6 gives the summary.

4.2 Array Signal Model

The array signal model used in this chapter is introduced here. Consider an array composed of $N+1$ equispaced omni-directional sensors, and assume one desired signal $s(t)$, M interference signals $i_m(t), m \in [0, M-1]$ impinge on the array with DOAs θ_s and θ_m, respectively. Therefore, the signals received by the array can be expressed as

$$\mathbf{x}(t) = \mathbf{v}(\theta_s)s(t) + \sum_{m=0}^{M-1} \mathbf{v}(\theta_m)i_m(t) + \mathbf{n}(t) \tag{4.1}$$

where $\mathbf{x}(t)$ is the $(N+1) \times 1$ vector

$$\mathbf{x}(t) = [x_0(t), x_2(t), \ldots, x_N(t)]^T \tag{4.2}$$

and $\mathbf{n}(t)$ is the white noise vector at each array element with a zero mean and variance σ^2. $\mathbf{v}(\theta_s)$ and $\mathbf{v}(\theta_m)$ are the array steering vectors (ASVs) of $s(t)$ and $i_m(t)$, respectively. T represents transpose.

As defined in (2.16), the covariance matrix $\mathbf{R}$ of array signal $\mathbf{x}(t)$ is given by

$$\mathbf{R} = E[\mathbf{x}(t)\mathbf{x}^H(t)] \tag{4.3}$$

where $E\{\cdot\}$ and H denote expectation and Hermitian transpose, respectively.

4.3 Covariance Matrix Taper Based Robust Beamformer

The conventional linearly constrained minimum variance (LCMV) beamformer is briefly discussed in Section 2.5. With narrowband interferers, LCMV beamformer produces sharp nulls in the spatial pattern of the array. The CMT based MVDR beamformer [15, 16] can be used to counter the effects of interferer motion by placing broad nulls in the direction of interferences.

The CMT based MVDR beamformer is realized by the following modification of the original covariance matrix in (4.3):

$$\mathbf{R}_{CMT} = \mathbf{R} \circ \mathbf{T}_{CMT} \tag{4.4}$$

where $\circ$ represents Haddamard (Schur) product. The taper $\mathbf{T}_{CMT}$ is, in general,

a real-valued positive definite matrix whose mnth element is given by

$$[\mathbf{T}_{CMT}]_{mn} = \frac{\sin((m-n)\Delta)}{(m-n)\Delta} \triangleq \text{sinc}((m-n)\Delta/\pi) \tag{4.5}$$

where $\Delta > 0$ represents the broad null width, and $\text{sinc}(x) \triangleq \sin(\pi x)/(\pi x)$. In [15], Δ was interpreted as the normalized angular extent over which a continuum of uncorrelated equal strength narrowband interferers is assumed to be present. In [16], Δ was interpreted as the amount of normalized frequency bandwidth occupied by a single interferer.

Formally, the CMT based MVDR beamformer is attempting to solve the following constrained optimization

$$\begin{cases} \min\limits_{\hat{\mathbf{w}}_{CMT}} & \hat{\mathbf{w}}_{CMT}^H \mathbf{R}_{CMT} \hat{\mathbf{w}}_{CMT} \\ s.t. & \mathbf{v}^H(\theta_s)\hat{\mathbf{w}}_{CMT} = 1. \end{cases} \tag{4.6}$$

Therefore, from (2.30), the optimal weight vector $\hat{\mathbf{w}}_{CMT}$ is given as

$$\hat{\mathbf{w}}_{CMT} = \frac{\mathbf{R}_{CMT}^{-1}\mathbf{v}(\theta_s)}{\mathbf{v}^H(\theta_s)\mathbf{R}_{CMT}^{-1}\mathbf{v}(\theta_s)}. \tag{4.7}$$

4.3.1 LMS Implementation of CMT Beamformer

In the discussion above, we only considered the optimum CMT beamformer but have not concerned ourselves with how such a beamformer would be implemented in practice. Optimality was only achieved because we assumed perfect knowledge of the second-order statistics of the received signal at the array, that is, the covariance matrix. In this subsection, we present the use of LMS adaptive method in implementing CMT beamformer.

The next theorem provides fundamental theorem for developing the LMS implementation of CMT beamformer.

Theorem 1: If given a positive definite covariance matrix $\mathbf{R}$ and a CMT $\mathbf{T}_{CMT}$, which is either positive definite or positive semidefinite with none zero diagonal entries, then the array coefficients $\hat{\mathbf{w}}_{CMT}$ satisfying (4.4)-(4.6) is an optimum MVDR beamformer with additive received signals $\tilde{\mathbf{x}} = \mathbf{x} \circ \mathbf{t}$, where $\mathbf{x}$ is the observed signals at the output of the sensor elements, $\text{cov}(\mathbf{x}) = \mathbf{R}, \text{cov}(\mathbf{t}) = \mathbf{T}_{CMT}$, $\mathbf{x}$ and $\mathbf{t}$ are uncorrelated, and where $\mathbf{t}$ is zero mean, wide sense stationary vector random process.

Proof: see [18].

Therefore, the introduction of a CMT is tantamount to solving an optimum MVDR beamforming problem where the additive received signals are assumed to have resulted from the Hadamard product of observed signals at sensor outputs and one vector random process. Assuming an $N+1$ element linear array, it has been shown in [18] that the vector random process $\mathbf{t}$ can be chosen as

$$\mathbf{t} = \begin{bmatrix} 1 \\ \vdots \\ e^{j\pi n\tilde{\phi}} \\ \vdots \\ e^{j\pi N\tilde{\phi}} \end{bmatrix} = \begin{bmatrix} 1 \\ \vdots \\ e^{jn\tilde{\omega}} \\ \vdots \\ e^{jN\tilde{\omega}} \end{bmatrix} \tag{4.8}$$

where $\tilde{\omega}$ (and, consequently, $\tilde{\phi}$) is a zero mean uniformly distributed random

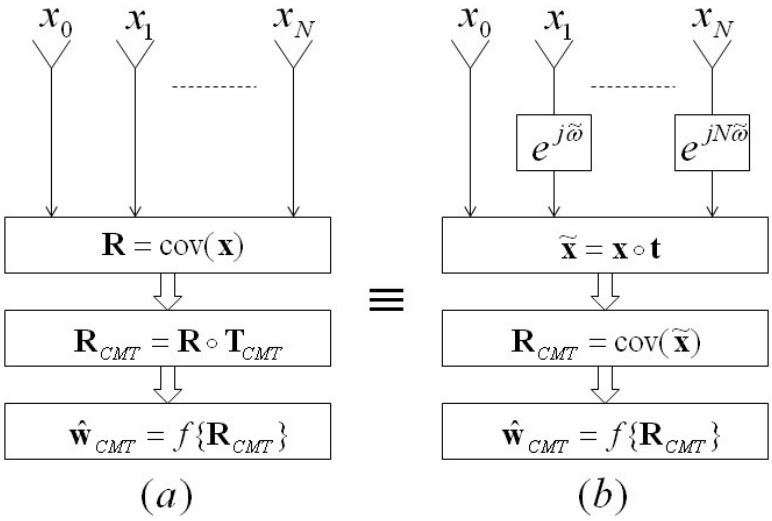

Figure 4.1: Equivalent interpretations for CMT beamformer

variable such that $-\Delta \leq \tilde{\omega} \leq \Delta$. From (4.4) and Theorem 1, we have

$$\begin{aligned} \mathbf{R}_{CMT} &= \mathbf{R} \circ \mathbf{T}_{CMT} = \mathrm{cov}(\mathbf{x}) \circ \mathrm{cov}(\mathbf{t}) \\ &= \mathrm{cov}(\mathbf{x} \circ \mathbf{t}) = \mathrm{cov}(\tilde{\mathbf{x}}) \end{aligned} \tag{4.9}$$

The equivalence in (4.9) is shown in Fig. 4.1, where $f\{\cdot\}$ represents the calculation of array coefficients using (4.7). With the equivalence in (4.9), we can implement the CMT beamformer using LMS adaptive algorithm [48] given as:

$$\hat{\mathbf{w}}_{CMT}(t+1) = \mathbf{v}(\theta_s) + \mathbf{P}[\hat{\mathbf{w}}_{CMT}(t) - \mu y^*(t)\tilde{\mathbf{x}}(t)] \tag{4.10}$$

where μ is the step-size parameter, $*$ denotes complex conjugate and $\mathbf{P}$ is the projection matrix given by:

$$\mathbf{P} = \mathbf{I} - \mathbf{v}(\theta_s)\mathbf{v}^H(\theta_s) \tag{4.11}$$

and

$$y(t) = \hat{\mathbf{w}}_{CMT}^{H}(t)\tilde{\mathbf{x}}(t) \tag{4.12}$$

For LMS adaptive CMT beamformer, the time constant associated with the mth interference source is given by [31]

$$\tau_m \approx \frac{1}{4\mu\sigma_m}; \quad m = 0, 1, \ldots, M-1 \tag{4.13}$$

where σ_m is the eigenvalue of covariance matrix $\mathbf{R}_{CMT}$ corresponding to the mth interference source. Therefore, the convergence behavior of LMS adaptive CMT beamformer is dependent on the eigenvalue spread of $\mathbf{R}_{CMT}$ and the algorithm may be unacceptably slow in the situation where strong interferences exist.

4.3.2 QR-RLS Implementation of CMT Based MVDR Beamformer

As discussed above, the convergence of LMS adaptive CMT beamformer can be very slow for large eigenvalue spread of covariance matrix $\mathbf{R}_{CMT}$. One alternative to LMS is the exponentially weighted RLS algorithm. The convergence of RLS to the optimum weight vector is often faster than that obtained using the LMS algorithm because it is independent of the eigenvalue spread of $\mathbf{R}_{CMT}$. The RLS adaptive filter is formulated as [48]

$$\begin{cases} \min\limits_{\mathbf{w}(t)} \sum\limits_{i=1}^{t} \lambda^{t-i}|e(i)|^2 \\ \quad e(i) = d(i) - \mathbf{w}^H(t)\mathbf{u}(i) \end{cases} \tag{4.14}$$

where $0 < \lambda < 1$ is the exponential forgetting factor. $e(i)$ is the difference between the desired signal $d(i)$ and the output signal of adaptive filter $\mathbf{w}^H(t)\mathbf{u}(i)$. $\mathbf{w}(t)$ is tap-weight vector and $\mathbf{u}(i)$ is tap-input vector.

The optimal solution of the conventional RLS problem can be obtained using QR based method. Detail discussion of QR-RLS can be found in [48].

To apply QR-RLS method in CMT based MVDR beamforming, the constrained optimization in (4.6) is reformulated as

$$\begin{cases} \min\limits_{\hat{\mathbf{w}}_{CMT}(t)} \sum\limits_{i=1}^{t} \lambda^{t-i}|e(i)|^2, \quad e(i) = \hat{\mathbf{w}}_{CMT}^H(t)\tilde{\mathbf{x}}(i) \\ s.t. \quad \mathbf{v}^H(\theta_s)\hat{\mathbf{w}}_{CMT}(t) = 1 \end{cases} \tag{4.15}$$

The optimal solution $\hat{\mathbf{w}}_{CMT}(t)$ in (4.7) can be reexpressed as

$$\hat{\mathbf{w}}_{CMT}(t) = \frac{\mathbf{R}_{CMT}^{-H/2}(t)\mathbf{a}(t)}{\|\mathbf{a}(t)\|^2} \tag{4.16}$$

where

$$\mathbf{a}(t) = \mathbf{R}_{CMT}^{-\frac{1}{2}}(t)\mathbf{v}(\theta_s). \tag{4.17}$$

Therefore, the output error signal $e(t)$ is

$$e(t) = \hat{\mathbf{w}}_{CMT}^H(t)\tilde{\mathbf{x}}(t) = \frac{\mathbf{a}^H(t)\mathbf{R}_{CMT}^{-\frac{1}{2}}(t)\tilde{\mathbf{x}}(t)}{\|\mathbf{a}(t)\|^2} \triangleq \frac{e^{'}(t)}{\|\mathbf{a}(t)\|^2}. \tag{4.18}$$

With the help of the correspondence between the QR-RLS adaptive filtering [48] and CMT beamforming variables, the QR-RLS based CMT beamformer

can be formulated as following:

$$\begin{bmatrix} \lambda^{\frac{1}{2}}\mathbf{R}_{CMT}^{\frac{1}{2}}(t-1) & \tilde{\mathbf{x}}(t) \\ \lambda^{\frac{1}{2}}\mathbf{a}^H(t-1) & 0 \\ \mathbf{0}^T & 1 \end{bmatrix} \Theta(t) = \begin{bmatrix} \mathbf{R}_{CMT}^{\frac{1}{2}}(t) & \mathbf{0} \\ \mathbf{a}^H(t) & \frac{e'(t)}{\gamma^{\frac{1}{2}}(t)} \\ \tilde{\mathbf{x}}^H(t)\mathbf{R}_{CMT}^{-\frac{H}{2}}(t) & \gamma^{\frac{1}{2}}(t) \end{bmatrix} \tag{4.19}$$

The matrix $\Theta(t)$ is any unitary rotation that operates on the elements of the input data vector $\tilde{\mathbf{x}}(t)$ in the prearray, annihilating them one by one so as to produce a block zero entry in the top block row of the postarray. With the postarray matrix elements, the coefficients $\hat{\mathbf{w}}_{CMT}(t)$ can be obtained using (4.16).

The potential advantages of QR-RLS algorithm include numerical stability, fully pipelined structure and robustness to finite precision problem. However, as was shown in [41], the computational complexity for QR-RLS is much higher than the LMS adaptive method.

4.4 Proposed Adaptive Null Steering Beamformer Implementation For Flexible Broad Null Control

In Chapter 3, we presented the null steering algorithm with multiple constraints for beamforming application. The algorithm can handle well in environments where stationary interfering sources exist. In this section, the algorithm will be further developed for the scenario when interferences are moving. By using the new design, broader null can be generated using the same null steering struc-

ture. This beamforming algorithm for broad null control is of great advantage for sensor array in which the number of array elements is very large compared with the number of interferences the array is designed to suppress. The method is useful and effective in environments where both stationary and moving interfering signals exist, since the beamformer can steer both sharp and controlled broad nulls in the appropriate directions.

The new null steering beamformer implementation for flexible broad null control is presented here. First the equivalence between FIR filtering and linear array processing is stated. This equivalence motivates us to incorporate the impulse response of an FIR filter in the new beamformer design. With the help of the equivalence, the desired broad null in the array spatial response can be mapped to the equivalent frequency response of a corresponding FIR filter. The procedures to generate FIR filter coefficients and apply the FIR filter as the aperture function of the new beamformer design are given. Details of the new beamformer structure and implementation are presented. The computational complexity and convergence behaviour are then discussed.

4.4.1 Equivalence Between FIR Filtering and Linear Array Processing

The equivalence between a temporal FIR filter structure and a uniform linear array (ULA) is given in this subsection.

The frequency response of an FIR filter with an impulse response $h(n)$, $0 \leq n \leq N$ is

$$H(\omega) = \sum_{n=0}^{N} h(n) \exp(-j\omega n) \tag{4.20}$$

which represents the response of the filter to a complex sinusoid of frequency ω. It should be noted that (4.20) is the discrete-time Fourier transformer (DTFT) of $h(n)$. Similarly, the beamformer response is defined as the amplitude and phase presented to a complex plane wave $e^{j\omega k}$, as a function of DOA θ relative to broadside and frequency ω.

For an $(N+1)$-sensor beamformer with an aperture function $w(n)$, $0 \leq n \leq N$, the beamformer response is [3],

$$W(\theta, \omega) = \sum_{n=0}^{N} w(n) \exp(-j\omega\tau_n(\theta)) \tag{4.21}$$

where $\tau_0(\theta) = 0$ and $\tau_n(\theta)$, $1 \leq n \leq N$, represents the time delay due to propagation relative to the first sensor element. We also refer to (4.21) as discrete-space Fourier transform (DSFT) of array coefficients $w(n)$. The analogy between FIR filtering and beamforming is closest when the ULA beamformer operates at a single temporal frequency $\omega = \omega_0$ and the array geometry is linear and equispaced. The time delay $\tau_n(\theta)$ is

$$\tau_n(\theta) = 2\pi n \frac{d \sin\theta}{\lambda \omega_0} \tag{4.22}$$

and the relationship between the temporal frequency ω in FIR filtering and the direction θ in array beamforming is

$$\omega = 2\pi \frac{d \sin\theta}{\lambda}. \tag{4.23}$$

Thus, the temporal frequency in FIR filtering corresponds to sine of the DOA in narrowband ULA beamforming. To avoid spatial ambiguity and increase the spatial resolution of a ULA beamformer, $d = \lambda/2$ is usually chosen and in this

case, (4.23) becomes

$$\omega = \pi \sin\theta \tag{4.24}$$

and each $\theta \in [-\frac{\pi}{2}, \frac{\pi}{2}]$ is uniquely mapped to $\omega \in [-\pi, \pi]$.

4.4.2 Spatial FIR Filter Design Procedures

The interchange of beamforming and FIR filtering methods discussed above motivates us to incorporate the impulse response of temporal FIR filter in the new beamformer design. The application of temporal FIR filter in beamformer design can be referred to as spatial filtering using sensor array. We propose using the spatial FIR filter to eliminate the interference from moving interfering signals. This is achieved by first designing a highpass FIR filter then in the spatial domain placing it at the angle of interference.

The highpass spatial filter design steps for windowing method can be summarized as follows:

Step 1: Determine the "cutoff" angle θ_c. Due to the symmetry property of the filter response, the cutoff angle of highpass filter is set to be half of the desired broad null width, i.e., $\theta_c = \Delta\theta/2$, where $\Delta\theta$ is the desired broad null width.

Step 2: Obtain ideal impulse response, $\hat{h}(n)$ of the desired highpass FIR fitler, we have the following:

$$\hat{h}(n) = \begin{cases} 1 - \dfrac{\theta_c}{\pi} & n = 0 \\ -\dfrac{\sin(\theta_c n)}{\pi n} & n \neq 0 \end{cases} \tag{4.25}$$

we note here (4.25) leads to the weight with infinite number of terms that is

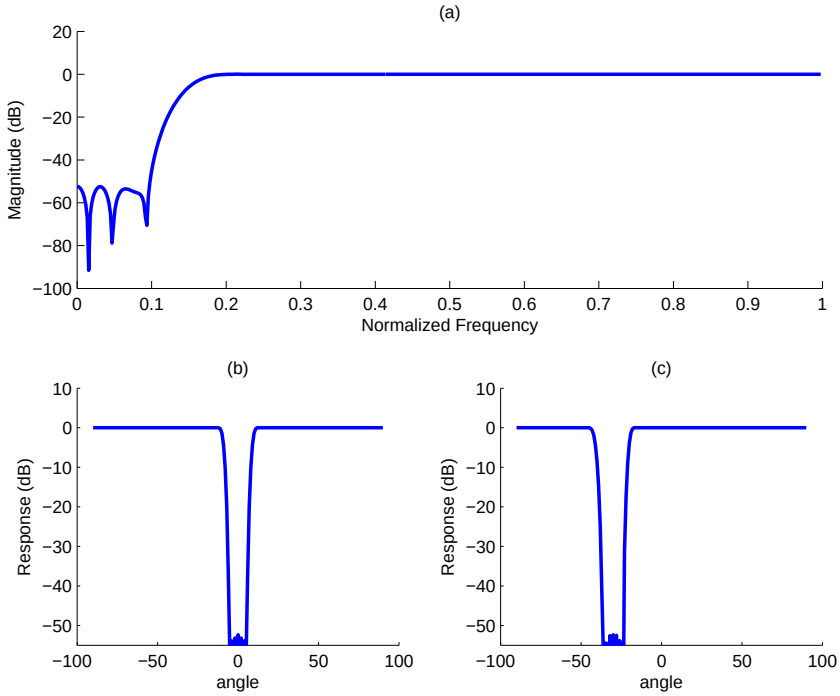

Figure 4.2: (a) Magnitude response (b) Equivalent spatial response (c) Spatial-shifted response of a highpass FIR filter

physically unrealizable. Truncating $\hat{h}(n)$ is equivalent to multiplying the ideal solution $\hat{h}(n)$ by a finite-length window function $g(n)$. Several window functions that are widely applied in the design of FIR digital filter can be utilized for weight design.

Step 3: Select a window function.

Step 4: Obtain the values of $g(n)$ for the chosen window function and the values of the actual FIR filter coefficients, $h(n)$, by multiplying $\hat{h}(n)$ with $g(n)$.

$$h(n) = \hat{h}(n)g(n) \tag{4.26}$$

Fig. 4.2(a) shows the magnitude of the frequency response of a 64th-order

highpass filter with stopband $0 \leq \omega \leq 0.15$. The FIR filter order depends on the stopband attenuation and the transition width and can be obtained by using the formulas for FIR filter order estimation [54]. For example, for FIR filter design technique using Kaiser Window, the filter order N can be estimated using

$$N \approx \frac{A_s - 7.95}{14.36\Delta f} + 1 \tag{4.27}$$

where A_s is the stopband attenuation, Δf is the transition width. For FIR filter design technique using Hamming Window and with a minimum stopband attenuation of 53 dB, the filter order N is inversely proportional to the transition width given as

$$N \approx \frac{8\pi}{\Delta f} \tag{4.28}$$

Here, a high order FIR filter is used since a sharp cut-off and large stopband attenuation are preferred. Among the window functions Hamming is the best choice for many applications [54]. Therefore, the Hamming window with window function [43]

$$g(n) = 0.54 - 0.46\cos\left(\frac{2\pi n}{N-1}\right),\ 0 \leq n \leq N \tag{4.29}$$

is used in the filter design. The window length is $N + 1$. From (4.24), we can obtain the equivalent spatial response of the designed highpass filter as shown in Fig. 4.2(b).

Next, we shift the spatial response of designed highpass filter to the band of unwanted arriving angles centered at direction θ_1 in the spatial domain. This can be achieved by using the frequency shifting property of DTFT: multiplication by a complex exponential corresponds to a shift in the frequency domain.

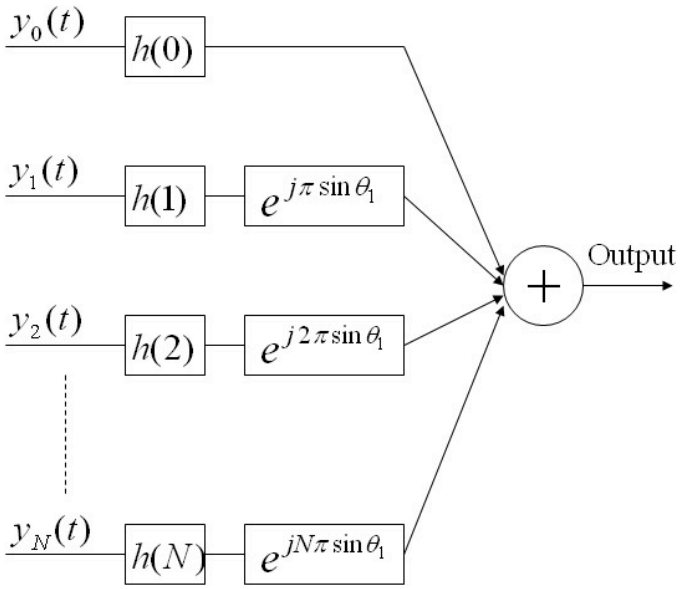

Figure 4.3: Structure of the spatial FIR filter

Therefore, the final designed spatial FIR filter coefficients are given by

$$\tilde{h}_1(n) = h(n)\exp(j\pi \sin(\theta_1)n),\ 0 \leq n \leq N \tag{4.30}$$

Fig. 4.2(c) shows the spatial response of the final designed filter. As seen in the figure, the original response of highpass filter is shifted to the band of rejecting angles centered at $-30°$. The structure of the spatial FIR filter is shown in Fig. 4.3.

4.4.3 New Beamformer Structure And Implementation

The details of new beamformer structure and implementation for broad null control is presented in this subsection. The new beamformer design uses a cascade configuration so that it can steer both sharp and controlled broad nulls in the appropriate directions.

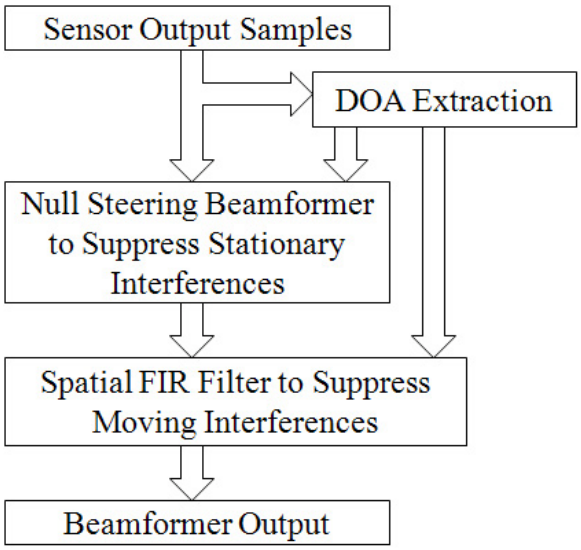

Figure 4.4: Flow chart of new beamformer for broad null control

Fig. 4.4 shows the flow chart of new beamformer for broad null control. The DOAs of desired signal and interferences are estimated using the fast null steering algorithm discussed in Section 3.3.2. Although this null steering system was designed originally for interference suppression, it can also be used to estimate the DOA and details will be discussed in Chapter 6. It is assumed that the DOAs of all signals in the environment are fixed during the very short DOA extraction period. The information on DOAs of all signals will be used to implement the null steering beamformer and the spatial FIR filter. The null steering beamformer is implemented using the null steering algorithm with multiple constraints presented in Chapter 3. The purpose is to suppress all the stationary interferences and preserve the desired signal. Next, spatial FIR filter designed in last subsection is used to eliminate the moving interference. Here, after the DOAs of the desired signal and interferences are estimated, it is assumed that the DOA of the moving interference is known.

Fig. 4.5 shows the structure of the proposed implementation for one broad

null. The new design includes the concept of subarrays. Consider a ULA with $N+1$ identical sensors. We divide this array into overlapping subarrays of L sensors each, with sensors $\{0, 1, \ldots, L-1\}$ forming the first subarray, sensors $\{1, 2, \ldots, L\}$ forming the second subarray and so on. The DOAs are estimated from the data samples received by the first subarray, provided the degree of freedom (DOF) of the subarray is larger than the number of signals existing in the environment. It should be noted here that the whole ULA system should have a large number of elements compared with the number of signals the array is designed to handle, since the ULA consists of several subarrays. For each subarray, the same null steering beamformer discussed in Chapter 3 is implemented. The signals $y_n, 0 \leq n \leq N-L$, are then fed to a spatial FIR filter with coefficients $\tilde{h}_1(n), 0 \leq n \leq N-L$. Note that, signals y_n contain only desired signal and moving interference. From (4.23), the delay of the nth output y_n with respect to the previous output y_{n-1} is $(2\pi d \sin\theta)/\lambda$.

Therefore, the new design in Fig. 4.5 can suppress interferences by steering sharp nulls toward the directions of stationary interfering signals and applying broad null to eliminate the interference from one interfering source that is moving around the central direction.

In order to steer another broad null centered at direction θ_2, the structure shown in Fig. 4.6 can be used. As seen in the figure, the data samples y_n are fed into a series of spatial FIR filters with coefficients $\tilde{h}_1(n), 0 \leq n \leq f-1$, which can be presented as a subarray representation with subarray size f. Note that, the stationary and first moving interferences are suppressed by the series of null steering beamformers and first set of spatial FIR filters, respectively. The second moving interference will be eliminated by the spatial FIR filter 2

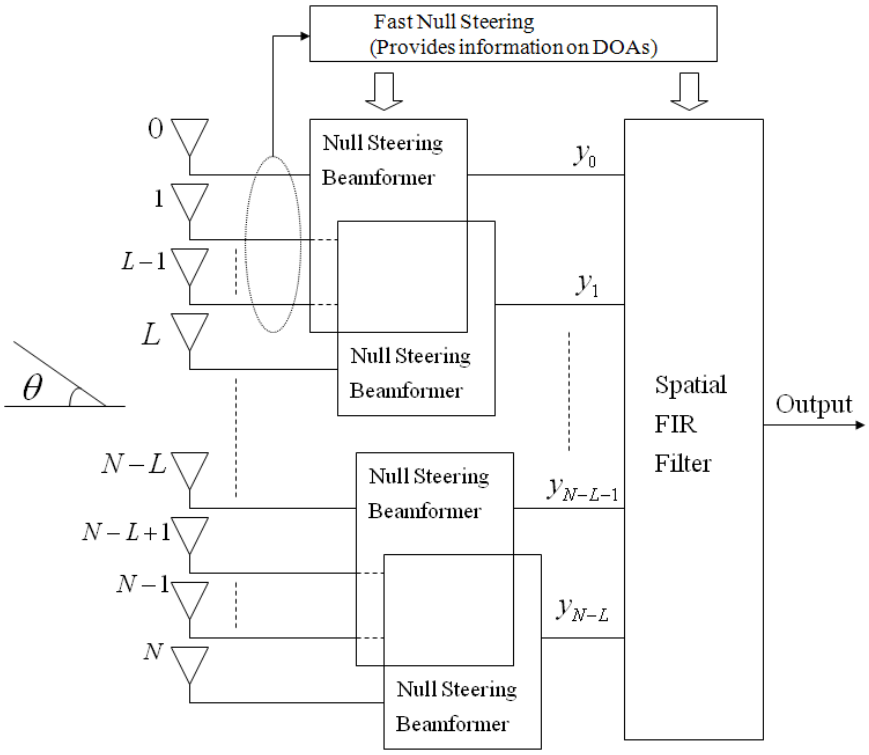

Figure 4.5: Structure of the proposed beamformer implementation for one broad null control

with coefficients $\tilde{h}_2(n), 0 \leq n \leq N-L-f$ while the desired signal will still be preserved at the system output. Here, coefficients $\tilde{h}_2(n)$ is generated according to (4.30) and given by

$$\tilde{h}_2(n) = h(n)\exp(j\pi \sin(\theta_2)n),\ 0 \leq n \leq N-L-f \tag{4.31}$$

A summary of the proposed implementation method in this section is given in Table 4.1. It should be noted that the highpass FIR filter is designed offline, and therefore step 1b) can be carried out concurrently with step 1a).

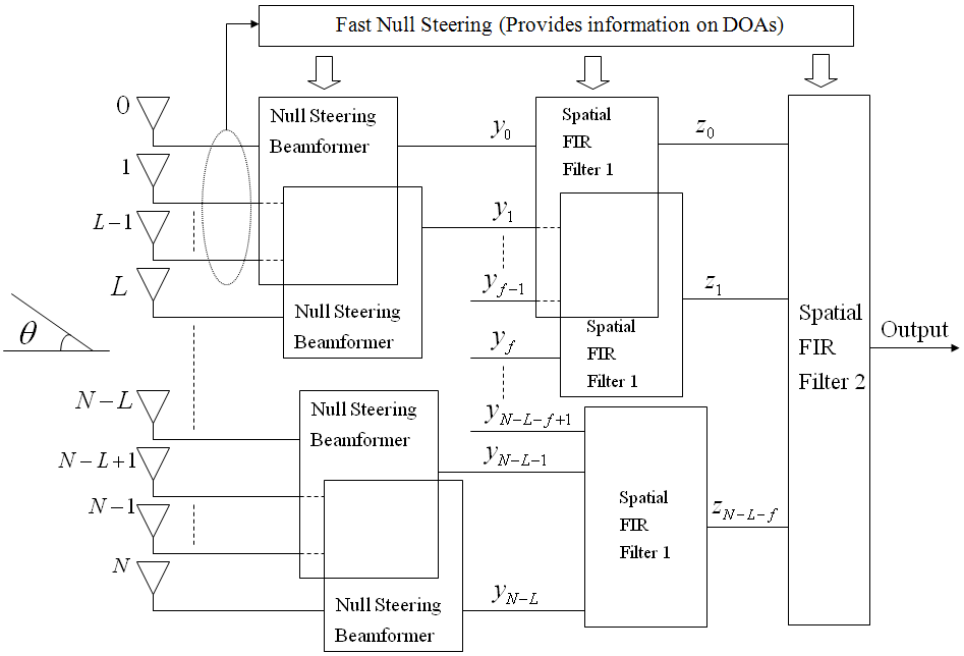

Figure 4.6: Structure of the proposed beamformer implementation for two broad nulls control

4.4.4 Computational Complexity Analysis

The computational complexity in terms of multiplication for implementing the proposed method is calculated and compared to the complexity of the CMT beamformers discussed in Section 4.3.1 and 4.3.2. Table 4.2 shows the comparison of computational complexity for different methods using N elements and K data samples. For the proposed method, Hamming window is used for designing the FIR filter. The subarray size is L in Fig. 4.5. In Fig. 4.6, the sizes of first and second subarray are L and f, respectively.

As can be seen in Table 4.2, for sensor array in which the number of array elements N is very large compared with the number of interferences the array is designed to suppress, the proposed method becomes convenient in terms of computational complexity with respect to the CMT beamformer with QR-RLS

Table 4.1: Summary of the proposed implementation method

Step 1a). Obtain DOAs of desired signal and interference sources using fast null steering method (Section 3.3.2).	Step 1b). (Offline) Design highpass FIR filter using equations (4.25), (4.26) and (4.29).
Step 2. Design null steering beamformer (Section 3.5)	
Step 3. Shift spatial response of designed highpass filter to band of unwanted arriving angles in spatial domain. Obtain final spatial FIR filter coefficients using equation (4.30).	
Step 4. Implement null steering beamformer for flexible broad null control shown in Fig. 4.5 or 4.6.	

Table 4.2: Comparison of computational complexity for implementing CMT based method with LMS/QR-RLS and proposed method per output sample

Method	Number of real multiplications
CMT w/LMS	$3N + 2$
CMT w/QR-RLS	$11N + 30N^2$ [41]
New method	$\{(L+1)N - L^2 + 2L + 4 + \frac{N+9L-12}{K}$ (Fig. 4.5)$\}$
	$\left\{ \begin{array}{l} (L+f+1)N - L^2 - (f-2)L - (f+1)^2 \\ +3 + \dfrac{N+9L-12}{K} \quad \text{(Fig. 4.6)} \end{array} \right\}$

scheme. Even though the complexity of new method is relatively higher than that of CMT based method with LMS, as will be shown later, the convergence rate of new method is significantly faster in comparison with that of LMS based CMT beamformer.

4.4.5 Average Convergence Behaviour

As discussed in Section 3.6, the convergence behaviour of proposed implementation is totally controlled by step 1a) in Table 4.1, since the processing in other steps are not involved in the iterative process. Therefore, for the new beam-

former design, the time constant associated with the mth interference source is

$$\tau_m \approx \frac{1}{2\rho_m}; \quad m = 0, 1, \ldots, M-1 \tag{4.32}$$

where M is number of signals in the environment. ρ_m is the misadjustment corresponding to the mth interference source. The convergence behaviour depends only on the misadjustment and is significantly faster. For the CMT beamformer with LMS scheme discussed in Section 4.3.1, as can be seen from (4.13), the convergence rate is governed by the eigenvalue spread of array input covariance matrix. For large eigenvalue spread, convergence can be very slow.

4.5 Simulation Results

Some simulation results will now be presented to verify the above theoretical results. The simulated array is assumed to be a 65-sensor ULA with intersensor spacing of $\lambda/2$. The subarray size L in Fig. 4.5 is chosen to be 4.

The simulated environment consists of a desired signal of power 20 dB arriving from broadside direction, and two independent interference signals of power 40 dB, assumed to be located at 40° and -30° to the array normal. Finally, independent white Gaussian noise of power 0 dB is added to each sensor element to account for the presence of ambient isotropic noise and other broadband sources of noise.

The estimated DOA values for signals and their errors are shown in Table 4.3.

Now we wish to generate a broad spatial null region to reject the interference from interfering signal that is moving around the central direction 39.9951°.

Table 4.3: Estimated DOA values and their errors

m	0	1	2
θ_m	0.1001	39.9951	-30.0986
Errors	0.1001	-0.0049	-0.0986

Hence, θ_1 in (4.30) is set to be 39.9951°. Fig. 4.7 illustrates the response using the proposed beamformer implementation. The broad null width is set to be 10°. It can be seen from the figure that the new beamformer steers a sharp null toward the direction of $-30.0986°$ and one broad null centered at the direction of 39.9951°. Now the effect of the choice of broad null width $\Delta\theta$ will be shown by simulation. For the same environment of Fig. 4.7, the directional patterns for new method with broad null widths 16°, 20° and 24° are shown in Fig. 4.8. As can be seen, both sharp and controlled broad nulls can be steered in the appropriate directions. Therefore, the new array structure is useful and effective in environments where both stationary and moving interfering signals exist.

The computational requirement for the proposed method was presented in Table 4.2. So, for the same scenario above, the new method requires $5N - 4$ multiplications to produce an output sample. It should be noted that the term $(N + 9L - 12)/K$ is ignored as K is large. On the other hand, as given in Table 4.2, the computational requirement for the CMT beamformer with QR-RLS scheme is $11N + 30N^2$ multiplications per output sample. Clearly, the new method has a lower complexity with respect to the QR-RLS based CMT beamformer.

As mentioned in Section 4.4.5, the convergence behaviour of proposed implementation is totally controlled by step 1a) in Table 4.1, i.e., DOA extraction

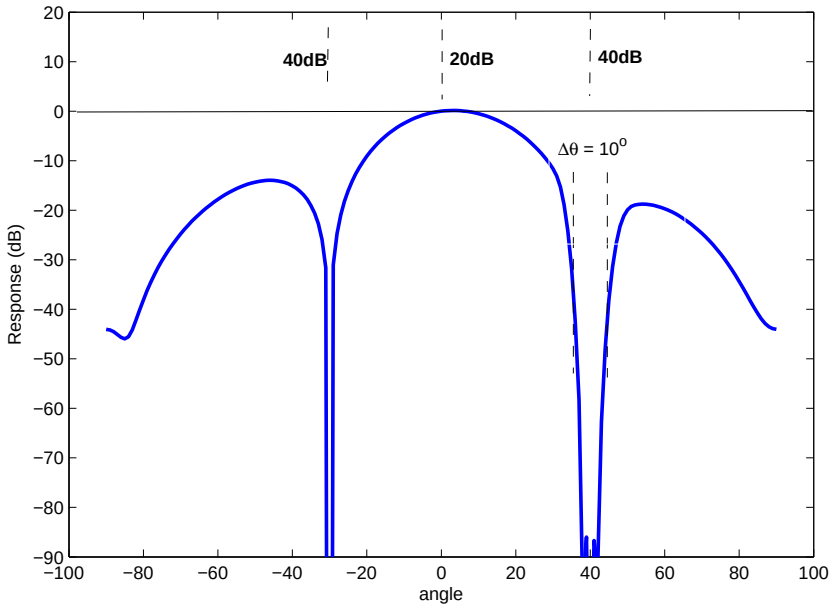

Figure 4.7: Directional pattern for new design with one broad null, $\Delta\theta$ set to be 10°

stage using fast null steering method. Considering the same scenario as Fig. 4.7, Fig. 4.9 compares the average output power convergence curves of using CMT with LMS, CMT with QR-RLS and new method, averaged over 500 runs. The desired misadjustment for all algorithms is 5%. As can be seen, the proposed method converges in a faster manner compared with the CMT based method with LMS. The CMT based method with QR-RLS and the proposed method have very similar convergence behavior.

Now consider the same scenario as Fig. 4.7, the array pattern with two controlled broad nulls is presented in Fig. 4.10. This pattern is obtained by using the proposed implementation shown in Fig. 4.6. The second subarray size f is set to be 35. It can be seen from Fig. 4.10 that two broad nulls with $\Delta\theta = 16^{\circ}$ and 30° are achieved over the spatial region centered at 39.9951° and -30.0986°, respectively.

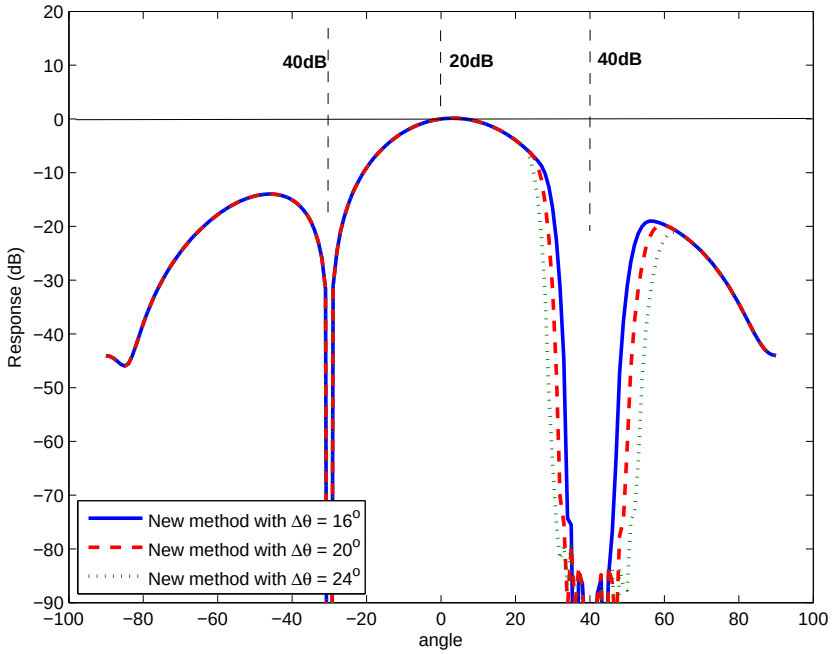

Figure 4.8: Directional patterns for new design with one broad null, $\Delta\theta$ set to be 16°, 20° and 24°

Now we look at another environment where three 40 dB interferences are located at $-60°$, 24° and 27° to the array normal and the desired signal of power 20 dB arrives from $-15°$. Note here that, the difference in DOA of the two interferences coming from 24° and 27° is chosen to be small. We use the same 65-sensor ULA in this scenario. The subarray sizes L and f in Fig. 4.5 and 4.6 are set to be 5 and 35, respectively. The estimated DOA values for signals and their errors are shown in Table 4.4. The dash line in Fig. 4.11 shows the array response using the new beamformer design in Fig. 4.5 with one broad null centered at 23.9967°. The broad null width $\Delta\theta$ is chosen to be 20°. The dot line in Fig. 4.11 gives the array response obtained by implementing the new beamformer in Fig. 4.6 with two broad nulls centered at 23.9967° and 27.0597°. The widths for both broad nulls are set to be 20°. One can observe from the

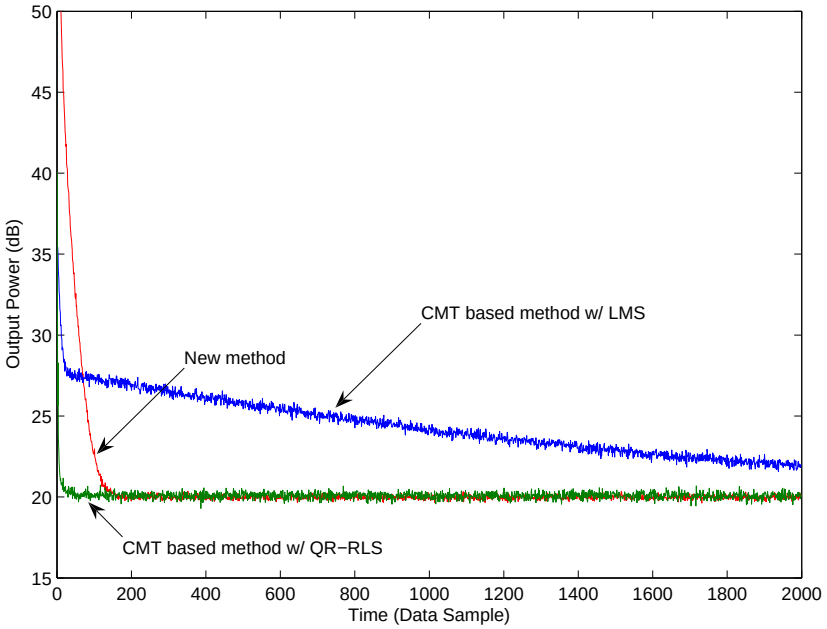

Figure 4.9: Stochastic output power convergence behaviors of CMT w/ LMS, CMT w/ QR-RLS and new method

Table 4.4: Estimated DOA values and their errors for another scenario

m	0	1	2	3
θ_m	-14.9827	-59.9642	23.9967	27.0597
Errors	0.0173	0.0358	-0.0033	0.0597

figure that the new method for one broad null control can handle well when two (or even more) closely located moving interferences exist in the environment, provided the broad null width is set to be a bigger value compared to the DOA difference.

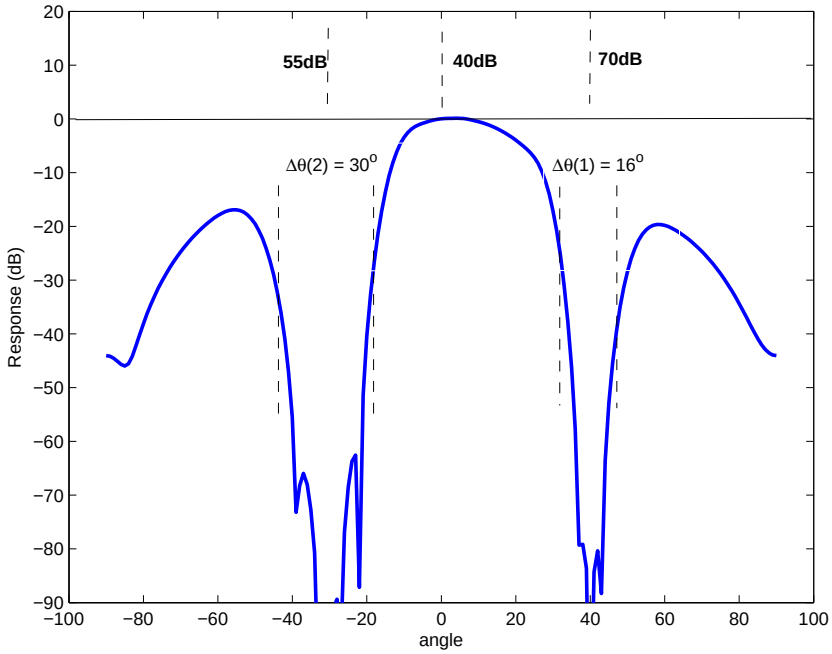

Figure 4.10: Directional patterns for new method with two broad nulls

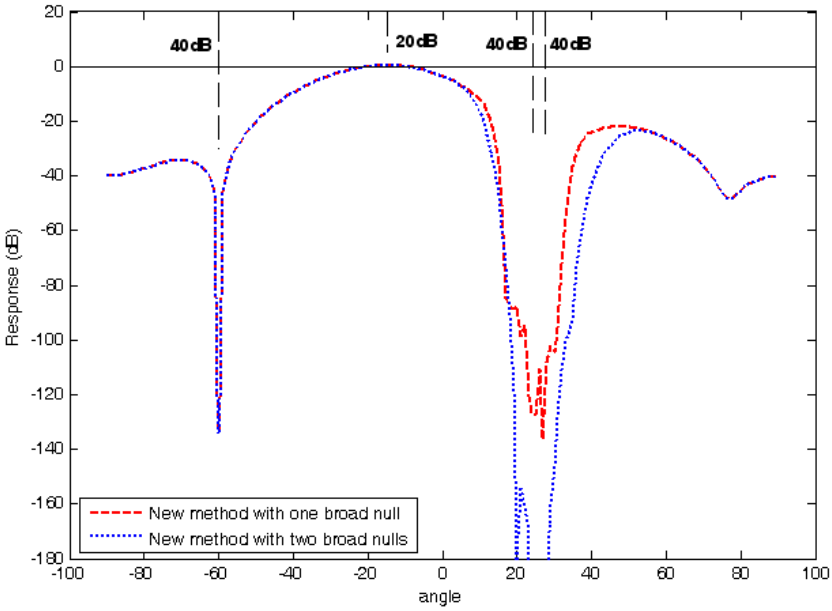

Figure 4.11: Directional patterns for new method in another scenario

4.6 Summary

In this chapter, we further developed the null steering beamformer discussed in Chapter 3 for the scenario when interferences are moving. Consequently, the implementation of adaptive null steering beamformer for flexible broad null control, based on constrained recursive updating of array response zeros and spatial FIR filters, was presented. The proposed implementation is of great advantage for sensor array in which the number of array elements is very large compared with the number of interferences the array is designed to suppress. The new beamformer is useful and effective in environments where both stationary and moving interfering signals exist since it can steer both sharp and controlled broad nulls in the appropriate directions. When compared with LMS CMT based broad null synthesis method, the proposed beamformer has a faster convergence rate; and the complexity required to implement the new design is far less than that for QR-RLS CMT based broad null synthesis method.

Chapter 5

IIR Array Processing Based Fast Adaptive Null Steering Algorithm Using Shift-Invariant Subarrays

5.1 Introduction

In this thesis, the basic structure of the Davies beamformer is used as the basis of our research work. In [12], a fast null steering algorithm based on Davies beamformer was proposed. In Chapter 3, we developed an adaptive beamformer derived from a constrained null steering design. The adaptive null steering beamformer implementation for flexible broad null control was proposed in Chapter 4. As mentioned in Chapter 3, the basic structure of null steering algorithm discussed so far assumes an all-zero model. It will be useful

to investigate the design and performance if it is extended to take the form of a pole-zero model and the discussion will be presented in this chapter.

Infinite impulse response (IIR) notch filter [37, 38, 39] is widely used in many signal processing applications to extract, eliminate or trace narrowband or sinusoidal signals embedded in broadband noise. With the similarity between uniform linear array (ULA) in spatial domain and finite impulse response (FIR) filter in time domain, it is possible to implement an IIR array structure in spatial domain [55]. The main advantage of IIR array processing is the small variation in its response over the non-notch angular directions.

In this chapter, a new fast null steering system employing IIR array processing will be presented and analyzed. The new algorithm is of considerable interest in communications where the desired signal is weak compared with the interfering signals or where the desired signal can be easily separated out. With the proposed algorithm, the nulls of the array system are repetitively updated one by one in a cyclical manner through a sequence of adjustment cycles. In each adjustment cycle, a particular null is updated by using the least mean square (LMS) algorithm and the update of each particular null will not affect other null positions. The proposed method is very effective and useful in the sense that it will result in a nearly flat gain in the antenna pattern, except zero gains at the null directions. Moreover, as will be demonstrated later from both analysis and simulation results, the convergence behavior of the new algorithm is significantly faster than the linearly constrained minimum variance (LCMV) method [31] and is almost independent of the external noise environment.

The remainder of this chapter is organized as follows. The next section provides the theory of IIR notch filter and implementation of IIR array process-

ing. The proposed adaptive null steering algorithm is presented in Section 5.3. Sections 5.4 and 5.5 discuss the optimal performance and average convergence behaviour. The simulation results are given in Section 5.6. Finally, Section 5.7 gives the summary.

5.2 IIR Notch Filter and Implementation of IIR Array Processing

IIR notch filter is widely used in many signal processing applications to extract, eliminate or trace narrowband or sinusoidal signals embedded in broadband noise. So far, several IIR notch filter structures have been proposed. Three typical ones are IIR lattice notch filter [49], bilinear second-order IIR notch filter [50], and IIR notch filter with constrained poles and zeros [51]. In this chapter, the third one will be considered. A complex Mth order IIR notch filter is characterized by the following transfer function

$$\begin{aligned} H(z) &= \frac{A(z)}{A(rz)} \\ &= \prod_{m=1}^{M} \left(\frac{1 - e^{j\omega_m} z^{-1}}{1 - r e^{j\omega_m} z^{-1}} \right) \\ &= \frac{1 + \sum_{m=1}^{M} a_m^* z^{-m}}{1 + \sum_{m=1}^{M} r^m a_m^* z^{-m}} \end{aligned} \tag{5.1}$$

where ω_m represents the mth notch frequency and $0 < r < 1$ is the constant pole radius close to 1. The zeros are constrained to locate on the unit circle at the notch frequency, and the poles are at the same radial lines as zeros to compensate for the frequency response to be an approximately unity gain for

the non-notch band. The bandwidth of the notch created by each pole-zero pair is $B = \pi(1-r)$ [40]. The closer r is to one, the narrower the band width of the notch. a_m is a complex coefficient and the notation $(\cdot)^*$ denotes the complex conjugate. Note that the above notch filter consists of cascades of M first-order filters which have their zeros on the unit circle, resulting in exactly zero gain at each notch frequency. For a complex input signal $x(n)$, the output of the filter $y(n)$ is given by

$$y(n) = \frac{A(z)}{A(rz)} x(n). \tag{5.2}$$

The input-output description of the IIR notch filter can also be expressed in difference equation form

$$y(n) = x(n) + \sum_{m=1}^{M} a_m^* x(n-m) - \sum_{m=1}^{M} r^m a_m^* y(n-m). \tag{5.3}$$

As understood in Section 4.4.1, the ULA in spatial domain is equivalent to a FIR filter in time domain. Using this equivalence, we introduce the IIR structure to ULA in spatial domain with the following response

$$\begin{aligned} \hat{H}(z) &= \prod_{m=1}^{M} \left(\frac{1 - z_m z^{-1}}{1 - r z_m z^{-1}} \right) \\ &= \frac{1 + \sum_{m=1}^{M} a_m^* z^{-m}}{1 + \sum_{m=1}^{M} r^m a_m^* z^{-m}} \end{aligned} \tag{5.4}$$

where

$$z_m = \exp\left(j \frac{2\pi d}{\lambda} \sin\theta_m \right). \tag{5.5}$$

To implement the IIR array in the form of (5.4), it is necessary to have recursive spatial feedbacks. This can be realized using the concept of subarrays

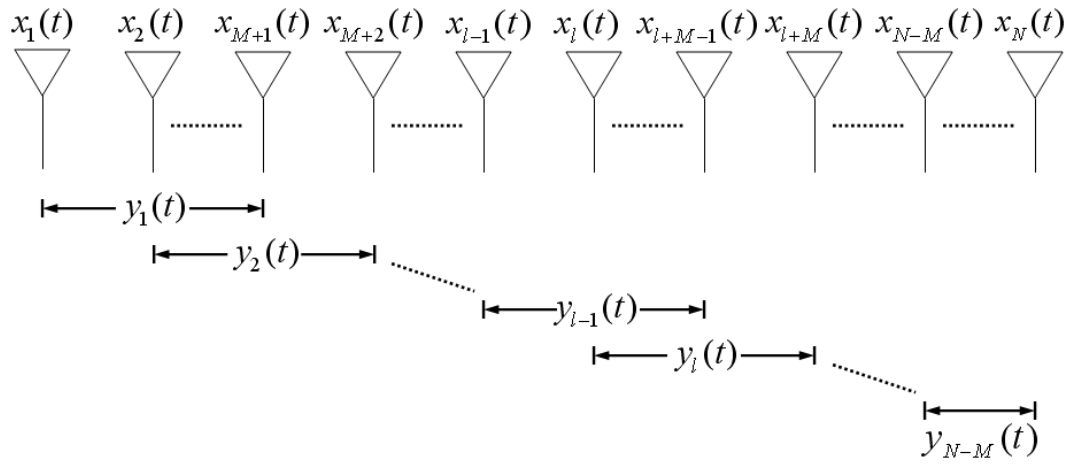

Figure 5.1: The structure of IIR array

[55]. The outputs of previous subarrays can be used for spatial feedbacks.

Consider a ULA with N identical sensors. We divide this array into overlapping subarrays of $M+1$ sensors each, with sensors $1, 2, \ldots, M+1$ forming the first subarray, sensors $2, 3, \ldots, M+2$ forming the second subarray and so on. As shown in Fig. 5.1, realizing each subarray using a Mth order IIR notch array structure, the output of lth, $1 \leq l \leq N-M$, subarray at time t is given by

$$y_l(t) = x_{l+M}(t) + \sum_{m=1}^{M} a_m^* x_{l+M-m}(t) - \sum_{m=1}^{M} r^m a_m^* y_{l-m}(t). \tag{5.6}$$

For convenience, we will drop the time index and assume that its presence is understood throughout the remainder of the chapter. From (5.4) and (5.5), each pole-zero pair of the IIR array response corresponds to a null direction $\theta_m, 1 \leq m \leq M$.

5.3 Proposed adaptive null steering algorithm

The advantage of IIR array processing is the small variation in its response over the non-notch angular directions. Therefore, we employ the IIR array processing into our new null steering system.

As discussed in Section 3.2, the directional pattern of the $(N+1)$-sensor power inversion array expressed in the polynomial form is given by:

$$D(z) = 1 + a_1 z^{-1} + a_2 z^{-2} + a_3 z^{-3} + \ldots + a_N z^{-N} \tag{5.7}$$

where

$$z = \exp\left(j\frac{2\pi d}{\lambda}\sin\theta\right). \tag{5.8}$$

Such a polynomial may be represented as the product of N factors giving the N zeros of the directional pattern.

$$D(z) = (1 - z_1 z^{-1})(1 - z_2 z^{-1}) \ldots (1 - z_N z^{-1}) \tag{5.9}$$

where $z_n, n = 1, \ldots, N$ is the nth complex response zero. Thus an $(N+1)$-sensor array has N degrees of freedom (DOFs) in its pattern and places maximum of N perfect nulls controlled by $z_n, n = 1, \ldots, N$. By choosing

$$z_n = \exp\left(j\frac{2\pi d}{\lambda}\sin\theta_n\right) \tag{5.10}$$

the array will direct its nulls at the directions $\theta_n, n = 1, \ldots, N$.

The algorithm proposed here repetitively updates the nulls of the array one by one in a cyclical manner through a sequence of adjustment cycles. In each

adjustment cycle, a particular null is updated by using the LMS algorithm such that the null being adjusted will be directed to one of the interferences at the end of the cycle.

Now suppose in the current adjustment cycle, the zero z_b (and, consequently, null direction θ_b) is to be updated. Let the response of the array system be expressed as

$$\begin{aligned} D(z) &= (1 - z_b z^{-1}) \hat{H}_{\text{int}}(z) \\ &= \hat{H}_{\text{int}}(z) - z_b z^{-1} \hat{H}_{\text{int}}(z) \end{aligned} \tag{5.11}$$

where $\hat{H}_{\text{int}}(z)$ is the initial response of the IIR array and given in (5.4) as follows:

$$\begin{aligned} \hat{H}_{\text{int}}(z) &= \prod_{m=1}^{M} \left(\frac{1 - z_m z^{-1}}{1 - r z_m z^{-1}} \right) \\ &= \frac{1 + \sum_{m=1}^{M} a^*_{m,\text{int}} z^{-m}}{1 + \sum_{m=1}^{M} r^m a^*_{m,\text{int}} z^{-m}}. \end{aligned} \tag{5.12}$$

The IIR array with the response $\hat{H}_{\text{int}}(z)$ is implemented using the structure shown in Fig. 5.1 with N sensors. The subarray size is $M + 1$. Therefore, the processing specified by (5.11) can be implemented by the structure of Fig. 5.2, where $\hat{H}_{\text{int}}(z)$ and $z^{-1}\hat{H}_{\text{int}}(z)$ are implemented by passing the signals from the first to the Nth sensor elements and from the second to the $(N + 1)$th sensor elements, respectively. With this preprocessing, the zero z_b can be seen to correspond to the complex weight in the last stage in the structure of Fig. 5.2. Clearly, with $\hat{H}_{\text{int}}(z)$ remaining unchanged in the current adjustment cycle, the updating of z_b is equivalent to the updating of the complex weight of a 2-sensor

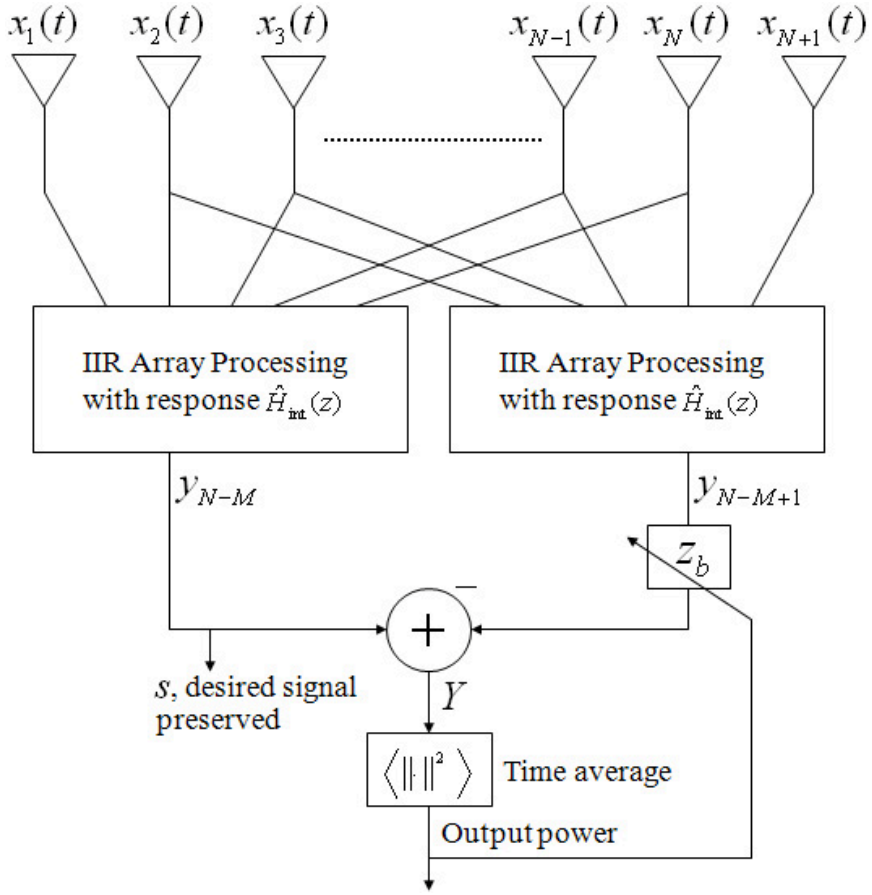

Figure 5.2: Array structure for updating z_b

power inversion array to minimize the output power according to (5.13):

$$z_b = \min_{z_b} E[|Y|^2] \tag{5.13}$$

Numerous algorithms can be used for updating z_b, but since only 1 complex weight is involved, the simple LMS algorithm is effective and efficient enough. With the LMS algorithm, the complex zero z_b is updated according to

$$z_b \rightarrow z_b + \mu_b Y^* y_{N-M+1} \tag{5.14}$$

with the arrival of each new data sample. y_{N-M+1} is the signal just in front of z_b in Fig. 5.2, while μ_b is the feedback factor of the algorithm and its significance will be discussed later.

Updating z_b in accordance with (5.14) K times using K data samples, z_b will converge towards its optimal value at the end of the current adjustment cycle. With the updated z_b, the response of the IIR array $\hat{H}_{\text{int}}(z)$ can be updated to $\hat{H}_b(z)$ given by

$$\begin{aligned} \hat{H}_b(z) &= \frac{(1 - z_b z^{-1})}{(1 - r z_b z^{-1})} \prod_{m=1, m \neq b}^{M} \left(\frac{1 - z_m z^{-1}}{1 - r z_m z^{-1}} \right) \\ &= \frac{1 + \sum_{m=1}^{M} a_{m,b}^{*} z^{-m}}{1 + \sum_{m=1}^{M} r^m a_{m,b}^{*} z^{-m}}. \end{aligned} \tag{5.15}$$

The update of $\hat{H}_{\text{int}}(z)$ to $\hat{H}_b(z)$ is essential because, with $\hat{H}_b(z)$, the interference with DOA θ_b can be suppressed by the IIR array processing, since one pole-zero pair of $\hat{H}_b(z)$ corresponds to the updated null direction θ_b.

Now suppose zero z_c is to be updated in the next cycle. The same updating procedure described above for z_b can be applied to the adjustment of z_c. The response of the proposed null steering array system now becomes

$$\begin{aligned} D(z) &= (1 - z_c z^{-1}) \hat{H}_b(z) \\ &= \hat{H}_b(z) - z_c z^{-1} \hat{H}_b(z). \end{aligned} \tag{5.16}$$

and the complex zero z_c is updated according to (5.14) with $\hat{H}_b(z)$ remaining unchanged. At the end of the cycle, z_c will converge to its optimal value. With updated z_c, the response of the IIR array $\hat{H}_b(z)$ can now be updated to $\hat{H}_c(z)$

given by

$$\begin{aligned}\hat{H}_c(z) &= \frac{(1-z_b z^{-1})(1-z_c z^{-1})}{(1-rz_b z^{-1})(1-rz_c z^{-1})} \prod_{m=1, m\neq b,c}^{M} \left(\frac{1-z_m z^{-1}}{1-rz_m z^{-1}}\right) \\ &= \frac{1+\sum_{m=1}^{M} a_{m,c}^* z^{-m}}{1+\sum_{m=1}^{M} r^m a_{m,c}^* z^{-m}}. \end{aligned} \tag{5.17}$$

so that the interferences with DOAs θ_b and θ_c can be suppressed by the IIR array processing with response $\hat{H}_c(z)$. As can be seen from (5.15) and (5.16), the updating of z_c will not affect the first updated zero z_b. Therefore, the zeros of the array are updated one after another without affecting other null positions so that all the interference signals existing in the environment can be rejected. As mentioned in Section 5.1, the new algorithm is of considerable interest in communications where the desired signal is weak compared with the interfering signals since the desired signal will not be in a null by using the new array system. The desired signal that is preserved can be taken as either y_{N-M} or y_{N-M+1} shown in Fig. 5.2.

The proposed method is very effective and useful in the sense that without applying any additional constraint it will result in an approximately unity gain in the antenna pattern, except zero gains at the null directions. It should be noted that, by employing IIR array processing, the proposed array system with $N+1$ sensors shown in Fig. 5.2 has M DOFs, which depends on the subarray size used in implementing the IIR array shown in Fig. 5.1. This is not really a disadvantage in the situation when the number of sensors within each subarray is larger than the number of interferences the array is designed to suppress, since the array can place enough nulls in the interference directions.

5.4 Optimal performance

Consider the updating of the complex zero z_b in the current adjustment cycle. From Fig. 5.2, the output of the array is given by

$$Y = y_{N-M} - z_b y_{N-M+1} \tag{5.18}$$

Thus, the output power is

$$\begin{aligned} E[|Y|^2] = E[|y_{N-M}|^2] - E[y_{N-M} y^*_{N-M+1}] z^*_b \\ -E[y^*_{N-M} y_{N-M+1}] z_b \\ +E[|y_{N-M+1}|^2] z_b z^*_b \end{aligned} \tag{5.19}$$

By carrying out differentiation with respect to z^*_b

$$\frac{\partial E[|Y|^2]}{\partial z^*_b} = E[|y_{N-M+1}|^2] z_b - E[y_{N-M} y^*_{N-M+1}] \tag{5.20}$$

From (5.20), the average output power will be minimized if z_b is given by its optimal value

$$z_{bopt} = \frac{E[y_{N-M} y^*_{N-M+1}]}{E[|y_{N-M+1}|^2]} \tag{5.21}$$

5.5 Average convergence behaviour

The average convergence behaviour of the zero being updated in the current adjustment cycle can be obtained by taking ensemble average of (5.14), giving

$$E[z_b] \rightarrow E[z_b] + \mu_b E[Y y^*_{N-M+1}] \tag{5.22}$$

Using (5.18) and (5.21) then yields

$$E[\Delta z_b] \rightarrow \{1 - \mu_b E[|y_{N-M+1}|^2]\} E[\Delta z_b] \tag{5.23}$$

where

$$\Delta z_b = z_b - z_{bopt} \tag{5.24}$$

is the difference between z_b and its optimal value.

From (5.23), after K iterations, the value of $E[\Delta z_b]$ at the end of the current adjustment cycle $E[\Delta z_{bend}]$ is related to that at the beginning of the cycle $E[\Delta z_{bint}]$ by

$$E[\Delta z_{bend}] = \{1 - \mu_b E[|y_{N-M+1}|^2]\}^K E[\Delta z_{bint}] \tag{5.25}$$

Clearly, if the feedback factor μ_b is such that

$$|1 - \mu_b E[|y_{N-M+1}|^2]| < 1 \tag{5.26}$$

$E[z_b]$ will converge towards its optimal value. As discussed in Chapter 3, the time constant for the convergence of $E[z_b]$ depends only on the desired misadjustment. Clearly, all the complex zeros will have the same convergence time constants if the misadjustments contributed by them are set to be roughly equal. It is the sameness in convergence time constants for all the zeros that leads to the fast convergence rate when the new method is employed. Whereas for LMS based LCMV method, the convergence behaviour is dependent on the external noise environment. The output power due to each individual interference converges with different time constants, and this leads to the slow overall convergence behaviour in the situation where strong interferences exist.

As discussed in Section 5.3, the update of each particular zero will not affect other null positions for the proposed method. Therefore, as can be seen from Fig. 5.3(a), the one-to-one relationship exists between the updated zeros of the array response and the interferences been tracked. Now assuming that the mth interferer i_m moves after we finish all the tracking process. Instead of updating all the zeros again, we can just update the zero z_m to re-track the moving interferer i_m, while all other zeros remain unchanged. Since only one zero needs to be adjusted, the convergence becomes even faster. Fig. 5.3(b) shows the relationship between the zeros of the array response and the interferences for LMS based LCMV method. The update of any zero will affect other null positions since all the zeros are interrelated. Hence, for the above assumed scenario, we need to repeat the whole LMS adaptive tracking process to update all the zeros of the array response, resulting in even slower convergence.

From the updating procedures described, Table 5.1 lists down the computational requirements for the new null steering algorithm. Note that the table includes an entry for the updating of the feedback μ_b and the recursive equation

$$\frac{1}{\mu_b} \rightarrow \left(1 - \frac{2\rho_T}{M}\right) \frac{1}{\mu_b} + |y_{N-M+1}|^2 \tag{5.27}$$

can be used to update μ_b every data sample so that the convergence time constant for $1/\mu_b$ is also roughly the same as that for $E[z_b]$. ρ_T is the total misadjustment tolerable. Ignoring the terms $2(M-2)/K$ and $3(M-1)/K$ in Table 5.1 as K will be large, the new algorithm requires 1 division, $2MN-(2M^2+2M-5)$ multiplications and $(2M+1)N-(2M^2+3M-3)$ additions to produce an output sample.

On the other hand, as listed in Table 5.2, the computational requirements

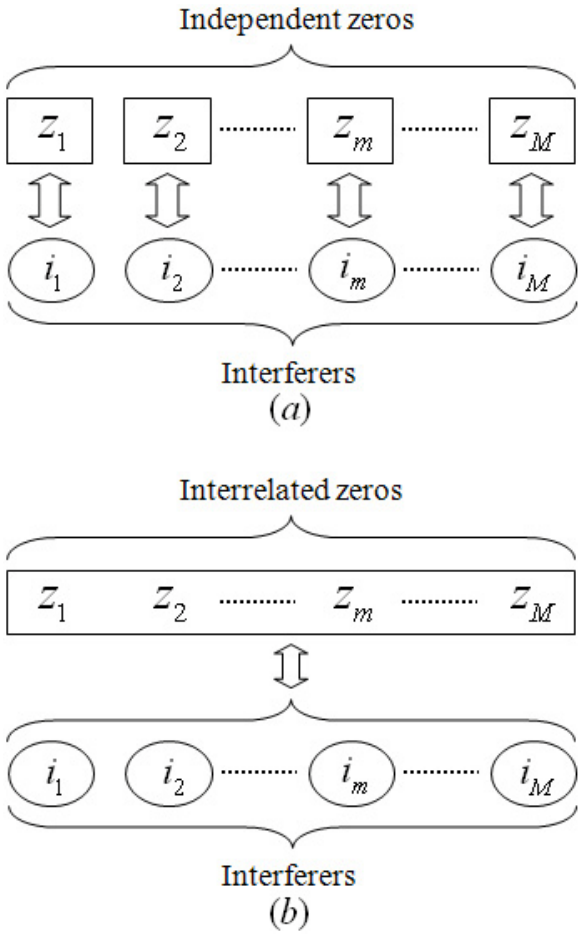

Figure 5.3: The relationship between zeros of array response and interferences for (a) proposed method (b) LMS LCMV method

for the LMS algorithm are 1 division, $2N + 2$ multiplications and $2N + 2$ additions per output sample. Clearly, for small subarray size M, the algorithm presented has an implementation complexity which is comparable to that of the LMS algorithm. Specifically, in the new algorithm, the entire adaptive array is implemented by using two IIR array processing and taking one power measurement, with the updating of the nulls being performed only sparingly. On the other hand, the LMS algorithm requires the implementation of one beamformer, but all the weights have to be updated every data sample.

Table 5.1: Computational requirements for implementing the new algorithm per output sample

Purpose	Multiplications	Additions	Divisions
Obtaining y_{N-M+1} and y_{N-M}	$2M(N-M-1)$	$(2M+1)(N-M-1)$	0
Obtaining Y	1	2	0
Updating z_b	2	1	1
Updating coefficients for IIR array processing	$\frac{2(M-2)}{K}$	$\frac{3(M-1)}{K}$	0
Updating μ_b	2	1	0
Total	$2MN+\frac{2(M-2)}{K}$ $-(2M^2+2M-5)$	$(2M+1)N+\frac{3(M-1)}{K}$ $-(2M^2+3M-3)$	1

Table 5.2: Computational requirements for implementing the LMS algorithm per output sample

Purpose	Multiplications	Additions	Divisions
Obtaining output	N	$N+1$	0
Updating weights	N	N	1
Updating feedback factor	2	1	0
Total	$2N+2$	$2N+2$	1

5.6 Simulation results

Some simulation results will now be presented to verify the above theoretical results. The simulated array is assumed to be a 50-sensor linear array with intersensor spacing of $\lambda/2$. The subarray size is set to be 5. The pole radius r in (5.12) is chosen to be 0.9.

The simulated environment consists of three independent interfering signals of power 40 dB, 30 dB and 20 dB, assumed to be located at 30° , -40° and 0°

to the array normal. Finally, independent white Gaussian noise of power 0 dB is added to each sensor element to account for the presence of ambient isotropic noise and other broadband sources of noise.

Fig. 5.4 shows the directional patterns of the new method. Note here that the directional patterns are generated at the IIR array output y_{N-M} or y_{N-M+1} shown in Fig. 5.2. Comparing Fig. 5.4(b) with the initial directional pattern of Fig. 5.4(a), the algorithm has steered a deep null towards the strongest interference after the first null update. As shown in Fig. 5.4(c), after adjusting the second zero, the new algorithm steers a null towards the second strongest interference. Then, from Fig. 5.4(d), the steering of the third null towards the weak interference is also achieved after the third zero update. Except nearly zero gains at the null directions, the directional pattern has an approximately unity gain at other directions, and this leads to the effectiveness and usefulness of the new method.

The updated null directions for interferences and their errors are shown in Table 5.3.

Table 5.3: Updated null directions and their errors

m	1	2	3
θ_m	29.9976	-39.9951	0.0204
Errors	-0.0024	0.0049	0.0204

In the new method, the nulls of the array system are repetitively updated one by one in a cyclical manner. One simple stopping criterion for the null updating process can be the array output power, since the information on whether untracked signals exist in the environment can be obtained by measuring the array output power as each zero is being updated. Table 5.4 summarizes the

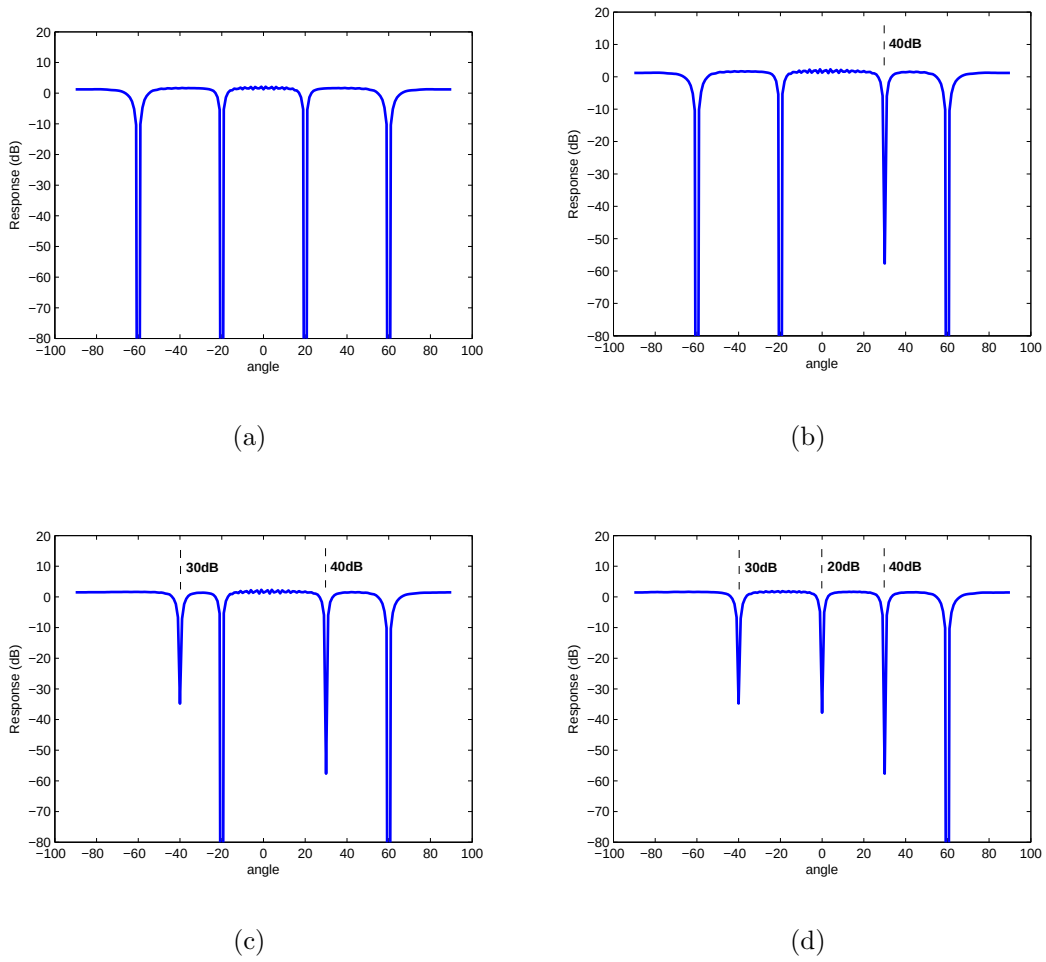

Figure 5.4: Directional patterns for new method (a) Initial, (b) After first null update, (c) After second null update, (d) After third null update.

null updating status at each stage. As can be seen in the table, the updating process will end after the third null has been adjusted since the output power becomes very low. Note here that the updated null directions have been rounded to integers.

Fig. 5.5 compares the average output power convergence curves of using the LMS based LCMV and new method, averaged over 500 runs. The desired misadjustment for both algorithms is 5%. As can be seen, the proposed method

Table 5.4: Summary of the null updating status

Actual interference directions (degree)	30	-40	0
Power of interferences (dB)	40	30	20
First updated null direction	30		
Output power after first null update	46		
Second updated null direction	-40		
Output power after second null update	20		
Third updated null direction	0		
Output power after third null update	-5		

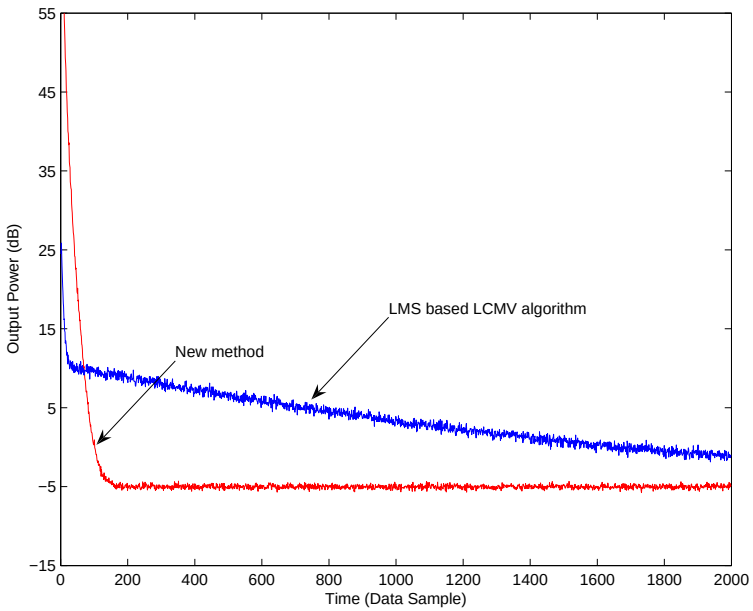

Figure 5.5: Stochastic output power convergence behaviors of LCMV and new method

converges in a faster manner compared with the LMS based LCMV method.

Now we look at another environment where three interfering signals of power 40 dB, 40 dB and 20 dB, located at 24° , 27° and −30°. Note here that, the difference in DOA of the two interferences with 40 dB power is chosen to be small and the same 50-sensor ULA is used. As can be seen from Fig. 5.6(d),

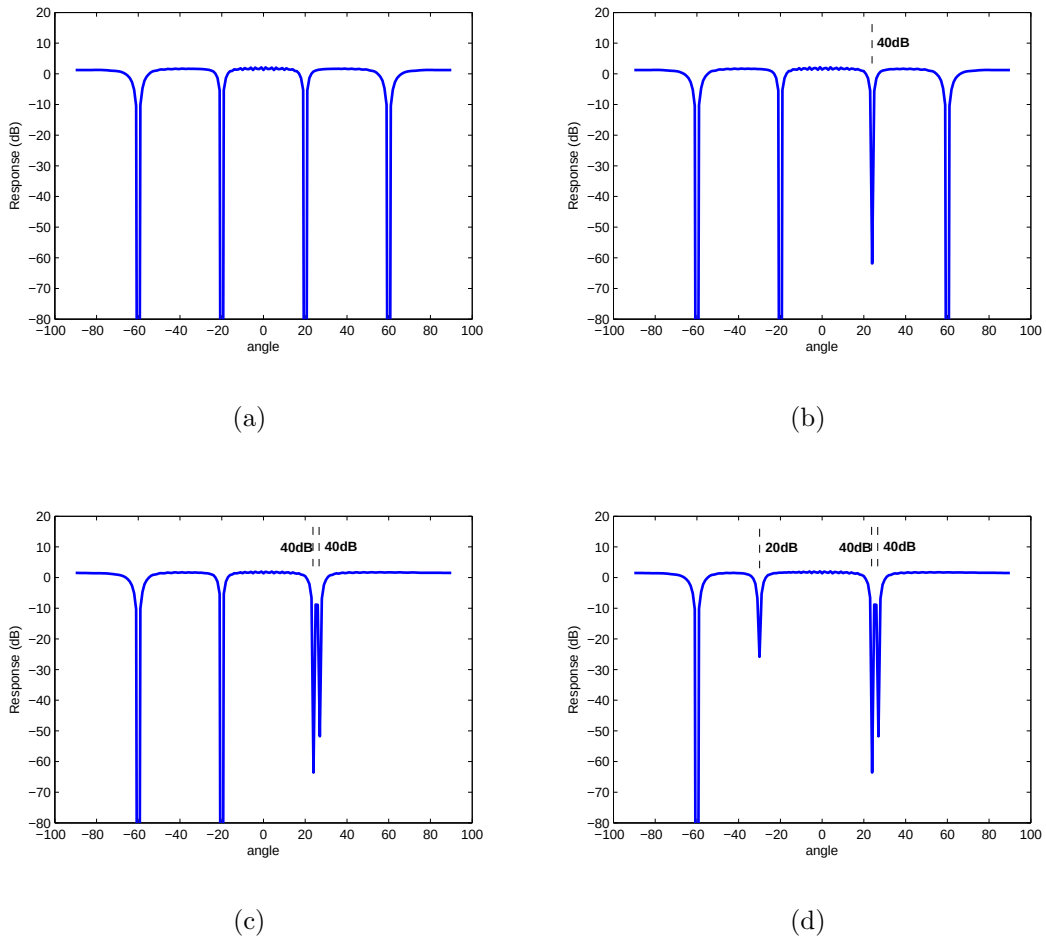

(a) (b)

(c) (d)

Figure 5.6: Directional patterns for new method (a) Initial, (b) After first null update, (c) After second null update, (d) After third null update.

the steering of two separate nulls towards the two closely spaced interferences is achieved and another null is steered towards the weak interference.

5.7 Summary

A fast IIR array processing based adaptive null steering algorithm is presented and discussed in this chapter. With this algorithm, the null positions can be

adaptively tracked one after another without affecting other null positions so that the interference signals can be rejected. The proposed method is very effective and useful in the sense that without applying any additional constraint it will result in a nearly flat gain in the antenna pattern, except zero gains at the null directions. Moreover, as demonstrated from both analysis and simulation results, the convergence behaviour of the new algorithm is significantly faster than the LMS based LCMV algorithm and is almost independent of the external noise environment.

As mentioned in Chapter 3, the same null steering structure discussed in this chapter can also be used for DOA extraction and details will be presented in next chapter.

Chapter 6

On the Application of the Null Steering Technique in Direction-of-Arrival Estimation

6.1 Introduction

The problem of determining directions of arrival (DOAs) of multiple narrowband plane waves using sensor arrays has received significant attention in the array signal processing literature. Many high-resolution direction-finding approaches have been presented to solve the problem in the recent years. Those approaches were based on the techniques such as maximum-likelihood [25], Capon [34], and multiple signal classification (MUSIC) [26]; However, the computational burden associated with those approaches is quite high and makes them difficult for high-speed applications. Comparing with Capon and MUSIC method, ESPRIT method [28] does not need to search for spectral peak, so it has advantage of less

calculation, higher precision and suitable for real time application. However, the ESPRIT method experiences significant performance degradation when the signal-to-noise ratio (SNR) is low.

In Section 3.3.2 of Chapter 3, we introduced the fast null steering algorithm that was originally designed for interference suppression. In Chapter 5, we presented the null steering algorithm with the form of a pole-zero model. It will be shown in this chapter that the same structures can also be used to estimate the DOA. With null steering algorithm, the complex zeros of the array directional pattern are repetitively updated one at a time by using the least mean square (LMS) algorithm. Then, a relationship between the updated zeros and the DOA angles is established so that the angles can be quickly estimated. Moreover, computer simulations show that the proposed approach is robust to the sensor gain and phase perturbations.

6.2 Problem Formulation

Consider an array composed of N equi-spaced omni-directional sensors, and assume M narrowband signals impinge on the array from the spatial sources with unknown DOAs $\theta_m, m \in [1, M]$ with respect to the array normal. Therefore, the signals received by the array can be expressed as

$$\mathbf{x}(t) = \sum_{m=1}^{M} \mathbf{v}(\theta_m) s_m(t) + \mathbf{n}(t) = \mathbf{V}(\theta)\mathbf{s}(t) + \mathbf{n}(t) \tag{6.1}$$

where $\mathbf{x}(t)$ is the $N \times 1$ vector

$$\mathbf{x}(t) = [x_1(t), x_2(t), \ldots, x_N(t)]^T \tag{6.2}$$

$\mathbf{V}(\theta)$ is a matrix consisting of the array steering vectors (ASVs). $\mathbf{s}(t)$ is the signal vector consisting of M different incidence signals, and $\mathbf{n}(t)$ is the white noise vector at each array element with a zero mean and variance σ^2. $\mathbf{V}(\theta)$, $\mathbf{s}(t)$ and $\mathbf{n}(t)$ can be expressed as

$$\mathbf{V}(\theta) = [\mathbf{v}(\theta_1), \mathbf{v}(\theta_2), \ldots, \mathbf{v}(\theta_M)] \tag{6.3}$$

$$\mathbf{s}(t) = [s_1(t), s_2(t), \ldots, s_M(t)]^T \tag{6.4}$$

and

$$\mathbf{n}(t) = [n_1(t), n_2(t), \ldots, n_N(t)]^T \tag{6.5}$$

respectively, where $\mathbf{v}(\theta_m)$ is the ASV of $s_m(t)$ and defined as

$$\mathbf{v}(\theta_m) = [1, e^{-j2\pi u_m}, \ldots, e^{-j2\pi u_m(N-1)}]^T \tag{6.6}$$

where

$$u_m = \frac{d \sin(\theta_m)}{\lambda} \tag{6.7}$$

d is the interelement spacing and λ is the wavelength. The covariance matrix of array signal is

$$\begin{aligned} \mathbf{R} &= E[\mathbf{x}(t)\mathbf{x}^H(t)] \\ &= \mathbf{V}(\theta)E[\mathbf{s}(t)\mathbf{s}^H(t)]\mathbf{V}^H(\theta) + E[\mathbf{n}(t)\mathbf{n}^H(t)] \\ &= \mathbf{V}(\theta)\mathbf{P}\mathbf{V}^H(\theta) + \sigma^2\mathbf{I} \end{aligned} \tag{6.8}$$

where $\mathbf{P}$ is received signal power matrix and I is an identity matrix of size N.

The DOA estimation problem is to estimate the directions $\theta_m, m \in [1, M]$ of

the sources from K samples of the received signals.

6.3 MUSIC DOA Estimation Algorithm

The MUSIC method [26] is a relatively simple and efficient eigenstructure method of DOA estimation. It has many variations and is perhaps the most studied method in its class. In its standard form, also known as spectral MUSIC, the method estimates the noise subspace from the available samples. This can be done by either eigenvalue decomposition of the estimated array covariance matrix or singular value decomposition of the data matrix. From Section 2.3.2, we know that the covariance matrix $\mathbf{R}$ can be written into the form

$$\mathbf{R} = \mathbf{U_s}\Lambda_\mathbf{s}\mathbf{U_s}^H + \mathbf{U_n}\Lambda_\mathbf{n}\mathbf{U_n}^H \tag{6.9}$$

where $\mathbf{U_s}$ and $\Lambda_\mathbf{s}$ are the eigenvector matrix and eigenvalue matrix of signal subspace, $\mathbf{U_n}$ and $\Lambda_\mathbf{n}$ are the eigenvector matrix and eigenvalue matrix of noise subspace.

Once the eigenvector matrix of noise subspace has been estimated, a search for M directions is made by looking for steering vectors that are as orthogonal to the noise subspace as possible. This is normally accomplished by searching for peaks in the MUSIC spectrum given by

$$\mathbf{G}(\theta) = \frac{1}{|\mathbf{v}^H(\theta)\mathbf{U_n}|^2} \tag{6.10}$$

One disadvantage of MUSIC is its high computational burden due to the eigenvalue decomposition (EVD) or singular value decomposition (SVD) of ar-

ray covariance matrix. Another disadvantage is that the searching for spectral peaks needs to be repeated for every angle if one of the M signals in the environment moves.

6.4 Application of Null Steering Technique in DOA Estimation

In Section 3.3.2 of Chapter 3, we introduced the fast null steering algorithm that was originally designed for interference suppression. In Chapter 5, we presented the null steering algorithm with the form of a pole-zero model. In this section, we present the application of null steering technique in DOA estimation. With the relationship established between the updated zeros and the direction, the DOA angles can be quickly estimated.

6.4.1 DOA estimation using null steering array with least-square based preprocessing

Consider a linear uniformly spaced narrowband array with N elements, and the first element has unity gain, the other elements are weighted by the complex weights $a_1, a_2, \ldots, a_{N-1}$. The directional pattern of the array expressed in the polynomial form is given by:

$$D(z) = 1 + a_1 z^{-1} + a_2 z^{-2} + a_3 z^{-3} + \ldots + a_{N-1} z^{-(N-1)} \qquad (6.11)$$

where

$$z = exp\left(j\frac{2\pi d}{\lambda}\sin\theta\right) \tag{6.12}$$

Such a polynomial may be represented as the product of $N-1$ factors giving the $N-1$ zeros of the directional pattern.

$$D(z) = (1 - z_1 z^{-1})(1 - z_2 z^{-1}) \ldots (1 - z_{N-1} z^{-1}) \tag{6.13}$$

where

$$z_n = exp\left(j\frac{2\pi d}{\lambda}\sin\theta_n\right) \tag{6.14}$$

where $z_n, n = 1, \ldots, N-1$ is the nth complex response zero. By using the null steering algorithm discussed in Section 3.3.2 of Chapter 3, the zeros of the array system will be repetitively updated one by one in a cyclical manner through a sequence of adjustment cycles.

Suppose zero z_a is to be updated to track the strongest signal. From (6.13), the directional pattern of the array is given by:

$$D_a(z) = (1 - z_a z^{-1})\hat{D}_a(z) \tag{6.15}$$

where

$$\begin{aligned} \hat{D}_a(z) &= \prod_{n=1, n\neq a}^{N-1} (1 - z_n z^{-1}) \\ &= c_{a0} + c_{a1} z^{-1} + \ldots + c_{aN-2} z^{-(N-2)} \end{aligned} \tag{6.16}$$

can be seen as the directional pattern of an $(N-1)$-element subarray with the coefficients $c_{a0}, c_{a1}, c_{a2}, \ldots, c_{aN-2}$. These initial coefficients can be chosen such

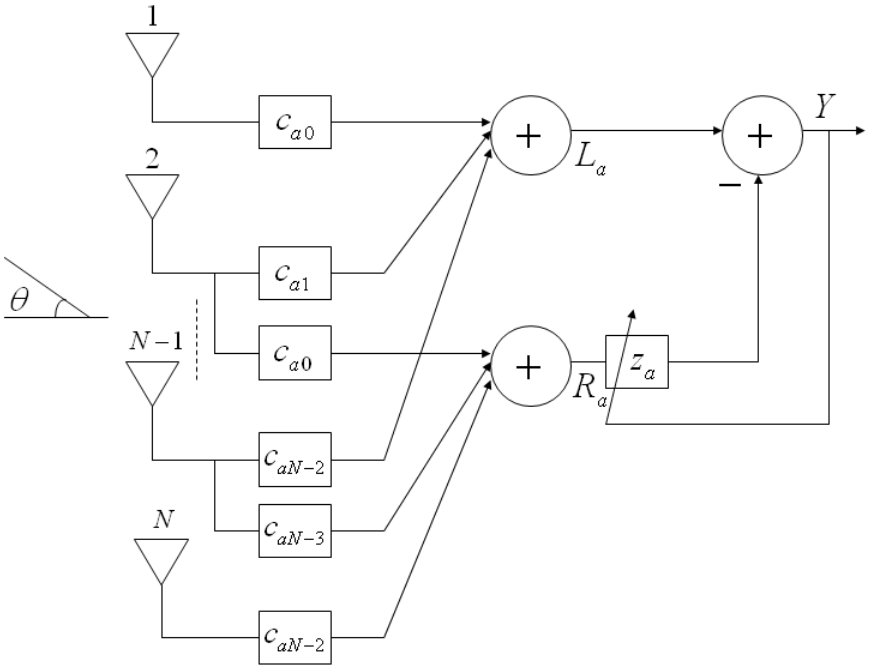

Figure 6.1: Array structure for updating z_a

that the first and last elements have unity equivalent weights and all the other elements have zero equivalent weights [52].

From (6.15) and (6.16), $D_a(z)$ can be expressed as

$$D_a(z) = \hat{D}_a(z) - z_a \hat{\hat{D}}_a(z) \tag{6.17}$$

where

$$\hat{\hat{D}}_a(z) = c_{a0}z^{-1} + c_{a1}z^{-2} + \ldots + c_{aN-2}z^{-(N-1)} \tag{6.18}$$

The processing of (6.15) can be implemented by using the structure in Fig. 6.1, where $\hat{D}_a(z)$ and $z^{-1}\hat{D}_a(z)$ are implemented by passing the signals from the first to the $(N-1)$th sensor elements and from the second to the Nth sensor elements, respectively. Therefore, the entire adaptive array in Fig. 6.1 is implemented by using two subarrays and with the preprocessing in the two

subarrays, the updating of z_a is equivalent to the updating of the complex weight of a 2-element power inversion array to minimize the output power. With the LMS algorithm, the complex zero z_a is updated according to

$$z_a \rightarrow z_a + \mu_a Y R_a^* \tag{6.19}$$

with the arrival of each new data sample. Y in (6.19) is the array output and is given by

$$Y = L_a - z_a R_a \tag{6.20}$$

μ_a is the feedback factor and as shown in Chapter 3, if μ_a is such that

$$|1 - \mu_a E[|R_a|^2]| < 1 \tag{6.21}$$

the value of updated zero z_{aend} at the end of the current adjustment cycle will converge towards its optimal value. Specifically, μ_a can be updated using the same recursive equation as that in (3.42). From (6.14), the following relationship between the updated zeros z_{aend} and the DOA θ_a can be established:

$$\theta_a = \arcsin\left\{\frac{\lambda \angle z_{aend}}{2\pi d}\right\} \tag{6.22}$$

Clearly, with z_{aend}, the DOA of the strongest signal θ_a can be easily computed using (6.22).

Now suppose zero z_b is to be updated in the next cycle to track the second strongest signal. The same updating procedure described above for z_a can be applied to the adjustment of z_b, except that the coefficients $c_{a0}, c_{a1}, c_{a2}, \ldots, c_{aN-2}$ in Fig. 6.1 will have to become $c_{b0}, c_{b1}, c_{b2}, \ldots, c_{bN-2}$.

In order to achieve a very low tracking error for z_b, intuitively, one desired property for the subarrays with coefficients $c_{b0}, c_{b1}, c_{b2}, \ldots, c_{bN-2}$ is that it should has a small variation in the directional pattern, except zero gain at the direction of θ_a. Therefore, the coefficients $c_{b0}, c_{b1}, c_{b2}, \ldots, c_{bN-2}$ can be obtained by solving the following constrained least-square optimization problem before updating zero z_b:

$$\begin{cases} \min\limits_{\mathbf{c}_b} \|\hat{\mathbf{V}}(\theta)\mathbf{c}_b - \mathbf{g}\|_2 \\ s.t.\ \ \hat{\mathbf{v}}^H(\theta_a)\mathbf{c}_b = 0 \end{cases} \tag{6.23}$$

where $\hat{\mathbf{V}}(\theta) = [\hat{\mathbf{v}}(\theta_1), \ldots, \hat{\mathbf{v}}(\theta_L)]^T$ is $L \times (N-1)$ matrix of ASVs and $L > N-1$ is the number of the sampled angular directions. $\mathbf{c}_b$ is the coefficient vector $[c_{b0}, c_{b1}, c_{b2}, \ldots, c_{bN-2}]^T$. $\mathbf{g}$ is a $L \times 1$ vector whose elements are all equal to 1. $\hat{\mathbf{v}}(\theta_a)$ is the steering vector towards the updated null direction θ_a. The above formulation can be efficiently solved using public domain software.

From (6.17), the directional pattern of the array now becomes

$$D_b(z) = (1 - z_b z^{-1})\hat{D}_b(z) \tag{6.24}$$

where

$$\begin{aligned} \hat{D}_b(z) &= c_{b0} \prod_{n=1, n\neq a,b}^{N-1} (1 - z_a z^{-1})(1 - z_n z^{-1}) \\ &= c_{b0} + c_{b1} z^{-1} + \ldots + c_{bN-2} z^{-(N-2)} \end{aligned} \tag{6.25}$$

and the complex zero z_b is updated according to (6.19). At the end of the cycle, z_b will converge to its optimal value z_{bopt}. With z_{bopt}, the DOA θ_b can be easily obtained from (6.22).

The same zero updating procedure can be applied to track all the remaining

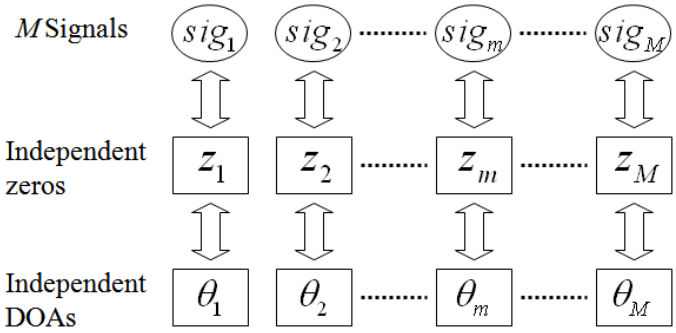

Figure 6.2: The relationship between zeros of array response, DOAs and signals for new method

untracked signals in the environment. One simple stopping criterion for the zero tracking process can be the array output power, since the information on whether untracked signals exist in the environment can be obtained by measuring the array output power as each zero is being updated. Since all the zeros (and, consequently DOAs) are repetitively obtained in a cyclical manner and only one DOA is estimated at any instant, the complexity required to implement the new method is relatively low and the convergence behaviour is significantly faster.

As discussed in Section 3.3.2, the estimate of each particular zero (and, consequently, the DOA) will not affect other DOAs for the new method. Therefore, as can be seen from Fig. 6.2, the one-to-one relationship exists between the zeros of array response, the DOAs and the signals in the environment. Now assuming that the mth signal sig_m moves after we finish all the tracking process. Instead of updating all the zeros again, we can just update the zero z_m to estimate the DOA of the moving signal sig_m, while all other zeros remain unchanged. Since only one DOA needs to be re-estimate, the convergence becomes even faster.

6.4.2 DOA estimation using null steering array with IIR array preprocessing

The method discussed in Section 6.4.1 uses least-square based preprocessing to reduce the tracking error. In Chapter 5, we presented an IIR array preprocessing based null steering system, which is very effective and useful in the sense that without applying any additional constraint it will result in a nearly flat gain in the antenna pattern, except zero gains at the null directions. Since the zeros of the IIR array preprocessing based null steering system is also repetitively updated one by one through a sequence of adjustment cycles, the same structure can be used to estimate the DOA. With updated zeros, the DOAs can be easily obtained from (6.22). Despite that, comparing to the method discussed in Section 6.4.1, a larger array is required to implement the IIR array preprocessing based null steering system, an even higher tracking accuracy can be achieved for low SNR situations due to its almost flat gain in the antenna pattern.

6.5 Simulation results

Some simulation results will now be presented to verify the above theoretical results. The simulated array is assumed to be a 7-element linear array with interelement spacing of $\lambda/2$.

The simulated environment consists of three independent signals of power 70 dB, 55 dB and 15 dB, assumed to be located at 24° , 27° and -30° to the array normal. Finally, independent white Gaussian noise of power 0 dB is added to each sensor element to account for the presence of ambient isotropic noise and other broadband sources of noise. Note here that, the difference in DOAs of

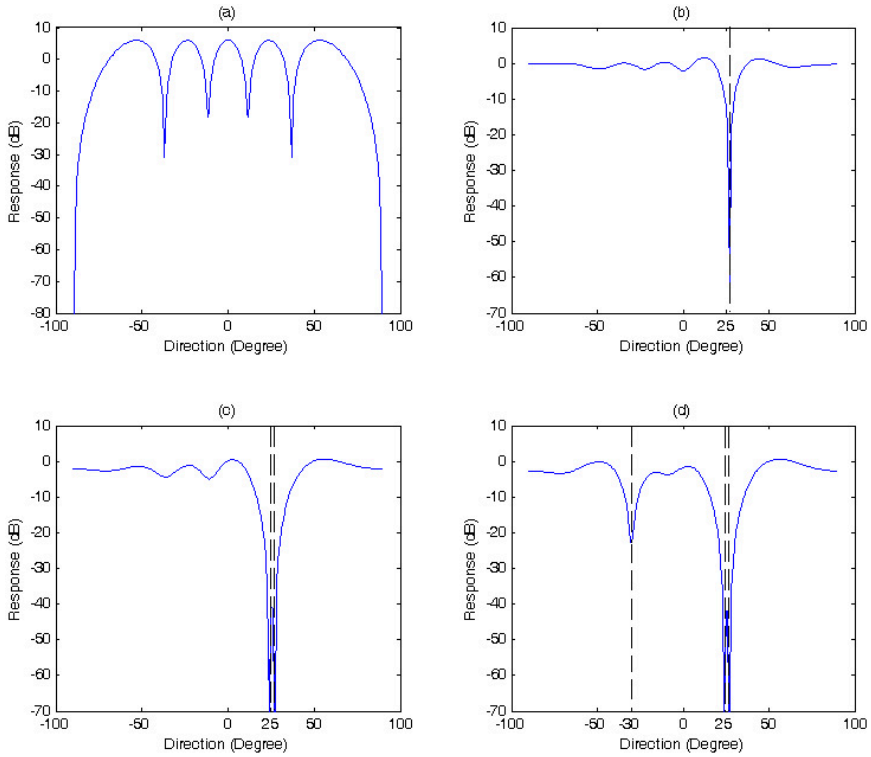

Figure 6.3: Directional patterns for new method (a) Initial pattern, (b) After first null update, (c) After second null update, (d) After third null update.

the two signals with 70 dB and 55 dB power is chosen to be small. The signal coming from -30° has a low power.

Fig. 6.3 shows the directional patterns of the proposed method at the end of the first, second and third null updates. As can be seen from Fig. 6.3(d), three zeros have been updated and the method has steered three nulls towards the signals in the environment. The steering of two separate nulls towards the two closely spaced signals is achieved. A null has also steered to the weak signal direction.

Clearly, from (6.22), the estimated DOA values for signals and their errors are shown in Table 6.1.

Consider the same simulated environment discussed above, the directional

Table 6.1: Estimated DOA values and their errors for new method

m	1	2	3
θ_m	23.9970	27.0056	-30.0932
Errors	0.0030	-0.0056	0.0932

patterns of the IIR array preprocessing based null steering system is shown in Fig. 6.4. The simulated array is assumed to be a 50-element linear array with interelement spacing of $\lambda/2$. The subarray size is set to be 5. The pole radius in (5.12) is chosen to be 0.9. As seen from Fig. 6.4(d), the method has steered three nulls towards the signals in the environment. Clearly by using the relationship in (6.22), the DOAs of the signals can be quickly estimated as given in Table 6.2.

Table 6.2: Estimated DOA values and their errors for new method

m	1	2	3
θ_m	24.0012	26.9982	-30.0226
Errors	-0.0012	0.0018	0.0226

Fig. 6.5 shows the DOA estimation errors using the new methods with different SNR values, averaged over 100 runs. It can be seen from the figure that high tracking accuracy can be achieved using the new method in Section 6.4.1 for a SNR as low as 10 dB. While using the new method in Section 6.4.2, a very low tracking error can be achieved even when the noise is comparable to the signal level.

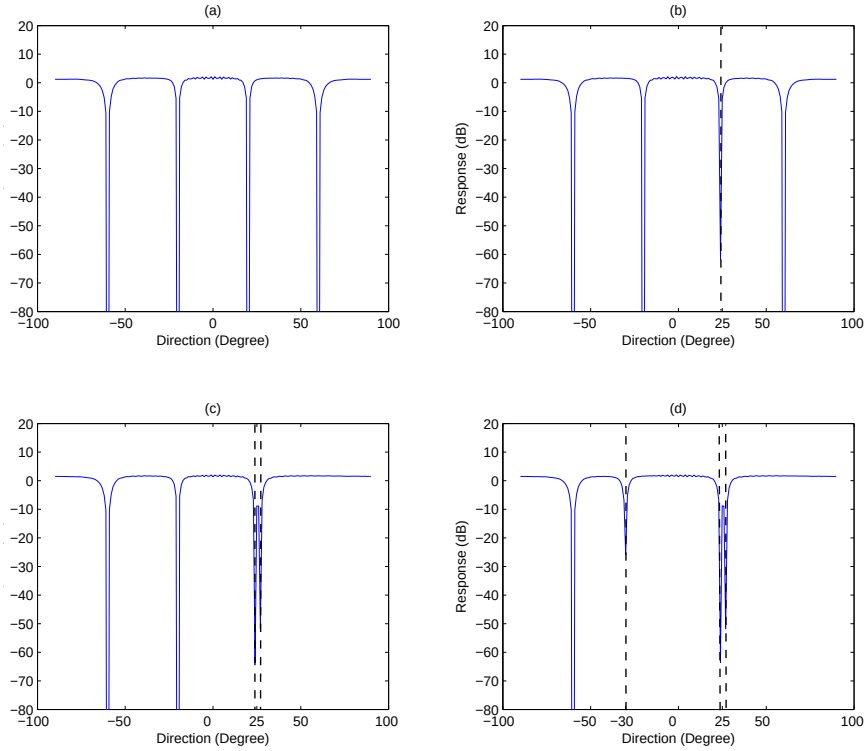

Figure 6.4: Directional patterns for new method (a) Initial pattern, (b) After first null update, (c) After second null update, (d) After third null update.

6.6 Effects of the sensor gain and phase perturbations

The effects of the sensor gain and phase perturbations for the new method in Section 6.4.1 are discussed in this section. The same effects exist for the new method in Section 6.4.2.

Imprecise knowledge of the gain and phase characteristics of the array sensors and the associated receivers, and of the sensor locations, can seriously degrade system performance [44, 45]. A simple model for random sensor gain and phase perturbations is to let each sensor have a perturbed response. Denoting the

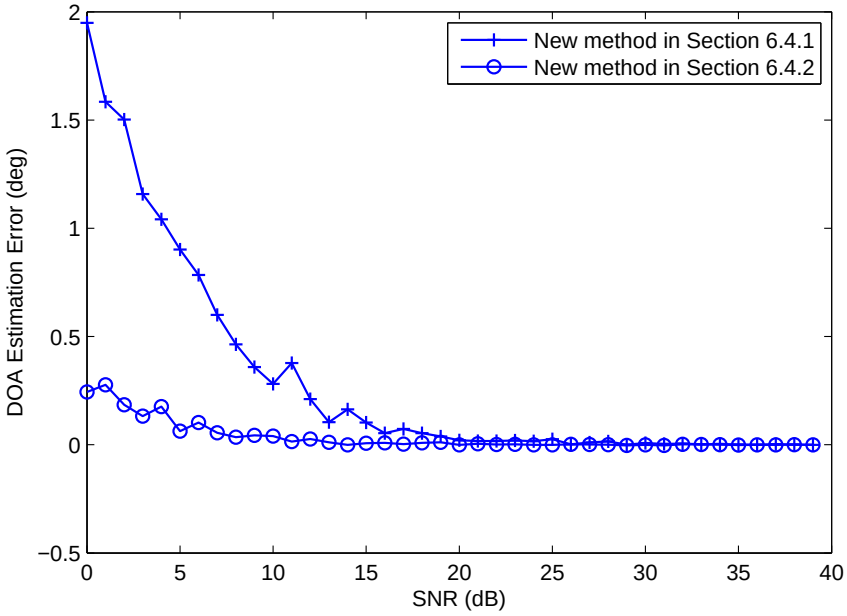

Figure 6.5: DOA estimation errors using new methods with different SNR values.

zero-mean random gain error of the nth sensor by ε_n and the zero-mean random phase error by ϕ_n, the perturbed output of the nth sensor can be written as

$$\mathbf{x}(t) = \sum_{m=1}^{M}(1+\varepsilon_n)\mathbf{v}(\theta_m)s_m(t)\exp(j\phi_n(t)) + \mathbf{n}(t) \tag{6.26}$$

The following computer simulation will show the effects of the sensor gain and phase perturbations on the performance of the proposed algorithm. Consider another environment where three signals of power 40 dB, 30 dB and 20 dB, located at $40°$, $-30°$ and $0°$. The 7-element ULA is used. Suppose that ε_n and ϕ_n are two zero-mean random variables with the following three random processes:

i. ε_n: uniform random process in the interval [-0.2, 0.2], ϕ_n: uniform random process in the interval [-0.2π, 0.2π].

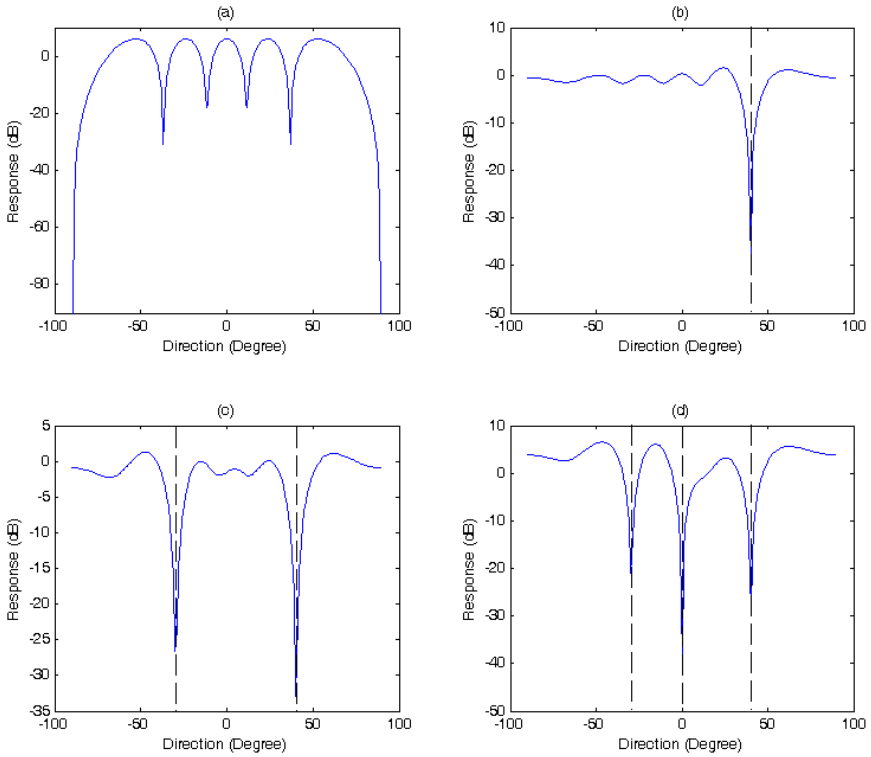

Figure 6.6: Directional patterns for new method with first random process (a) Initial pattern, (b) After first null update, (c) After second null update, (d) After third null update.

ii. ε_n: uniform random process in the interval [-0.3, 0.3], ϕ_n: uniform random process in the interval [-0.4π, 0.4π].

iii. ε_n: uniform random process in the interval [-0.2, 0.2], ϕ_n: Gaussian process with variance $\sigma_m^2 = (0.2\pi)^2$.

The directional patterns for the proposed method with the above three random processes of ε_n and ϕ_n are shown in Fig. 6.6, Fig. 6.7 and Fig. 6.8, respectively. The estimated DOA values are shown in Table 6.3. Here we assume that the zero-mean gain errors and the zero-mean phase errors are independent from sensor to sensor and stationary. Therefore, the multiplicative gain and phase errors in the sensors are equivalent to increasing the thermal internal noise.

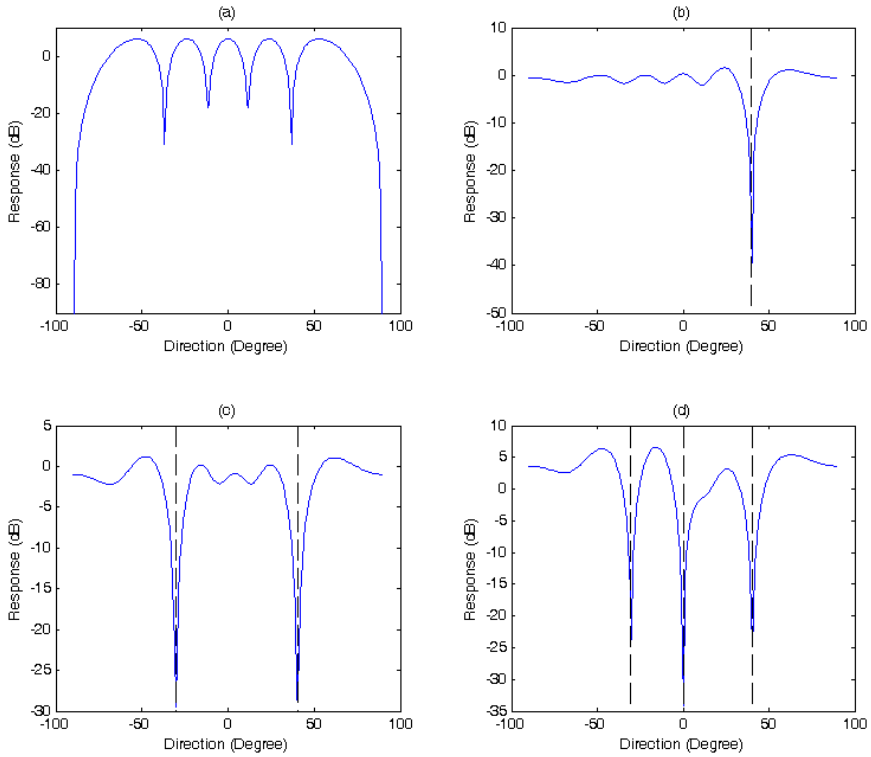

Figure 6.7: Directional patterns for new method with second random process (a) Initial pattern, (b) After first null update, (c) After second null update, (d) After third null update.

Table 6.3: Estimated DOAs with sensor gain and phase perturbations for new method

	m	1	2	3
i.	θ_m	40.2300	0.0673	-29.5845
ii.	θ_m	40.3690	-0.1258	-30.2946
iii.	θ_m	39.8856	-0.3412	-29.6494

More simulations can also reveal that the proposed method can be robust to the sensor gain and phase perturbations. Moreover the following observation can be made: these is no apparent relationship between the perturbation level

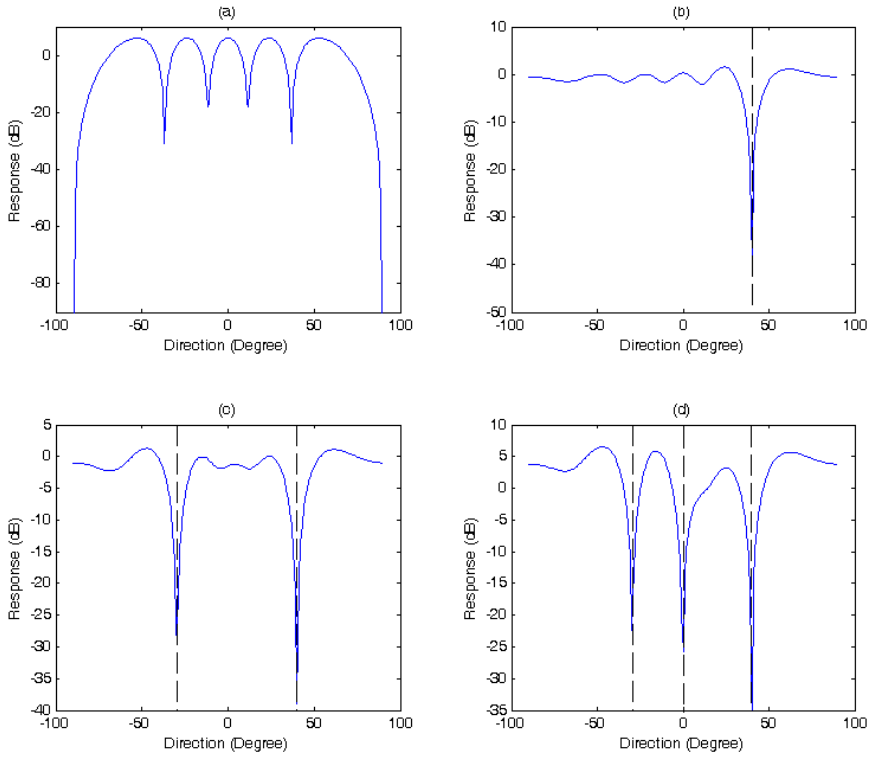

Figure 6.8: Directional patterns for new method with third random process (a) Initial pattern, (b) After first null update, (c) After second null update, (d) After third null update.

and the performance of the proposed method as long as the perturbations are controlled in a certain range.

6.7 Summary

This chapter presents and discusses the detailed application of null steering technique in DOA estimation. With this algorithm, the complex zeros of the array directional pattern are repetitively updated one at a time by using the LMS algorithm to minimize the output power. The relationship between the updated zeros and the DOA angles is established so that the angles can be quickly estimated. The advantages of the new DOA estimation method is its

relatively low computational complexity and faster convergence rate. The estimate of each particular DOA will not affect other extracted DOAs for the new method since one-to-one relationship exists between the estimated DOAs and the signals in the environment. From the simulation results, we can also observe the effectiveness and robustness to the sensor gain and phase perturbations of the proposed method.

Chapter 7

Conclusions and Recommendations

7.1 Conclusions

In this thesis, we have focused on the null steering algorithms for beamforming application.

Our work has been carried out in four aspects. Firstly, the null steering algorithms with single and multiple constraints (NSASC, NSAMC) were proposed. Using these methods, the zeros can be selectively tracked so that the interferences can be rejected while the desired signal is concentrated on by the array. Specifically, NSASC was designed for use as a fast null steering algorithm while maintaining unity gain in desired signal direction. By using NSAMC, the same null steering structure can also function like a beamformer, where the output signal-to-interference-plus-noise ratio (SINR) of the mainbeam is enhanced with a decreased sidelobe level. The main advantage of NSASC/NSAMC is the sim-

plicity. When compared with conventional least mean square (LMS) based linearly constrained minimum variance (LCMV) beamforming algorithm, NSASC and NSAMC converge in a faster manner; and compared with QR-recursive least squares (QR-RLS) based minimum variance distortionless response (MVDR) beamformer, NSASC and NSAMC have lower complexity. Furthermore, due to their cascade configurations, signal self-nulling problem for conventional beamformer can be resolved.

Secondly, we proposed an online implementation of adaptive null steering beamformer for flexible broad null control. This design is a further development of the NSAMC. Using the proposed design, the series of null steering beamformers are first implemented by decomposing the original array into several subarrays. A spatial finite impulse response (FIR) filter is used in the design to suppress any moving interference. The advantages of this proposed implementation are its relatively simple design and the ability to control the broad nulls. The new beamformer is useful and effective in the environment where both stationary and moving interfering signals exist since it can steer both sharp and controlled broad nulls in the appropriate directions. When compared with LMS covariance matrix taper (CMT) based broad null synthesis method, the proposed beamformer has a faster convergent rate; and compared with the QR-RLS CMT based broad null synthesis method, the proposed method has a lower complexity.

Thirdly, we investigated the design and performance if the structure of null steering algorithm is extended to take the form of a pole-zero model. The proposed null steering algorithm employs infinite impulse response (IIR) array preprocessing. Using the new method, the complex zeros of the array system

will be repetitively updated one by one in a cyclical manner through a sequence of adjustment cycles. In each adjustment cycle, a particular complex zero is updated by using the LMS algorithm. The proposed method is very effective and useful in the sense that without applying any additional constraint it will result in a nearly flat gain in the antenna pattern, except zero gains at the null directions.

Lastly, the application of null steering technique in direction of arrival (DOA) estimation was presented and discussed. With this algorithm, the complex zeros of the array directional pattern are repetitively updated one at a time by using the LMS algorithm to minimize the output power. Then, a relationship between the updated zeros and the DOA angles is established so that the angles can be quickly estimated. Moreover, computer simulations showed that the proposed approach is robust to the sensor gain and phase perturbations.

7.2 Recommendations for Further Research

Based on the techniques and schemes developed in this thesis, the scope of the current work may be further extended.

In this thesis, we have focused on the beamforming techniques using uniform linear array (ULA) system. Recently, there has been increased interest in using uniform circular array (UCA) [46, 47]. This is because circular arrays are suitable for scanning 360° without any variation in gain and radiation pattern.

As shown in Fig. 7.1, a uniform circular array consists of a number of N sensors arranged in a circular ring, with radius r in the azimuth plane. The nth component of the array response (or steering) vector $\mathbf{a}(\theta), n \in 1, 2, \ldots, N$, for a

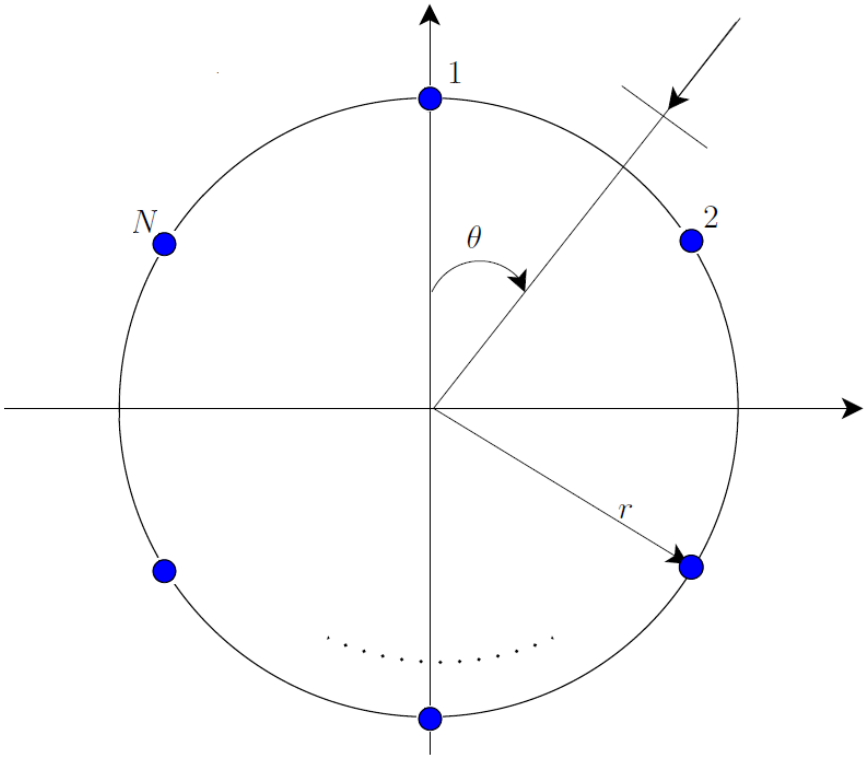

Figure 7.1: Circular array with N sensors

narrowband signal of wavelength λ arriving from angle θ is given by

$$[\mathbf{a}(\theta)]_n = \exp\left[jkr\cos\left(\theta - \frac{2\pi(n-1)}{N}\right)\right] \tag{7.1}$$

where $k = 2\pi/\lambda$. Therefore, adaptive zero-tracking methods based on the use of UCA can be further studied.

In Chapter 4, we proposed an implementation of adaptive zero tracking beamformer for flexible broad null control. In this new design, a spatial FIR filter was used to suppress any moving interference. A cascade configuration was employed in the new implementation. In future studies, it is possible to develop a robust zero tracking beamformer with broad null. From Equation

(4.1), the modified directional pattern of the array can be given as

$$D(\theta) = (1 - b_1 z^{-1})\hat{D}(\theta) \tag{7.2}$$

where

$$b_1 = \exp\{j[\pi \sin(\theta_1 + \phi_1)]\} \tag{7.3}$$

Note that in (7.3), $\phi_1 \in [\theta_1 - \triangle/2, \theta_1 + \triangle/2]$ and $\triangle$ is the null width. Therefore, we can try to minimize the system output power by placing a broad null in the spatial region centred around θ_1.

Author's Publications

1. S. Leng, W. Ser and C.C. Ko, "A simple constrained based adaptive null steering algorithm," *Proceedings of the 16th European Signal Processing Conference (EUSIPCO 2008)*, Lausanne, Switzerland, August 2008.

2. S. Leng, W. Ser and C. C. Ko, "Adaptive beamformer derived from a constrained null steering design," *Signal Processing*, vol. 90, issue 5, pp. 1530-1541, May 2010.

3. S. Leng and W. Ser, "Adaptive null steering beamformer implementation for flexible broad null control," *Signal Processing*, vol. 91, issue 5, pp. 1229-1239, May 2011.

4. S. Leng and W. Ser, "IIR Array Processing Based Fast Adaptive Zero Tracking Algorithm Using Shift-Invariant Subarrays," submitted to *Signal Processing*, under second review, 2011.

5. S. Leng and W. Ser, "On the Application of the Null Steering Technique in Direction-of-Arrival Estimation," submitted to *IEEE Communications Letters*, under review, 2011.

Bibliography

[1] G. V. Tsoulos, *Adaptive Antennas for Wireless Communications*. New York: IEEE Press, 2001.

[2] H. Krim and M. Viberg, "Two decades of array signal processing research: the parametric approach," *IEEE Signal Processing Mag.*, vol. 13, no. 4, pp. 67-94, Jul. 1996.

[3] B. D. Van Veen and K. M. Buckley, "Beamforming: a versatile approach to spatial filtering," *IEEE ASSP Mag.*, vol. 5, no. 2, pp. 4-24, Apr. 1988.

[4] R. Compton, *Adaptive Antennas: Concepts and Performance*. New Jersey: Prentice-Hall, 1988.

[5] J. E. Hudson, *Adaptive Array Principles*. Peter Peregrinus Ltd., 1981.

[6] D. H. Johnson and D. E. Dudgeon, *Array Signal Processing: Concepts and Techniques.* Prentice Hall, Inc., 1993.

[7] R. A. Monzingo and T. W. Miller, *Introduction to Adaptive Arrays*. New York: Wiley, 1980.

[8] P. S. Naidu, *Sensor Array Signal Processing*. CRC Press London, 2001.

[9] Y. Zhou and S. C. Chan, "A new family of approximate QR-LS algorithms for adaptive filtering," *IEEE Trans. on Statistical Signal Processing*, pp. 71-76, Jul. 2005.

[10] Z. L. Yu, W. Ser and S. Rahadja, "QR-RLS based minimum variance distortionless response beamformer," in *Proc. ICASSP*, vol. 3, pp. 984-987, May 2006.

[11] D. E. N. Davies, "Independent angular steering for each zero of directional pattern for a linear array," *IEEE Trans. Antennas Propagation*, vol. AP-15, pp. 296-298, 1967.

[12] C. C. Ko, K. L. Thum, W. Ser and T. S. Quek, "A simple fast adaptive zero tracking algorithm," *Signal Processing*, vol. 20, pp. 315-323, 1990.

[13] R. T. Compton, JR, "The power inversion array: Concept and performance," *IEEE Trans. on Aerospace and Electronic Systems*, vol. AES-15, pp. 803-814, 1979.

[14] H. M. Elkamchouchi and M. A. R. M. Adam, "A new constrained fast null steering algorithm, *IEEE Trans. on Antennas and Propagation*," vol. 2, pp. 926-929, Jul. 2000.

[15] R. J. Mailloux, "Covariance matrix augmentation to produce adaptive array pattern troughs," *Electronics Letters*, vol. 31, No. 10, pp. 771-772, May 1995.

[16] M. Zatman, "Production of adaptive array troughts by dispersion synthesis," *Electronics Letters*, vol. 31, No. 25, pp. 2141-2142, Dec 1995.

[17] J. Riba, J. Goldberg, and G. Vazquez, "Robust beamforming for interference rejection in mobile communications," *IEEE Trans. on Signal Processing*, vol. 45, pp. 271-275, Jan. 1997.

[18] J. R. Guerci, "Theory and application of covariance matrix tapers for robust adaptive beamforming," *IEEE Trans. on Signal Processing*, vol. 47, pp. 997-985, Apr. 1999.

[19] A. Jakobsson, S. R. Alty, and S. Lambotharan, "On the implementation of the linearly constrained minimum variance beamformer," *IEEE Trans. on Circuit and Systems II*, vol. 53, No. 10, pp. 1059-1062, Oct. 2006.

[20] S. R. Nagesh and T. S. Vedavathy, "A procedure for synthesizing a specified sidelobe topography using an arbitrary array," *IEEE Trans. on Antennas and Propagation*, vol. 43, No. 7, pp. 742-745, 1995.

[21] B. P. Ng, M. H. Er and C. Kot, "A flexible array synthesis method using quadratic programming," *IEEE Trans. on Antennas and Propagation*, vol 41, No. 11, pp. 1541-1550, 1993.

[22] C. Y. Tseng and L. J. Griffiths, "A simple algorithm to achieve desired patterns for arbitrary arrays," *IEEE Trans. on Antennas and Propagation*, vol 40, No. 11, pp. 2737-2746, 1992.

[23] L. J. Gudino, S. N. Jagadeesha and J. X. Rodrigues, "A novel design of design of sharp transition FIR filter for digital beamforming," in *International Symposium on CNSDSP*, pp. 247-250, Jul. 2008.

[24] W. C.Wu and Y. J.Wang, "A study of beam-pattern generation methods for antenna array systems," *Journal of Science and Engineering Technology*, vol. 1, No. 2, pp. 7-12, 2005.

[25] M. Pesavento and A. B. Gershman, "Maximum-likelihood direction-ofarrival estimation in the presence of unknown nonuniform noise," *IEEE Trans. on Signal Processing*, 49(7): pp. 1310-1324, 2001.

[26] H. Srinath and V. U. Reddy, "Analysis of MUSIC algorithm with sensor gain and phase perturbations," *Signal Processing*, 23(3): pp. 245-256, 1991.

[27] M. A. AI-Nuaimi., R. M. Shubair and K. O. AI-Midfa, "Direction of Arrival Estamation in Wireless Mobile Communications using Minimum Variance Distorsionless Response," *The second International conference on Innovations in information technology (IIT'05)*, pp. 1-6, 2005.

[28] A. Paulraj, R. Roy and T. Kailath, "A subspace rotation approach to signal parameter estimation," *Proc. IEEE*, vol. 74, pp. 1044-1046, July 1986.

[29] S. P. Applebaum, "Adaptive arrays," *IEEE Trans. on Antennas and Propagation*, vol. AP-24, pp. 650-662, Sept. 1976.

[30] B. Widrow, P. E. Mantey, L. J. Griffiths and B. B. Goode, "Adaptive antenna systems," *Proc. IEEE*, vol. 55, pp. 2143-2159, Dec. 1967.

[31] O. L. Frost, "An algorithm for linearly constrained adaptive array processing," *Proc. IEEE*, vol. 60, pp. 926-935, Aug. 1972.

[32] S. P. Applebaum, "Adaptive arrays," Syracuse Univ. Res. Corp., Special Projects Lab, Syracuse, N. Y., Tech. Rep. SPL-TR 66-1, Aug. 1966.

[33] M. H. Er, "Optimum antenna array processors with linear and quadratic constraints," Ph.D. dissertation, The University of Newcastle, New South Wales, 2308, Australia, May 1985.

[34] J. Capon, "High-resolution frequency wavenumber spectrum analysis," in *Proc. IEEE*, vol. 57, no. 8, 1969.

[35] M. S. Bazaraa and C. M. Shetty, *Nonlinear Programming: Theory and Algorithms*. John Wiley & Sons, 1979.

[36] L.C. Godara, "Application of Antenna Arrays to Mobile Communications, Part II: Beamforming and Direction-of-Arrival Considerations," *Proc. IEEE*, vol. 85, no. 8, pp. 1195-1245.

[37] J. Zhou and G. Li, "Plain gradient based direct frequency estimation using second-order constrained adaptive IIR notch filter," *Electronics Letters*, 40(5): pp. 351-352, 2004.

[38] Y. Xiao, Y. Takeshita and K. Shida, "Steady-state analysis of a plain gradient algorithm for a second-order adaptive IIR notch filter with constrained poles and zeros," *IEEE Trans. on Circuits and Systems II*, 48(7): pp. 733-740, 2001.

[39] X. Yegui, et al., "Statistical performance of the memoryless nonlinear gradient algorithm for the constrained adaptive IIR notch filter," *IEEE Trans. on Circuits and Systems I*, 52(8): pp. 1691-1702, 2005

[40] P. Stoica and A. Nehorai, "Performance analysis of an adaptive notch filter with constrained poles and zeros," *IEEE Trans on ASSP*, vol. ASSP-36, no. 6, pp. 911-919, 1998.

[41] M. Martone, *Multiantenna Digital Radio Transmission*, Artech House, MA, 2002.

[42] V. V. Zaharov, and M. Teixeira, "SMI-MVDR beamformer implementations for large antenna array and small sample size," *IEEE Trans. on Circuit and Systems I*, vol. 55, No. 10, pp. 3317-3327, Nov. 2008.

[43] Joyce Van de Vegte, *Fundamentals of Digital Signal Processing*, Prentice Hall, Upper Saddle River, NJ, 2002.

[44] A. P. -C. Ng, "Direction-of-arrival estimates in the presence of wavelength, gain, and phase errors," *IEEE Trans. on Signal Processing*, 43(1): pp. 225-232, 1995.

[45] G. V. Serebryakov, "Capability of minimum variance beamformer for direction finding for fast perturbations of array sensors," *The 1996 IEEE International Conference on Acoustics, Speech, and Signal Processing*, Allanta, GA, USA, vol. 6, pp. 3157-3160, 1996.

[46] J. A. Tsai, and B. D. Woerner, "Adaptive Beamforming of Uniform Circular Arrays (UCA) for Wireless CDMA System," *Proceedings of the 35th Asilomar Conference on Signal Systems and Computers*, Pacific Grove, CA, USA, 2001.

[47] J. A. Tsai, R. M. Buehrer, and B. D. Woerner, "BER Performance of a Uniform Circular Array Versus a uniform Linear Array in a Mobile Radio Environment," *IEEE Transactions on Wireless Communications*, Vol. 3, pp. 695-700, 2004.

[48] Simon Haykin, *Adaptive Filter Theory.* Prentice Hall, Inc., 2002.

[49] N. I. Cho, C. H. Choi, and S. U. Lee, "Adaptive line enhancement by using an IIR lattice notch filter," *IEEE Trans. Acoust., Speech, Signal Processing*, vol. 37, pp. 585-589, Apr. 1989.

[50] T. Kwan and K. Martin, "Adaptive detection and enhancement of multiple sinusoids using a cascade IIR filter," *IEEE Trans. Circuits Syst.*, vol. 36, pp. 937-947, Jul. 1989.

[51] J. F. Chicharo and T. S. Ng, "Gradient-based adaptive IIR notch filtering for frequency estimation," *IEEE Trans. Acoust., Speech, Signal Processing*, vol. 38, pp. 769-777, May 1990.

[52] C. C. Ko, "A fast adaptive null-steering algorithm based on output power measurements," *IEEE Trans. on Aerospace and Electronic Systems*, vol. 29, no. 3, pp. 717-725, July 1993.

[53] C. C. Ko, "A fast null steering algorithm for linearly constrained adaptive arrays," *IEEE Trans. on Antennas and Propagation*, vol. 39, no. 8, pp. 1098-1104, Aug 1991.

[54] Vinay K. Ingle and John G. Proakis, *Digital Signal Processing Using Matlab.* Brooks/Cole, 2000.

[55] F. X. Wen, "New algorithms for adaptive beamforming and direction of arrival estimation," *Progress report for qualifying examination*, Nanyang Technological University, 2008.